JOURNAL OF PETROLOGY | VOLUME 55 | NUMBER 3 | PAGES 549–583 | 2014 | doi:10.1093/petrology/egt077

A Record of Paleoproterozoic Subduction Preserved in the Northern Slave Cratonic Mantle: Sr–Pb–O Isotope and Trace-element Investigations of Eclogite Xenoliths from the Jericho and Muskox Kimberlites

KATIE A. SMART[1,2]*, THOMAS CHACKO[1], ANTONIO SIMONETTI[1,3], ZACHARY D. SHARP[4] AND LARRY M. HEAMAN[1]

[1]DEPARTMENT OF EARTH AND ATMOSPHERIC SCIENCES, UNIVERSITY OF ALBERTA, EDMONTON, AB, T6G 2E3, CANADA

[2]INSTITUT FÜR MINERALOGIE, WESTFÄLISCHE WILHELMS-UNIVERSITÄT, MÜNSTER 48149, GERMANY

[3]DEPARTMENT OF CIVIL AND ENVIRONMENTAL ENGINEERING AND EARTH SCIENCES, UNIVERSITY OF NOTRE DAME, NOTRE DAME, IN 46556, USA

[4]DEPARTMENT OF EARTH AND PLANETARY SCIENCES, UNIVERSITY OF NEW MEXICO, ALBUQUERQUE, NM 87131, USA

RECEIVED MAY 7, 2013; ACCEPTED DECEMBER 5, 2013
ADVANCE ACCESS PUBLICATION JANUARY 11, 2014

Paleoproterozoic eclogite xenoliths from the Jericho and Muskox kimberlites located in the northern Slave craton, Canada, display geochemical and isotopic evidence of a recycled oceanic lithosphere origin. The eclogites comprise a diverse suite of kyanite- and diamond-bearing and bimineralic xenoliths that have a wide range of geochemical compositions. Calculated whole-rock eclogite compositions are broadly basaltic to picritic, ranging from 5 to 13 wt % MgO. Calculated whole-rock trace-element compositions for the eclogites show three overall REE patterns: the first pattern resembles that of oceanic gabbros with prominent positive Eu anomalies and flat heavy REE; the second pattern is similar to the first but displays marked light REE depletion that is interpreted to record partial melt loss; the third pattern lacks Eu anomalies and instead displays both gradually increasing REE contents from La to Lu similar to boninitic melts and 'humped' middle REE patterns similar to those observed in eclogites formed by reaction with subduction fluids. Several eclogites have garnet and/or clinopyroxene $\delta^{18}O$ *values >6‰, which coupled with the trace-element systematics of all the eclogites is interpreted to reflect derivation from recycled oceanic lithosphere protoliths. Lead isotope data for eclogite clinopyroxenes form a broad array that extends from highly radiogenic isotope compositions similar to the host Jericho kimberlite to an intersection with the Stacey–Kramers terrestrial two-stage Pb evolution curve at* c. *2·2 Ga. The slope of this data array defines a secondary Pb isochron with an associated age of 1·7 ± 0·3 Ga. Although it is possible that the Pb isotope array is actually a mixing line between the eclogite protolith and the host Jericho kimberlite, both the secondary isochron age and the* c. *2·2 Ga Stacey–Kramers model age are consistent with Paleoproterozoic protolith oceanic crust formation. Eclogite xenoliths and eclogitic diamond inclusions from the Slave craton almost exclusively yield* c. *2 Ga ages, which are broadly compatible with formation during subduction associated with the* c. *1·9–1·8 Ga Wopmay orogeny at the western margin of the Slave craton. Trends in the Sr–Pb isotopic compositions of the eclogite clinopyroxene show that seawater alteration of the oceanic crust protoliths was an important process during protolith formation, and cryptic metasomatism further increased the Pb and Sr isotope values. This metasomatism is probably associated with the Jurassic kimberlite magmatism; however, contributions from the Mesoproterozoic Mackenzie event cannot be completely excluded.*

*Corresponding author. Present address: School of Geosciences, University of the Witwatersrand, Private Bag 3, Johannesburg 2050, South Africa. Telephone: +27 11 717 6549. Fax: +27 717 6579. E-mail: katie.smart2@wits.ac.za

KEY WORDS: *cratonic mantle lithosphere; diamond; recycled oceanic crust; Laser Ablation ICP-MS; metasomatism*

INTRODUCTION

The preservation of cratons since the Archean has largely been attributed to the presence of mantle roots that underlie the cratonic crust. Whether these mantle roots have remained coupled to the overlying cratonic crust since their inception is debated (e.g. Aulbach, 2012) but increasing recognition of the commonality of ages determined for the cratonic mantle lithosphere and the overlying crust suggest a shared history (Carlson *et al.*, 2005). Major peaks in crustal growth (or reworking; Dhuime *et al.*, 2012) in the Mesoarchean, Neoarchean, and the Paleoproterozoic are also observed in the age populations of mantle xenoliths and diamond inclusions (e.g. Pearson & Wittig, 2008; Shirey & Richardson, 2011), indicating that the cratonic crust and mantle lithosphere were at least partially coupled during growth and modification (e.g. Pearson, 1999). However, the exact mechanism of cratonic mantle lithosphere formation is highly controversial and debate continues on whether subduction-driven stacking of oceanic lithosphere (e.g. Helmstaedt & Schulze, 1989; Stachel *et al.*, 1998; Pearson & Wittig, 2008), vertical subcretion of mantle plumes (e.g. Griffin *et al.*, 2003; Aulbach, 2012), or a combination of the two processes was involved (e.g. Herzberg & Rudnick, 2012). Some of the arguments used in these petrogenetic models concentrate on the composition and age of kimberlite-hosted peridotite xenoliths; however, mantle eclogite xenoliths can provide equally important constraints because of their potential involvement in subduction cycles (e.g. Ringwood & Green, 1966), formation of mantle heterogeneities (e.g. Hirschmann & Stolper, 1996) and contribution to mantle melt generation (e.g. Kogiso *et al.*, 2004).

Similar to the debate surrounding the formation of cratonic mantle lithosphere, the origin of eclogite xenoliths is also controversial. Mantle eclogite xenoliths have been interpreted as both high-pressure cumulates of mantle-derived melts (e.g. O'Hara & Yoder, 1967; Smyth *et al.*, 1989) and remnants of subducted oceanic crust (e.g. Helmstaedt & Doig, 1975; MacGregor & Manton, 1986; Jacob *et al.*, 1994). Recent investigations of eclogite xenoliths and eclogitic diamond inclusions largely favor a recycled oceanic crust origin owing to the presence of hallmark geochemical signatures (Eu anomalies, non-'mantle' $\delta^{18}O$ signatures) in some samples (see review by Jacob, 2004) that are interpreted to indicate plagioclase-bearing, seawater-altered oceanic basaltic and gabbroic protoliths (e.g. Schulze *et al.*, 2003; Spetsius *et al.*, 2009; Smit *et al.*, 2013). However, on the basis of proposed correlations between the oxygen isotope compositions of eclogitic minerals and geochemical indices of metasomatism (Williams *et al.*, 2009; Gréau *et al.*, 2011), some recent studies have advocated deep magmatic processes and metasomatism as critical to eclogite formation (e.g. Huang *et al.*, 2012).

Ages determined for eclogite xenoliths and eclogitic diamond inclusions range from Neoarchean to Proterozoic, such that unraveling the petrogenesis of mantle eclogites will improve our understanding of the temporal evolution of cratonic mantle lithosphere and crust–mantle dynamics. Peridotite xenoliths and peridotitic diamond inclusions commonly yield ages older than eclogitic mantle material (e.g. Richardson *et al.*, 1993; Aulbach *et al.*, 2009*a*), and have been related to the initiation of cratonic mantle lithosphere formation (Shirey *et al.*, 2004). However, it is significant that ages determined for cratonic mantle eclogites are largely younger than 3 Ga, suggesting that the process(es) responsible for eclogite formation and/or preservation became important only in the late Meso- to Neoarchean (e.g. Shirey & Richardson, 2011). Furthermore, ages determined from worldwide occurrences of eclogite xenoliths and eclogitic diamond inclusions largely fall into two time periods, Meso- to Neoarchean (*c.* 3·0–2·5 Ga) or Paleoproterozoic (*c.* 1·8–2·2 Ga), with a subordinate Mesoproterozoic (*c.* 1–1·3 Ga) population [see compilation by Shirey & Richardson (2011)]. Significantly, these eras mark prominent episodes of worldwide continental crust formation (e.g. Hawkesworth & Kemp, 2006), amalgamation (e.g. Bleeker, 2003) and modification (e.g. Griffin *et al.*, 2004*a*), and the evidence of these events is preserved in cratons today.

Our study aims to further investigate the links between cratonic crust and mantle lithosphere through the study of a compositionally diverse suite of eclogite xenoliths from the Jericho and Muskox kimberlites of the northern Slave craton, Canada. Previous investigations of the eclogite xenoliths from the Jericho kimberlite have shown wide mineralogical and compositional ranges (Kopylova *et al.*, 1999*a*), but significant attention has been given to two unusual eclogite types: high-FeO zircon-bearing eclogites and high-MgO diamond-bearing eclogites. Detailed geochemical investigation of the high-MgO diamond-bearing eclogites revealed a complex origin (De Stefano *et al.*, 2009; Smart *et al.*, 2009, 2012), but isotopic investigations did not provide age constraints (Smart *et al.*, 2009). In contrast, the high-Fe zircon-bearing eclogite xenoliths yield *c.* 1·9 Ga formation ages, and are interpreted as remnants of oceanic crust subducted beneath the northern Slave craton during the Paleoproterozoic Wopmay orogeny (Schmidberger *et al.*, 2005). Despite detailed investigations of the more atypical Jericho eclogites, an integrated geochemical and isotopic study is lacking for the majority of the Jericho eclogites. To better understand the petrogenesis of the Jericho eclogite suite as a whole, and to investigate any relationship between their origin and processes occurring in the Slave cratonic crust and mantle, we have conducted a more comprehensive major- and trace-element, and

Sr–Pb–O isotopic study of a wide range of eclogite types from the Jericho kimberlite, and two additional diamond-bearing eclogites from the nearby Muskox kimberlite.

GEOLOGY OF THE SLAVE CRATON

The Archean Slave craton of NW Canada (Fig. 1) comprises an ancient (4·03–2·85 Ga) basement complex in the central and western parts of the craton and a juvenile, 2·72–2·55 Ga volcanic and granitoid terrane in the east (Bleeker & Hall, 2007). The two terranes were amalgamated at *c.* 2·7–2·6 Ga and stitched together by intrusion of 2·60–2·58 Ga granites (Bleeker *et al.*, 1999; Davis *et al.*, 2003). The Slave craton was modified in the Paleoproterozoic at its southern and eastern margins by the Taltson–Thelon orogeny, and at the western margin by the Wopmay orogeny (Hoffman, 1989). The Wopmay orogeny was accompanied by subduction of oceanic crust beneath the craton, which is hypothesized to be responsible for extensive eclogite and diamond formation in the cratonic mantle (Schmidberger *et al.*, 2005, 2007; Aulbach *et al.*, 2009*a*, 2009*b*). This paleo-subduction zone has been geophysically imaged dipping eastward below the craton (Cook *et al.*, 1999). Abundant mafic dykes intruded the craton between 2·2 and 1·8 Ga (Le Cheminant & van Breemen, 1994), and again at 1·27 Ga as part of the Mackenzie Igneous Event, which radiated from the NW of the craton (Le Cheminant & Heaman, 1989). Phanerozoic kimberlites occur throughout the Slave craton and are particularly concentrated in the Lac de Gras area in the center of the craton (Creaser *et al.*, 2004).

The lithospheric mantle underlying the Slave craton is vertically and horizontally stratified with respect to its chemical composition (e.g. Griffin *et al.*, 1999). Based on the CaO–Cr_2O_3 compositions of garnet xenocrysts from Slave kimberlites, Grütter *et al.* (1999) divided the Slave cratonic mantle into NE–SW-trending northern, central and southern domains. The Jurassic-age Jericho (173·1 ± 1·3 Ma, Heaman *et al.*, 2006) and Muskox kimberlites lie in the northern domain (Fig. 1), and in contrast to the central and southern domains, which contain a shallow ultra-depleted harzburgitic and dunitic layer, the mantle lithosphere of the northern domain is composed of more fertile lherzolites with a significant metasomatic signature in the deeper cratonic mantle lithosphere (Griffin *et al.*, 2004*b*).

ECLOGITE XENOLITHS FROM THE JERICHO AND MUSKOX KIMBERLITES

Previous investigations of Jericho eclogites

Eclogite xenoliths from the Jericho kimberlite have been the subject of several studies in the last 15 years. The Jericho xenolith population contains a high proportion of eclogite (25%) and pyroxenite or wehrlite (16%) xenoliths, in which the eclogites record a wide range of equilibration temperatures from 600 to 1150°C [calculated at 5 GPa using the calibration of Ellis & Green (1979)], whereas the pyroxenitic xenoliths record exclusively high temperatures of 1100–1200°C (Kopylova *et al.*, 1999*a*, 1999*b*). Integrated textural and major-element classification [using the geochemical parameters of Coleman *et al.* (1965)] of 41 Jericho eclogite xenoliths found that eclogites with massive textures fall into Groups A and B and those with anisotropic textures into Groups B and C (Kopylova *et al.*, 1999*a*). The Jericho kimberlite also contains two distinct eclogite suites that have been intensively studied; these include high-FeO, zircon-bearing eclogites (Schmidberger *et al.*, 2005; Heaman *et al.*, 2006) and high-MgO, diamond-bearing eclogites (Heaman *et al.*, 2006; Smart *et al.*, 2009, 2012). The Jericho zircon-bearing eclogites contain exceptionally Fe-rich garnet (up to 27·5 wt % FeO) and Na-rich clinopyroxene (up to 9·33 wt % Na_2O) and classify as Group C (Heaman *et al.*, 2006). Zircons yield U–Pb ages ranging from 2·0 to 0·8 Ga, and Lu–Hf ages of 2·1 and 2·3 ± 0·1 Ga (Schmidberger *et al.*, 2005), whereas whole-rock Nd model ages determined for select zircon-bearing eclogites range from 1 to 1·3 Ga (Heaman *et al.*, 2006). From the age information, the Jericho zircon eclogites are interpreted as remnants of subducted oceanic crust associated with accretion of *c.* 1·9 Ga magmatic arcs (e.g. Hottah or Great Bear) to the western margin of the Slave craton occurring during the Wopmay orogeny (Schmidberger *et al.*, 2005), and underwent later modification by metasomatism related to the 1·27 Ga Mackenzie Igneous Event (Heaman *et al.*, 2006).

In contrast, the Jericho high-MgO diamond-bearing eclogites are exclusively Group A, containing pyrope-rich garnet (up to 21·2 wt %) and jadeite-poor, CaO-rich clinopyroxene (Heaman *et al.*, 2006; Smart *et al.*, 2009). The Jericho high-MgO diamond-bearing eclogites have unique compositions compared with diamond-bearing eclogites worldwide (Heaman *et al.*, 2006); the high concentrations of incompatible trace elements and radiogenic Sr–Pb isotope compositions of these xenoliths suggest a complex, multi-stage petrogenesis (Smart *et al.*, 2009). Garnet and clinopyroxene inclusions in diamond derived from the high-MgO eclogites have lower MgO and higher Na_2O contents than the host eclogite garnet and clinopyroxene, indicating that post-diamond formation secondary processes were critical to the petrogenesis of this eclogite suite (Smart *et al.*, 2009, 2012). Diamonds from the high-MgO eclogites have the lowest diamond $\delta^{13}C$ values reported to date (−41‰; De Stefano *et al.*, 2009). Smart *et al.* (2011) proposed that the carbon source for these highly ^{13}C-depleted diamonds was derived from ancient subducted organic matter.

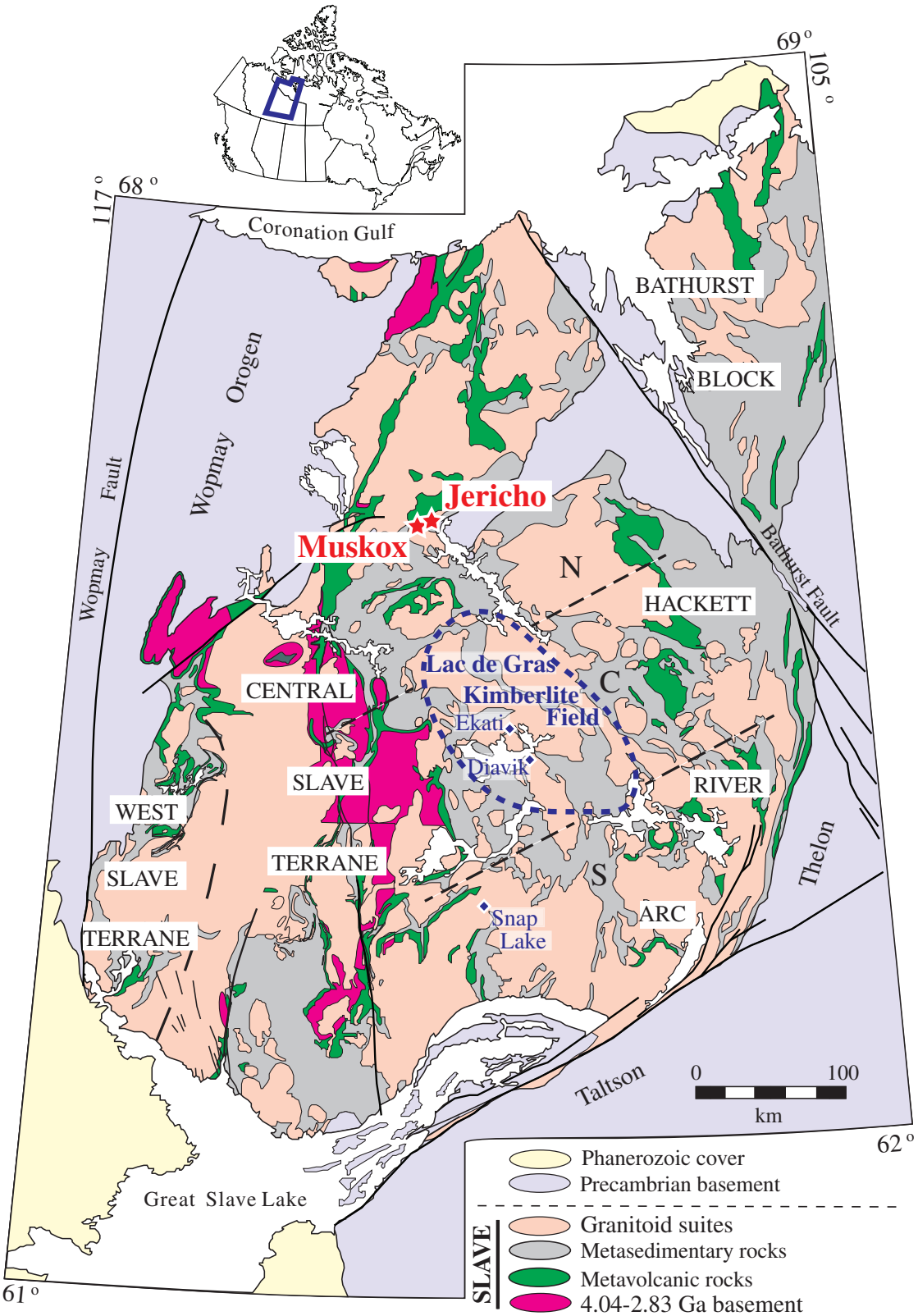

Fig. 1. Simplified geological map of the Slave craton of northwestern Canada, modified from Tappe *et al.* (2013). The Jericho and Muskox kimberlites are located in the northern Slave craton (indicated by stars), *c.* 150 km north of the Lac de Gras kimberlite field that hosts the Diavik and Ekati diamond mines. Based on xenocrystic garnet compositions, the Slave craton has been divided into Northern (N), Central (C) and Southern (S) mantle domains, which are delineated by NE–SW-trending dashed lines (from Grütter *et al.*, 1999).

In this study, we have investigated 23 eclogites and one pyroxenite (Jer 5) from the Jericho kimberlite, two additional diamond-bearing eclogites from the nearby Muskox kimberlite (~15 km SW of Jericho; Hayman & Cas, 2011), and garnet separates from a previously investigated zircon-bearing Jericho eclogite (MX8A; Schmidberger *et al.*, 2005). Some of the eclogite data were presented as a range by Smart *et al.* (2009) for comparative purposes, but the single xenolith data were not presented. Six of the xenoliths presented here were previously studied for their major-element compositions by Kopylova *et al.* (1999*a*, 2004).

Eclogite xenolith descriptions

A summary of the mineralogy and texture of all the eclogites in this study and from Smart *et al.* (2009, 2011, 2012) is given in Table 1. Garnet is orange, red–orange, red–pink and light lilac–pink. Clinopyroxene is dark to bright medium green and, in kyanite-bearing eclogites, pale green. Most of the eclogites are bimineralic, but some contain trace amounts of red–brown rutile and glassy apatite, which are often found as inclusions within garnet. Bright to light blue, oriented kyanite grains are found in six eclogites, and light blue needles of corundum are present in one eclogite. One pyroxenite (Jer 5; 85 modal % pyroxene content) contains minor (<5 modal %) orthopyroxene. Secondary fine veins with phlogopite, calcite and apatite are common. The eclogites range from very fresh with transparent clinopyroxene and garnet with clear grain boundaries, to more altered, with irregularly shaped garnet and milky or cloudy clinopyroxene in which only small 'islands' of fresh clinopyroxene remain. The eclogites have both massive, interlocking textures (generally found in bimineralic eclogites) and anisotropic, oriented textures (generally found in kyanite-bearing eclogites). Type I and II textural eclogite types, as described from South African eclogites by MacGregor & Carter (1970), are not apparent in the eclogites. Whereas major-element compositions were calculated for all eclogites (see Table 1), trace-element and isotope compositions were determined only for eclogites deemed to contain minimally altered clinopyroxene.

Smart *et al.* (2009) reported on a large ($n = 13$) suite of high-MgO diamond-bearing eclogites from Jericho; here we include the chemical composition of two additional diamond-bearing eclogites (Jde15, Jde25) which have markedly lower MgO contents and were first reported by Smart *et al.* (2011). In addition, we also present data for two diamond-bearing eclogites from the nearby Muskox kimberlite (Mox001, Mox023). The Jericho diamond-bearing eclogites reported here contain 5–10 modal % diamond, light green, milky clinopyroxene and orange garnet and show high degrees of alteration, in contrast to the very fresh high-MgO Jericho diamond-bearing eclogites from Smart *et al.* (2009). The two diamond-bearing eclogites from the Muskox kimberlite contain only trace amounts of diamond and have deep red garnet and dark green clinopyroxene.

ANALYTICAL TECHNIQUES

Major- and minor-element analysis

Garnet and clinopyroxene from all xenoliths were analyzed for major and minor elements using a JEOL 8900 electron microprobe at the University of Alberta with a 20 nA beam current and 20 kV accelerating voltage. Effort was taken to analyze touching garnet and clinopyroxene pairs in core-to-rim mineral grain transects; however, for some of the diamond-bearing eclogites (Jde15 and Jde25), mineral separates mounted in epoxy mounts were used instead. Three to five grains of garnet and clinopyroxene with 10 analyses per mineral grain were obtained for each xenolith.

Trace-element analysis

Garnet and clinopyroxene were analyzed for their trace-element compositions in both grain mounts and 'thick'-sections by laser ablation quadrupole inductively coupled plasma mass spectrometry (ICP-MS) at the University of Alberta using a New Wave Research Nd:YAG UP213 laser system coupled to a Perkin Elmer Elan 6000 Quadrupole ICP-MS system. A spot size of 160 μm and a fluence of *c.* 15 J cm^{-3} were used for all analyses. Background counting time was 20 s followed by 50 s of ablation. Each analytical session was bracketed by three to four analyses of the NIST 612 glass standard to monitor accuracy. Repeated analyses of the NIST 612 standard over four analytical sessions yielded relative standard deviations generally <5% (excluding <9% for Ni and Ti) and differences from the accepted values of <3 % for the trace elements of interest (excluding one session where the per cent differences were <6%). The ^{44}Ca content of garnet and clinopyroxene (from electron microprobe analysis) was used for calibration. All data were reduced using GLITTER data reduction software (van Achterbergh *et al.*, 2001). The uncertainty for most elements is *c.* 10% relative (2σ), but for elements present in very low abundance [e.g. U, Th, Rb; heavy rare earth elements (HREE) in clinopyroxene; light REE (LREE) in garnet] the uncertainty can be up to 40%. Between five and 40 grains of garnet and clinopyroxene were analyzed per xenolith with generally one spot per grain.

Sr and Pb isotope analysis

The Sr and Pb isotopic compositions of clinopyroxene separated from the Jericho xenoliths were determined using a NuPlasma multi-collector (MC)-ICP-MS system coupled to the New Wave laser system described above. When possible, Sr and Pb isotope analyses were determined on the same grain for which trace-element contents were previously analyzed. The Jericho and Muskox

Table 1: Jericho and Muskox eclogite petrography

Eclogite xenolith	Class. (grt)	Class. (trace)	Mineralogy						Texture	Comments
			Gt	Cpx	Dia	Ky	Rut	Other		
8-12	B		x	x			x		m	secondary phlog + cc + ap
35-2	B	peaked	x	x			x	ap	a	phlog
1-1	B	peaked	x	x			x		m	secondary phlog + cc + ap
55-7	C	depleted	x	x					m	secondary phlog + cc + ap
Jd6Fn	B	depleted	x	x			x		a	secondary phlog + cc + ap
R183	B	peaked	x	x			x		a	secondary phlog + cc + ap
53-11	C		x	x		x		ap	a	
54-5	B		x	x					m	secondary phlog + cc + ap
44-9	A		x	x					m	secondary phlog + cc + ap
10-13	C	peaked	x	x			x		a	secondary phlog + cc + ap
53-6	B		x	x			x		m	secondary phlog + cc + ap
51-10	C		x	x		x	x	ap	m	
11-17	C		x	x		x	x		a	secondary phlog + cc + ap
7-5	B		x	x					m	secondary phlog + cc + ap
Jer 1	B	depleted	x	x		x			m	
Jer 2	B	peaked	x	x		x		ap, cor	m	
Jer 3	C	depleted	x	x		x			m	
Jer 4	B	depleted	x	x					m	
Jer 5	B		x	x			x	opx	a	
Jer 6	B	depleted	x	x			x	ap	a	
Jer 7	B	peaked	x	x			x		a	
Jer 8	C	depleted	x	x				ap	m	
Jde01	A		x	x	x				m	phlog, cc, glass, sulf
Jde02	A		x	x	x				m	phlog, cc, glass, sulf
Jde03	A		x	x	x				m	phlog, cc, glass, sulf
Jde07	A		x	x	x				m	phlog, cc, glass, sulf
Jde15	B	sloped	x	x	x				m	
Jde16	A		x	x	x				m	phlog, cc, glass, sulf
Jde17	A		x	x	x				m	phlog, cc, glass, sulf
Jde18	A		x	x	x				m	phlog, cc, glass, sulf
Jde19	A		x	x	x				m	phlog, cc, glass, sulf
Jde20	A		x	x	x				m	phlog, sulf
Jde21	A		x	x	x				m	phlog, sulf
Jde22	A		x	x	x				m	phlog, cc, glass, sulf
Jde23	A		x	x	x				m	phlog, cc, glass, sulf
Jde24	A		x	x	x				m	phlog, cc, glass, sulf
Jde25	B	sloped	x	x	x				m	
Mox001	B	sloped	x	x	x				m	from Muskox kimberlite
Mox023	B	sloped	x	x	x				m	from Muskox kimberlite

Class (grt) is classification based on garnet composition from Coleman *et al*. (1965) (see Fig. 2). Class (trace) is grouping based on the calculated whole-rock trace-element pattern (see Fig. 7). Gt, garnet; cpx, clinopyroxene; dia, diamond; ky, kyanite; rut, rutile; ap, apatite; phlog, phlogopite; cc, calcite; opx, orthopyroxene; sulf, sulfide; cor, corundum. Texture follows Kopylova *et al*. (1999*a*); m, massive; a, anisotropic.

diamond-bearing eclogites (Jde15, Jde25, Mox001, Mox023) were not suitable candidates for Sr and Pb isotope analysis owing to their low Sr (<83 ppm) and Pb (<0·16 ppm) contents (NIST 614 = 2·1–2·3 ppm Pb). A beam diameter of 160 μm was used for Sr isotope analysis and data were collected using an array of five Faraday collectors, following the procedures of Schmidberger *et al.* (2003). Sr analyses of the unknowns were bracketed by analysis of a modern coral sample (accepted thermal ionization mass spectrometry $^{87}Sr/^{86}Sr$ value of 0·709098 ± 0·00019; Bizzarro *et al.*, 2003) and values obtained (0·709115 ± 0·000071, 0·709011 ± 0·000074) were within error of the accepted value. The techniques employed for collection of Pb isotope data are similar to those described by Simonetti *et al.* (2005). Pb isotope data were collected using three ion counters for increased sensitivity and two Faraday detectors were employed for Tl collection. A beam diameter of 160 μm and 320 μm × 320 μm raster patterns were used for Pb isotope data collection. Each session included measurement of an NIST 614 standard glass and measured $^{206}Pb/^{204}Pb$ values deviated by less than 0·7% from the accepted values.

Oxygen isotope analysis

The oxygen isotope composition of garnet and clinopyroxene separates was obtained by laser fluorination at the University of New Mexico, following the procedure of Sharp (1990). Inclusion- and crack-free garnet and clinopyroxene grains (1–2 mg) were loaded into a Ni block, dried in an oven and then transferred into the sample chamber to be placed under vacuum. Samples were reacted with BrF_5 and heated with a Merchantek 25 W CO_2 laser. The extracted O_2 gas sample was purified over liquid N and KCl traps before being measured on-line using a dual-inlet Finnigan MAT Delta XL mass spectrometer. Mineral standards were measured throughout the analytical session (Gee Whiz quartz $\delta^{18}O = 12{\cdot}5 \pm 0{\cdot}1$‰, Larson & Sharp, 2005; UWG-2 garnet $\delta^{18}O = 5{\cdot}74 \pm 0{\cdot}15$‰, 1σ, Valley *et al.*, 1995) and were within error of the accepted values (measured Gee Whiz quartz: $\delta^{18}O = 12{\cdot}6 \pm 0{\cdot}1$‰, 1σ, $n = 18$; UWG-2 garnet: $\delta^{18}O = 5{\cdot}7 \pm 0{\cdot}1$‰, 1σ, $n = 5$).

MINERAL CHEMISTRY

The major- and trace-element compositions of garnet and clinopyroxene from the Jericho eclogites are listed in Tables 2 and 3, respectively.

Major and minor elements

All garnets from the Jericho and Muskox eclogites studied here are Cr-poor (<0·13 wt %) pyrope–grossular–almandine solid solutions, and broadly overlap in composition with garnet from the Jericho eclogites investigated by Kopylova *et al.* (1999*a*) and De Stefano *et al.* (2009). Garnet has variable FeO (11·6–26·4 wt %), MgO (5·0–15·3 wt %) and CaO (4·0–17·7 wt %) contents with Mg-numbers ranging from 27 to 71. The Ca–Mg–Fe compositions of garnet from the present study are plotted in Fig. 2 and classify as Group 'B' and 'C' using the geochemical classification of Coleman *et al.* (1965). The new garnet compositions overlap with those from previous studies of Jericho and Slave eclogites (Fig. 2). Group C garnets on average have higher CaO contents than group B garnets (mean CaO of 13·1 vs 8·0 wt %), which are more Mg-rich (Mg number 57 vs 39). Garnet from the diamond-bearing Jericho and Muskox eclogites studied here (white diamond symbols in Fig. 2) is more pyropic than the non-diamond-bearing eclogites, falling within the Group B field (Fig. 2), and has uniform Mg-numbers (66–67) with a much smaller range in CaO contents (6·8–9·1 wt %). It should be noted that the Group B diamond-bearing eclogites reported here have much lower MgO contents compared with the Jericho high-MgO diamond-bearing eclogites (Group A in Fig. 2) from Smart *et al.* (2009).

Clinopyroxenes from the Jericho eclogites also have a wide range of compositions, and overlap with clinopyroxenes from previous Jericho eclogite studies (Fig. 3). The Jericho clinopyroxenes classify as Group B and C using the MgO vs Na_2O diagram from Taylor & Neal (1989) (Fig. 3), in agreement with the garnet classification in Fig. 2. Clinopyroxenes from Group C eclogites have on average higher Na_2O (7·3 vs 5·0 wt %; Fig. 3a) and Al_2O_3 (13·3 vs 8·9 wt %) contents than the Group B clinopyroxene, but also have lower CaO contents (12·1 vs 15·6 wt %; Fig. 3b) and Mg-numbers (75 vs 83). The diamond-bearing eclogite clinopyroxenes have more jadeite-poor and diopside-rich compositions compared with clinopyroxene from the diamond-free eclogites, and classify as Group B (Fig. 3a). Of note, the Group B diamond eclogites reported here have significantly lower MgO and CaO, but higher Na_2O contents than the clinopyroxene from the high-MgO diamond-bearing eclogites from Jericho.

Trace elements

Garnet

A subset of the 26 Jericho eclogites analyzed for major elements was selected for trace-element analysis based on degree of freshness and preservation of fresh clinopyroxene. Grain mounts were made from mineral separates for ten of the eclogites (eclogites 35-2 to JD6fn; Mox001; Mox023 in Table 3), whereas thick-sections were made of the remaining ten eclogites (Jer 1 to Jer 8; Jde15; Jde25) owing to their small size.

Garnets from the Jericho eclogites exhibit chondrite-normalized REE patterns similar to those commonly observed in eclogitic garnets worldwide (e.g. Jacob, 2004; Gonzaga *et al.*, 2010). The REE patterns for Group B, C

Table 2: Major-element composition of garnet, clinopyroxene and calculated whole-rocks of Jericho and Muskox eclogites

Eclogite:	8-12	35-2	1-1	55-7	Jd6Fn	R183	53-11	54-5	44-9	10-13	53-6	51-10	11-17
Mineral:	Grt	Grt	Grt	Grt	Grt	Grt	Grt	Grt	Grt	Grt	Grt	Grt	Grt
Mode:	50	60	40	55	50	40	40	50	50	65	50	50	60
SiO_2	39·0	38·6	39·6	38·6	39·6	40·5	39·2	40·0	41·5	38·7	39·5	39·3	38·8
TiO_2	0·04	0·07	0·12	0·12	0·07	0·11	0·12	0·09	0·49	0·11	0·09	0·16	0·11
Al_2O_3	22·7	22·8	23·3	22·7	22·7	23·2	22·4	22·8	22·6	22·0	22·6	22·3	22·0
Cr_2O_3	0·13	0·04	0·05	0·04	0·11	0·07	0·03	0·02	0·54	0·01	0·07	0·04	0·01
FeO	22·0	21·2	13·5	15·4	19·3	13·5	16·9	15·6	9·2	22·5	17·4	14·0	22·5
MnO	0·33	0·36	0·25	0·32	0·35	0·25	0·32	0·31	0·37	0·30	0·30	0·32	0·29
MgO	11·1	11·7	12·9	7·02	8·86	12·7	6·51	9·67	20·1	5·91	9·51	5·50	5·76
CaO	4·58	4·54	9·22	14·6	9·33	9·34	14·1	11·4	4·42	10·6	10·1	17·7	10·6
Na_2O	0·03	0·05	0·05	0·05	0·04	0·06	0·05	0·04	0·06	0·05	0·04	0·06	0·05
K_2O		0·01											
Total	99·9	99·4	99·1	98·9	100·4	99·7	99·7	99·8	99·2	100·1	99·7	99·3	100·2
Mg #	47	49	63	45	45	63	41	53	80	32	49	41	31
Class.	B	B	B	C	B	B	C	B	A	C	B	C	C

Eclogite:	7-5	Jer 1	Jer 2	Jer 3	Jer 4	Jer 5	Jer 6	Jer 7	Jer 8	Jde15	Jde25	Mox1	Mox23
Mineral:	Grt	Grt	Grt	Grt	Grt	Grt	Grt	Grt	Grt	Grt	Grt	Grt	Grt
Mode:	50	50	60	60	65	10	60	50	75	50	50	60	60
SiO_2	40·1	40·4	41·1	39·8	39·7	39·6	39·2	40·2	38·5	41·0	40·4	41·0	40·9
TiO_2	0·23	0·08	0·04	0·15	0·05	0·06	0·07	0·04	0·09	0·28	0·37	0·32	0·19
Al_2O_3	22·6	23·4	23·8	22·9	22·8	22·6	22·5	23·2	22·1	23·4	22·5	23·1	23·1
Cr_2O_3	0·07	0·07	0·11	0·04	0·01	0·12	0·02	0·11	0·01	0·02	0·07	0·07	0·08
FeO	16·7	11·6	11·9	14·4	18·6	22·4	23·6	17·4	26·5	13·7	13·7	12·4	12·9
MnO	0·40	0·23	0·22	0·27	0·29	0·50	0·42	0·29	0·39	0·25	0·22	0·27	0·28
MgO	12·0	11·0	15·3	7·55	10·1	11·6	9·24	12·9	4·97	14·7	13·4	14·4	14·6
CaO	7·56	13·8	8·12	15·59	8·43	3·99	5·75	6·23	8·60	6·8	8·26	9·06	7·84
Na_2O	0·10	0·04	0·04	0·07	0·04	0·03	0·06	0·04	0·06	0·11	0·14	0·13	0·11
K_2O													
Total	99·8	100·6	100·7	100·7	99·9	100·9	100·9	100·5	101·3	100·2	99·0	100·8	99·8
Mg #	56	63	71	52	49	48	44	59	27	66	64	67	67
Class.	B	B	B	C	B	B	B	B	C	B	B	B	B

Eclogite:	8-12	35-2	1-1	55-7	Jd6Fn	R183	53-11	54-5	44-9	10-13	53-6	51-10	11-17
Mineral:	Cpx	Cpx	Cpx	Cpx	Cpx	Cpx	Cpx	Cpx	Cpx	Cpx	Cpx	Cpx	Cpx
Mode:	50	40	60	45	50	60	60	50	50	35	50	50	40
SiO_2	55·8	55·6	55·9	56·0	56·1	55·9	56·3	56·1	54·5	55·9	56·0	56·0	56·2
TiO_2	0·12	0·11	0·15	0·12	0·12	0·15	0·14	0·12	0·23	0·14	0·12	0·15	0·14
Al_2O_3	7·54	7·50	9·40	13·4	10·8	9·00	14·6	11·7	1·92	12·9	12·2	14·3	13·0
Cr_2O_3	0·16	0·08	0·06	0·04	0·09	0·06	0·04	0·02	0·71	0·01	0·07	0·01	0·01
FeO	5·53	5·47	2·36	2·58	3·71	2·33	2·81	2·55	3·30	5·12	2·71	2·44	5·06
MnO	0·04	0·04	0·03	0·02	0·02	0·03	0·02	0·03	0·10	0·03	0·02	0·03	0·02
MgO	10·9	11·0	11·5	8·13	9·28	11·7	7·20	9·46	17·2	6·88	8·67	7·70	6·66
CaO	15·7	15·9	16·7	13·1	14·4	16·5	12·0	14·6	19·9	11·4	13·7	12·8	11·2
Na_2O	4·66	4·58	4·34	6·88	5·92	4·82	7·50	6·09	1·63	7·33	6·30	7·14	7·9
K_2O		0·01	0·03		0·01	0·03	0·01		0·04		0·01		
Total	100·4	100·3	100·6	100·2	100·5	100·5	100·6	100·6	99·6	99·8	99·9	100·5	100·1
Mg #	78	78	90	85	82	90	82	87	90	71	85	85	70

(continued)

Table 2: Continued

Eclogite:	7-5	Jer 1	Jer 2	Jer 3	Jer 4	Jer 5	Jer 6	Jer 7	Jer 8	Jde15	Jde25	Mox1	Mox23
Mineral:	Cpx	Cpx	Cpx	Cpx	Cpx	Cpx	Cpx	Cpx	Cpx	Cpx	Cpx	Cpx	Cpx
Mode:	50	50	40	40	35	90	40	50	25	50	50	40	40
SiO_2	55·5	55·0	55·5	55·1	55·0	54·2	54·5	54·9	55·1	55·0	55·7	54·8	55·1
TiO_2	0·31	0·11	0·11	0·22	0·12	0·08	0·11	0·10	0·17	0·34	0·39	0·14	0·13
Al_2O_3	8·49	10·7	11·4	14·0	9·87	3·89	6·53	7·67	11·2	8·7	10·7	6·39	7·45
Cr_2O_3	0·08	0·08	0·15	0·04	0·02	0·09	0·02	0·14	0·01	0·09	0·08	0·06	0·06
FeO	4·24	1·83	1·67	2·28	3·59	6·44	6·22	3·54	7·54	3·46	3·23	3·82	3·55
MnO	0·05	0·02	0·02	0·02	0·03	0·08	0·05	0·03	0·03	0·04	0·03	0·05	0·05
MgO	10·7	10·3	9·86	7·76	9·61	12·9	10·9	11·5	6·36	11·6	9·63	12·7	12·2
CaO	15·0	16·2	14·6	13·5	14·8	18·1	16·3	16·6	11·0	14·6	13·3	17·0	16·3
Na_2O	5·70	4·96	5·96	6·51	5·58	3·00	4·49	4·57	7·90	4·88	6·44	3·95	4·02
K_2O	0·01		0·004	0·01	0·01		0·01			0·10	0·05	0·07	
Total	100·0	99·2	99·2	99·4	98·5	98·8	99·1	99·0	99·4	98·7	99·5	99·0	99·1
Mg #	82	88	85	78	83	78	73	81	55	86	84	86	86

Eclogite:	8-12 WR	35-2 WR	1-1 WR	55-7 WR	Jd6Fn WR	R183 WR	53-11 WR	54-5 WR	44-9 WR	10-13 WR	53-6 WR	51-10 WR	11-17 WR
SiO_2	47·4	45·4	49·4	46·4	50·3	49·7	49·5	48·0	48·0	44·7	47·8	47·6	47·5
TiO_2	0·08	0·09	0·14	0·12	0·10	0·13	0·1	0·10	0·36	0·12	0·10	0·16	0·12
Al_2O_3	15·1	16·7	15·0	18·5	15·0	14·7	17·7	17·2	12·3	18·8	17·4	18·3	17·5
Cr_2O_3	0·14	0·06	0·06	0·04	0·10	0·07	0·0	0·02	0·63	0·01	0·07	0·03	0·01
FeO	13·8	14·9	6·82	9·65	9·16	6·80	8·4	9·05	6·25	16·4	10·1	8·20	13·8
MnO	0·19	0·23	0·12	0·18	0·14	0·11	0·1	0·17	0·24	0·21	0·16	0·17	0·15
MgO	11·0	11·4	12·1	7·52	9·13	12·1	6·9	9·57	18·6	6·25	9·09	6·60	6·21
CaO	10·1	9·09	13·7	13·9	12·6	13·7	12·8	13·0	12·2	10·9	11·9	15·3	10·9
Na_2O	2·35	1·86	2·63	3·12	3·86	2·91	4·5	3·06	0·85	2·60	3·17	3·60	3·99
K_2O	0·003	0·01	0·02	0·002	0·005	0·02	0·0	0·004	0·02	0·004	0·005	0·004	0·004
Total	100·2	99·7	100·0	99·5	100·4	100·2	100·3	100·2	99·4	100·0	99·8	99·9	100·2
Mg #	63	61	79	63	63	79	65·5	70	85	46	67	63	45
T_{KR}(°C)	903	932	862	920	894	843	940	883	1121	994	863	931	1000

Eclogite:	7-5 WR	Jer 1 WR	Jer 2 WR	Jer 3 WR	Jer 4 WR	Jer 5 WR	Jer 6 WR	Jer 7 WR	Jer 8 WR	Jde15 WR	Jde25 WR	Mox1 WR	Mox23 WR
SiO_2	47·8	47·7	46·8	45·9	45·0	52·8	45·3	47·6	42·7	48·0	48·1	46·5	46·6
TiO_2	0·27	0·10	0·06	0·18	0·08	0·08	0·09	0·07	0·11	0·31	0·38	0·25	0·17
Al_2O_3	15·6	17·1	18·9	19·3	18·2	5·76	16·1	15·4	19·4	16·1	16·6	16·4	16·8
Cr_2O_3	0·08	0·07	0·12	0·04	0·01	0·09	0·02	0·12	0·01	0·06	0·08	0·06	0·07
FeO	10·5	6·70	7·83	9·53	13·3	8·04	16·7	10·5	21·8	8·58	8·46	8·95	9·13
MnO	0·22	0·13	0·14	0·17	0·20	0·12	0·27	0·16	0·30	0·15	0·125	0·18	0·19
MgO	11·3	10·6	13·1	7·63	9·93	12·8	9·89	12·2	5·32	13·1	11·5	13·7	13·6
CaO	11·3	15·0	10·7	14·8	10·6	16·7	9·97	11·4	9·21	10·70	10·78	12·3	11·2
Na_2O	2·90	2·50	2·41	2·64	1·98	2·71	1·83	2·31	2·02	2·50	3·29	1·66	1·67
K_2O	0·01	0·002	0·004	0·004	0·004	0·003	0·002	0·002	0·002	0·05	0·03	0·03	0·001
Total	99·9	99·9	100·1	100·2	99·4	99·0	100·2	99·8	100·8	99·5	99·29	100·0	99·5
Mg #	69	75	77	62	61	74	55	70	34	76	74	75	75
T_{KR}(°C)	1053	1085	1408	1414	903	885	1207	1164	1252	1065	1113	1217	1124

Oxides are given as wt % and modes in vol. %. Blanks indicate that the element of interest was below detection limit (generally 0·01 wt % for most oxides). Mg # = Mg/(Mg + Fe) calculated from cations. Class. is eclogite classification based on the geochemical parameters of Coleman *et al.* (1965). T_{KR}(°C) is temperature calculated iteratively at 5 GPa using Krogh Ravna (2000).

Table 3: Trace-element composition of garnet and clinopyroxene from Jericho and Muskox eclogites

Eclogite:	35-2		1-1		R183		10-13		53-11		55-7		44-9		Jd6fn		Jer 1		Jer 2	
Mineral:	Grt	1σ	Grt	1σ	Grt	1σ	Grt	1σ	Grt	1σ	Grt	1σ	Grt	1σ	Grt	1σ	Grt	1σ	Grt	1σ
Li	0·36	0·09	0·43	0·12	0·56	0·12	0·41	0·1	0·36	0·09	0·23	0·08	0·13	0·06	0·24	0·07	0·64	0·3	0·46	0·17
V	590	4	794	3	851	4	664	5	1070	1	771	2	3360	8	378	2	497	6	216	2
Ni	10·3	1	23·2	2	24·8	3	2·17	0·3	7·69	0·7	7·91	0·7	27·9	2	9·46	0·8	19·5	5	19·0	5
Sc	39·7	2	51·3	2	49·9	2	61·2	2	35·7	1	56·4	2	102	4	53·5	2·0	64·5	4	39·0	3
Rb	0·03	0·01	b.d.	–	0·11	0·02	0·02	0·01	0·14	0·02	0·05	0·02	0·00	0·02	0·04	0·02	0·30	0·05	0·05	0·02
Ba	0·30	0·02	0·15	0·01	0·28	0·01	0·06	0·01	0·13	0·02	0·12	0·02	0·06	0·01	0·61	0·03	0·26	0·05	0·06	0·02
Th	b.d.	–	0·18	0·10	b.d	–	b.d	–	0·28	0·10	b.d.	–	b.d.	–	b.d.	–	b.d	–	0·19	0·08
U	b.d.	–	b.d.	–	0·01	0·003	0·4	0·02	0·02	0·01	b.d.	–	b.d.	–	0·04	0·01	0·03	0·01	0·02	0·01
Nb	0·03	0·1	0·09	0·03	0·06	0·02	0·02	0·02	0·16	0·03	0·08	0·02	0·2	0·04	b.d.	–	0·05	0·03	b.d.	–
Ta	0·12	0·02	0·03	0·02	0·02	0·01	b.d.	–	0·03	0·02	0·04	0·02	0·04	0·02	0·03	0·01	b.d.	–	0·05	0·02
La	0·12	0·01	0·04	0·02	0·06	0·01	0·02	0·01	0·03	0·02	0·07	0·02	0·04	0·02	0·04	0·01	0·04	0·03	0·04	0·03
Ce	0·18	0·02	0·15	0·03	0·19	0·02	0·10	0·02	0·29	0·03	0·15	0·03	0·12	0·02	0·15	0·03	0·31	0·06	0·13	0·04
Pr	0·08	0·01	0·08	0·02	0·07	0·01	0·07	0·02	0·19	0·02	0·10	0·02	0·05	0·01	0·09	0·02	0·13	0·03	0·09	0·03
Pb	0·05	0·02	0·13	0·03	0·04	0·02	0·04	0·03	b.d.	–	0·09	0·03	0·00	0·03	0·07	0·03	0·34	0·05	0·08	0·04
Sr	0·59	0·05	0·52	0·06	0·62	0·06	0·74	0·06	2·65	0·1	1·54	0·1	0·17	0·03	0·44	0·04	0·84	0·08	0·35	0·05
Nd	1·17	0·1	0·88	0·1	0·84	0·1	0·93	0·1	2·98	0·2	1·84	0·2	0·57	0·1	1·64	0·2	2·15	0·4	1·35	0·3
Sm	1·84	0·3	1·23	0·3	1·16	0·2	0·94	0·2	2·13	0·3	2·35	0·3	0·60	0·2	2·58	0·3	1·54	0·4	1·56	0·5
Zr	4·50	0·3	9·04	0·6	9·05	0·5	3·42	0·2	24·4	0·9	14·1	0·6	34·4	1·3	3·94	0·3	11·5	0·7	5·38	0·4
Hf	0·11	0·05	0·15	0·06	0·15	0·05	0·09	0·04	0·19	0·06	0·19	0·06	1·17	0·1	0·13	0·05	0·19	0·09	0·18	0·09
Eu	1·52	0·1	0·77	0·08	0·76	0·06	0·97	0·08	1·83	0·1	1·55	0·1	0·28	0·04	1·66	0·1	0·87	0·1	1·35	0·2
Ti	590	52	794	97	851	67	664	38	1070	61	771	44	3360	189	378	22	497	150	216	65
Gd	4·12	0·4	2·45	0·3	2·48	0·3	2·29	0·3	3·25	0·3	4·93	0·4	1·56	0·2	6·31	0·5	2·31	0·4	3·50	0·6
Tb	0·78	0·06	0·47	0·05	0·44	0·04	0·35	0·04	0·56	0·05	0·94	0·06	0·40	0·04	1·24	0·08	0·36	0·07	0·52	0·09
Dy	5·59	0·4	2·99	0·3	2·96	0·2	2·09	0·2	4·33	0·3	5·99	0·3	3·48	0·2	9·35	0·5	2·72	0·5	2·97	0·5
Y	30·3	1·3	15·6	0·8	15·1	0·7	9·69	0·4	20·7	0·7	26·2	0·9	15·7	0·6	40·5	1·4	13·0	0·6	11·2	0·6
Ho	1·18	0·08	0·62	0·06	0·61	0·05	0·38	0·04	0·98	0·07	1·22	0·08	0·76	0·06	1·93	0·1	0·52	0·09	0·52	0·09
Er	3·39	0·3	1·62	0·2	1·58	0·1	0·89	0·1	2·71	0·2	3·04	0·2	2·11	0·2	5·41	0·3	1·63	0·3	1·16	0·2
Tm	0·51	0·05	0·24	0·04	0·23	0·03	0·09	0·02	0·40	0·04	0·42	0·04	0·30	0·03	0·82	0·06	0·27	0·05	0·14	0·04
Yb	3·77	0·3	1·59	0·2	1·51	0·2	0·64	0·1	2·78	0·2	2·92	0·2	1·81	0·2	5·27	0·3	1·73	0·3	0·89	0·2
Lu	0·64	0·05	0·23	0·04	0·22	0·03	0·10	0·02	0·40	0·04	0·47	0·05	0·26	0·03	0·81	0·06	0·27	0·05	0·15	0·04
Eu/Eu*	1·6		1·3		1·3		1·9		2·1		1·4		0·8		1·2		1·4		1·7	
Lu_N	26·1		9·3		9·0		4·1		16·3		19·1		10·6		32·9		11·0		6·1	
Lu_N/Gd_N	1·26		0·76		0·72		0·36		1·00		0·77		1·35		1·04		0·94		0·34	
No. grains	28		20		29		6		9		6		7		6		5		5	

Eclogite:	Jer 3		Jer 4		Jer 5		Jer 6		Jer 7		Jer 8		Jde15		Jde25		Mox001		Mox023
Mineral:	Grt	1σ	Grt	1σ	Grt	1σ	Grt	1σ	Grt	1σ	Grt	1σ	Grt	1σ	Grt	1σ	Grt	1σ	Grt
Li	0·42	0·2	0·43	0·2	0·49	0·15	0·5	0·17	0·41	0·15	0·32	0·14	0·85	0·15	0·3	0·01	0·39	0·2	0·89	0·4
V	919	8	326	3	430	7	422	4	212	3	385	5	74·9	5	80·3	0·5	156	14	126	11
Ni	12·7	3	12·2	3	8·39	0·7	6·51	0·7	16·7	1	2·72	0·5	21·8	2	n.d.	–	66·5	15	65·6	15
Sc	51·7	3	35·0	2	96·7	4	58·6	2	52·6	2	33·0	2	46·4	2	37	0·2	64·7	4	69·2	4
Rb	0·67	8	0·07	0·03	0·12	0·03	0·35	0·1	0·18	0·1	0·07	0·04	0·15	0·04	b.d.	–	0·15	0·08	0·94	0·1
Ba	0·07	0·02	0·09	0·03	0·04	0·02	0·18	0·03	0·08	0·02	0·03	0·02	0·81	0·03	0·04	0·02	0·36	0·06	1·53	0·1
Th	b.d.	–	b.d	–	0·15	0·05	0·24	0·11	0·26	0·14	b.d.	–	0·03	0·01	b.d.	–	0·26	0·11	b.d	–
U	0·07	0·01	b.d.	–	b.d.	–	0·05	0·01	0·03	0·01	b.d.	–	0·04	0·01	b.d.	–	0·25	0·08	0·09	0·02
Nb	b.d.	–	0·10	0·03	b.d.	–	0·03	0·02	b.d.	–	b.d.	–	0·18	0·05	0·2	0·03	0·42	0·07	0·28	0·06
Ta	0·05	0·03	0·12	0·03	b.d.	–	0·03	0·02	b.d.	–	b.d.	–	b.d.	–	0·1	0·03	0·06	0·03	0·03	0·03
La	0·05	0·03	0·06	0·02	0·04	0·01	0·04	0·02	0·04	0·02	b.d.	–	0·19	0·02	b.d.	–	0·17	0·04	0·11	0·04
Ce	0·67	0·1	0·11	0·03	0·07	0·02	0·11	0·02	0·07	0·02	0·22	0·03	0·12	0·03	0·09	0·03	0·73	0·1	0·2	0·04
Pr	0·35	0·05	0·06	0·02	0·05	0·01	0·04	0·01	0·06	0·02	0·09	0·02	0·05	0·02	0·05	0·02	0·13	0·03	0·05	0·02

(continued)

Table 3: Continued

Eclogite:	Jer 3		Jer 4		Jer 5		Jer 6		Jer 7		Jer 8		Jde15		Jde25		Mox001		Mox023	
Mineral:	Grt	1σ	Grt	1σ	Grt	1σ	Grt	1σ	Grt	1σ	Grt	1σ	Grt	1σ	Grt	1σ	Grt	1σ	Grt	
Pb	0·09	0·03	0·09	0·04	0·07	0·04	0·13	0·05	0·17	0·04	0·17	0·05	0·06	0·03	b.d.	–	0·18	0·05	0·14	0·04
Sr	2·06	0·1	0·56	0·06	0·22	0·03	0·43	0·05	0·31	0·04	0·62	0·06	0·51	0·1	0·52	0·05	1·04	0·08	0·58	0·06
Nd	4·58	0·6	0·88	0·2	0·78	0·1	0·53	0·1	0·90	0·10	1·53	0·2	0·38	0·2	0·45	0·1	1·01	0·2	0·38	0·1
Sm	3·66	0·6	1·75	0·4	1·24	0·3	1·02	0·3	1·12	0·30	2·54	0·4	0·43	0·2	0·93	0·1	0·61	0·2	n.d.	–
Zr	19·4	1	6·24	0·4	8·26	0·5	4·21	0·3	4·07	0·30	7·88	0·6	7·86	0·5	18·9	0·4	13·6	0·7	3·4	0·3
Hf	0·27	0·09	0·19	0·08	0·20	0·06	0·17	0·07	0·07	0·05	0·20	0·06	0·21	0·07	0·62	0·1	0·35	0·1	0·2	0·08
Eu	1·78	0·3	1·15	0·2	0·72	0·07	0·82	0·08	0·82	0·07	2·16	0·1	0·20	0·04	0·7	0·08	0·22	0·06	0·12	0·04
Ti	919	276	326	98	430	47	423	52	212	32	385	65	2026	117	1765	7	1940	582	1245	374
Gd	5·17	0·8	4·92	0·7	3·72	0·3	3·32	0·4	2·44	0·3	8·61	0·7	0·99	0·2	2·44	0·2	0·79	0·2	0·52	0·2
Tb	0·90	0·1	1·04	0·2	0·96	0·07	0·97	0·07	0·39	0·04	1·86	0·1	0·23	0·03	0·49	0·06	0·20	0·05	0·12	0·04
Dy	5·99	0·9	7·49	1	8·45	0·5	8·72	0·5	2·69	0·2	13·6	0·8	1·86	0·2	3	0·2	1·57	0·3	1·42	0·3
Y	26·1	1	33·9	2	49·4	1·9	54·9	2	13·9	0·7	74·6	4	9·84	0·6	13·2	0·2	10·6	0·5	9·88	0·5
Ho	1·19	0·2	1·58	0·2	1·96	0·1	2·31	0·1	0·59	0·06	3·07	0·2	0·38	0·04	0·39	0·05	0·43	0·08	0·43	0·08
Er	3·26	0·4	3·96	0·5	6·50	0·4	7·32	0·5	1·70	0·2	7·80	0·6	1·03	0·1	1·07	0·1	1·47	0·2	1·3	0·2
Tm	0·51	0·08	0·57	0·08	0·96	0·07	1·20	0·09	0·28	0·04	0·97	0·08	0·14	0·03	0·13	0·02	0·20	0·04	0·24	0·05
Yb	3·59	0·5	3·55	0·5	7·50	0·3	8·69	0·5	1·87	0·2	5·76	0·4	0·98	0·1	0·87	0·1	1·53	0·3	1·93	0·3
Lu	0·51	0·08	0·48	0·08	1·20	0·08	1·51	0·1	0·26	0·04	0·84	0·07	0·13	0·02	0·12	0·02	0·25	0·05	0·3	0·06
Eu/Eu*	1·2		1·1		0·9		1·2		1·5		1·3		0·9		1·3		1·0		–	
Lu_N	20·8		19·5		48·8		61·6		10·5		34·1		5·1		4·9		10·0		12·2	
Lu_N/Gd_N	0·80		0·79		2·61		3·69		0·85		0·79		1·03		0·40		2·51		4·67	
No. grains	5		5		5		5		5		5		7		5		5		5	

Eclogite:	35-2		1-1		R183		10-13		55-7		44-9		Jd6fn		Jer 1		Jer 2		Jer 3	
Mineral:	Cpx	1σ	Cpx	1σ	Cpx	1σ	Cpx	1σ	Cpx	1σ	Cpx	1σ	Cpx	1σ	Cpx	1σ	Cpx	1σ	Cpx	1σ
Li	4·68	0·43	5·18	0·7	5·58	0·42	2·89	0·6	5·57	0·39	0·25	0·06	5·66	0·4	10·9	3·7	11·1	3·8	9·61	3·3
V	360	14	182	9	191	9	156	17	127	5	258	9	248	9	180	16	135	12	191	17
Ni	209	11	264	18	280	21	136	2	146	7	193	9	203	9	282	65	267	62	167	38
Sc	20·4	0·8	12·8	0·6	12·4	0·6	31·1	0·8	17·5	1	24·9	1	17·8	0·7	17·6	1	8·04	0·6	14·7	1
Rb	0·45	0·01	0·03	0·01	0·08	0·02	0·12	0·01	0·25	0·07	0·12	0·03	0·02	0·01	0·04	0·02	b.d.	–	0·21	0·03
Ba	1·32	0·1	0·12	0·02	0·13	0·02	0·39	0·01	0·04	0·01	0·39	0·03	0·03	0·01	0·09	0·02	0·07	0·02	0·07	0·03
Th	0·18	0·1	b.d.	–	0·26	0·1	b.d.	–	b.d.	–	0·03	0·01	0·01	0	0·19	0·08	0·13	0·06	b.d.	–
U	0·02	0·00	0·01	0·01	0·01	0·003	0·01	0·01	b.d.	–	b.d.	–	0·02	0·01	b.d.	–	0·03	0·01	0·02	0·01
Nb	b.d.	–	b.d.	–	b.d.	–	b.d.	–	b.d.	–	b.d.	–	0·02	0·01	b.d.	–	b.d.	–	b.d.	–
Ta	0·03	0·01	0·03	0·01	0·02	0·01	0·04	0·01	b.d.	–	0·04	0·02	b.d.	–	b.d.	–	b.d.	–	b.d.	–
La	4·17	0·2	1·07	0·07	1·00	0·06	1·08	0·04	0·04	0·02	3·04	0·1	0·54	0·05	0·24	0·05	1·07	0·2	0·56	0·1
Ce	14·1	0·5	3·63	0·2	3·49	0·2	3·62	0·07	0·14	0·02	9·39	0·3	2·37	0·1	1·32	0·2	4·57	0·6	2·85	0·4
Pr	2·83	0·1	0·64	0·04	0·60	0·03	0·71	0·03	0·04	0·01	1·58	0·07	0·59	0·04	0·39	0·06	0·95	0·1	0·67	0·09
Pb	1·10	0·1	0·39	0·05	0·37	0·04	0·35	0·04	0·22	0·04	0·27	0·04	0·30	0·04	0·31	0·06	0·32	0·05	0·66	0·09
Sr	678	23	209	8	201	7	182	5	169	5	131	4	211	7	201	8	231	10	240	10
Nd	16·4	0·6	3·14	0·2	3·03	0·2	4·25	0·1	0·33	0·07	7·93	0·4	3·88	0·3	2·58	0·4	6·07	0·8	3·86	0·6
Sm	4·29	0·3	0·90	0·2	0·84	0·2	1·71	0·1	0·26	0·1	1·67	0·2	1·16	0·2	0·69	0·3	1·17	0·3	0·79	0·3
Zr	12·3	0·5	11·0	0·6	10·5	0·5	9·41	0·2	6·24	0·3	8·35	0·4	7·10	0·3	6·94	0·4	6·02	0·4	24·9	1
Hf	1·00	0·1	0·62	0·09	0·57	0·07	0·44	0·04	0·41	0·07	0·77	0·1	0·59	0·08	0·37	0·1	0·31	0·08	1·00	0·2
Eu	1·68	0·1	0·31	0·04	0·31	0·03	0·89	0·03	0·08	0·02	0·48	0·04	0·41	0·04	0·20	0·05	0·54	0·09	0·18	0·05
Ti	856	60	1030	108	1013	64	856	56	836	48	1411	80	826	47	610	183	595	179	1221	367
Gd	2·54	0·2	0·62	0·1	0·55	0·1	2·13	0·07	0·24	0·07	1·41	0·2	0·95	0·1	0·47	0·2	0·96	0·2	0·48	0·2
Tb	0·21	0·02	0·06	0·02	0·05	0·01	0·33	0·01	0·03	0·01	0·15	0·02	0·10	0·02	0·05	0·02	0·06	0·02	0·05	0·02

(continued)

Table 3: Continued

Eclogite:	35-2		1-1		R183		10-13		55-7		44-9		Jd6fn		Jer 1		Jer 2		Jer 3	
Mineral:	Cpx	1σ	Cpx	1σ	Cpx	1σ	Cpx	1σ	Cpx	1σ	Cpx	1σ	Cpx	1σ	Cpx	1σ	Cpx	1σ	Cpx	1σ
Dy	0·75	0·07	0·22	0·07	0·19	0·05	2·12	0·04	0·15	0·05	0·68	0·09	0·29	0·06	0·22	0·07	0·20	0·07	0·25	0·08
Y	2·02	0·1	0·56	0·06	0·52	0·05	10·7	0·03	0·26	0·04	1·99	0·1	0·81	0·06	0·27	0·04	0·34	0·05	0·32	0·05
Ho	0·09	0·01	0·03	0·01	0·03	0·01	0·43	0·01	0·02	0·01	0·10	0·02	0·04	0·01	0·03	0·02	b.d.	–	b.d.	–
Er	0·15	0·03	0·08	0·03	0·07	0·02	1·15	0·02	b.d.	–	0·20	0·04	0·07	0·03	0·05	0·04	0·05	0·03	0·13	0·06
Tm	0·02	0·01	0·02	·01	b.d.	–	0·17	0·01	0·02	0·01	0·02	0·01	0·01	0·01	b.d.	–	b.d.	–	0·01	0·01
Yb	0·10	0·03	0·07	0·04	0·05	0·03	1·18	0·03	0·05	0·03	0·10	0·04	0·06	0·03	0·02	0·95	b.d.	–	b.d.	–
Lu	0·02	0·01	0·02	0·01	b.d.	–	0·19	0·01	b.d.	–	0·02	0·01	b.d.	–	b.d.	–	b.d.	–	b.d.	–
Eu/Eu*	1·4		1·2		1·3		1·4		1·0		0·9		1·2		1·0		1·5		0·8	
La_N	17·6		4·5		4·2		4·5		0·2		12·8		2·3		1·0		4·5		2·3	
La_N/Sm_N	0·61		0·74		0·75		0·39		0·09		1·14		0·29		0·22		0·57		0·44	
No. grains	40		24		27		6		8		7		7		5		5		5	

Eclogite:	Jer 4		Jer 5		Jer 6		Jer 7		Jer 8		Jde15		Jde25		Mox1		Mox23	
Mineral:	Cpx	1σ	Cpx	1σ	Cpx	1σ	Cpx	1σ	Cpx	1σ	Cpx	1σ	Cpx	1σ	Cpx	1σ	Cpx	1σ
Li	11	3·7	5·73	0·6	6·92	0·74	7·32	0·9	8·75	1·2	6·12	0·15	2·72	0·03	1·6	0·6	5·48	1·9
V	182	16	378	20	267	15	207	14	236	18	221	15	187	0·6	224	20	220	20
Ni	231	53	201	10	144	7	298	17	79·9	5	139	12	n.d.	–	333	76	357	82
Sc	10·6	0·7	52·8	2	32·3	1	17·6	0·9	15·8	0·8	11·3	0·5	7·7	0·04	12·5	0·8	13·2	0·9
Rb	0·03	0·02	0·02	0·01	0·05	0·02	b.d.	–	0·05	0·01	0·12	0·04	b.d.	–	0·05	0·02	0·07	0·02
Ba	0·05	0·02	0·17	0·02	0·16	0·02	0·08	0·02	0·08	0·02	0·09	0·02	0·14	0·03	0·31	0·05	0·25	0·04
Th	0·31	0·12	0·09	0·04	0·28	0·14	0·17	0·10	0·15	0·09	0·01	0·01	b.d.	–	0·3	0·12	0·16	0·07
U	b.d.	–	0·02	0·01	0·02	0·01	0·03	0·01	0·02	0·01	0·01	0·01	b.d.	–	0·04	0·01	b.d.	–
Nb	b.d.	–	0·02	0·01	0·04	0·01	0·03	0·02	b.d.	–	0·13	0·04	0·24	0·02	0·23	0·04	0·08	0·03
Ta	0·03	0·02	b.d.	–	0·03	0·01	0·06	0·01	b.d.	–	b.d.	–	0·03	0·02	0·03	0·02	0·02	0·02
La	0·38	0·07	3·51	0·2	1·00	0·07	1·58	0·1	0·64	0·06	0·35	0·03	0·17	0·03	1·04	0·2	0·42	0·07
Ce	2·19	0·3	15·3	0·6	4·42	0·2	6·25	0·3	2·56	0·2	1·27	0·09	0·87	0·07	3·2	0·4	1·28	0·2
Pr	0·53	0·07	3·23	0·1	1·01	0·06	1·44	0·08	0·54	0·04	0·23	0·02	0·17	0·03	0·54	0·07	0·19	0·04
Pb	0·51	0·07	2·11	0·2	1·18	0·1	0·63	0·08	0·27	0·05	0·11	0·03	n.d.	–	0·16	0·04	0·11	0·04
Sr	310	13	732	25	537	19	400	16	205	9	79·5	4	56·1	0·4	82·8	4	66·5	3
Nd	3·96	0·5	17·2	0·7	6·44	0·4	9·22	0·5	3·41	0·3	1·12	0·1	0·96	0·1	2·4	0·4	0·97	0·2
Sm	1·26	0·3	4·14	0·3	2·00	0·2	2·13	0·3	0·84	0·2	0·30	0·1	0·25	0·05	0·44	0·2	n.d.	–
Zr	8·16	0·5	9·46	0·5	12·5	0·7	7·58	0·6	15·4	1	6·97	0·4	7·32	0·2	4·45	0·3	1·1	0·1
Hf	0·61	0·1	0·79	0·1	0·88	0·1	0·50	0·09	1·1	0·1	0·53	0·06	0·46	0·1	0·17	0·06	0·12	0·05
Eu	0·44	0·08	1·37	0·08	0·84	0·06	0·66	0·06	0·40	0·05	0·12	0·01	0·13	0·02	0·11	0·03	0·07	0·03
Ti	643	193	451	51	643	83	402	65	586	104	2424	140	2204	5	762	230	728	220
Gd	0·91	0·2	3·43	0·3	1·70	0·2	1·05	0·2	0·90	0·2	0·35	0·09	0·26	0·04	0·37	0·1	0·27	0·1
Tb	0·10	0·03	0·41	0·03	0·19	0·02	0·09	0·02	0·09	0·02	0·05	0·01	0·03	0·01	0·04	0·01	0·03	0·02
Dy	0·32	0·1	1·79	0·2	1·09	0·1	0·25	0·07	0·36	0·08	0·19	0·05	0·19	0·03	0·16	0·07	0·26	0·08
Y	0·74	0·07	4·97	0·2	3·08	0·2	0·57	0·06	1·21	0·1	0·68	0·06	0·44	0·03	0·54	0·06	0·64	0·07
Ho	0·05	0·02	0·20	0·03	0·12	0·02	0·02	0·01	0·05	0·02	0·04	0·01	0·02	0·01	0·04	0·02	0·03	0·02
Er	0·10	0·04	0·46	0·07	0·28	0·05	0·07	0·03	0·06	0·03	0·07	0·03	0·04	0·01	0·1	0·04	0·081	0·04
Tm	b.d.	–	0·04	0·01	0·05	0·01	b.d.	–	b.d.	–	0·02	0·01	b.d.	–	b.d.	–	0·03	0·01
Yb	b.d.	–	0·22	0·06	0·10	0·04	0·06	0·01	0·05	0·04	b.d.	–	b.d.	–	0·10	0·05	0·037	0·06
Lu	0·03	0·01	0·03	0·01	0·02	0·01	b.d.	–	0·02	0·01	b.d.	–	b.d.	–	0·016	0·01	0·014	0·01
Eu/Eu*	1·2		1·1		1·3		1·2		1·4		1·1		–		0·8		–	
La_N	1·6		14·8		4·2		6·7		2·7		1·5		5·2		4·4		1·8	
La_N/Sm_N	0·19		0·53		0·31		0·46		0·48		0·74		0·89		1·48		–	
No. grains	5		5		5		5		5		5		5		5		5	

Trace-element contents in ppm. $Eu^* = 2Eu_N/(Gd_N + Sm_N)$. Subscript N indicates normalization to chondrite from McDonough & Sun (1995). b.d., below detection limit; n.d., not detected.

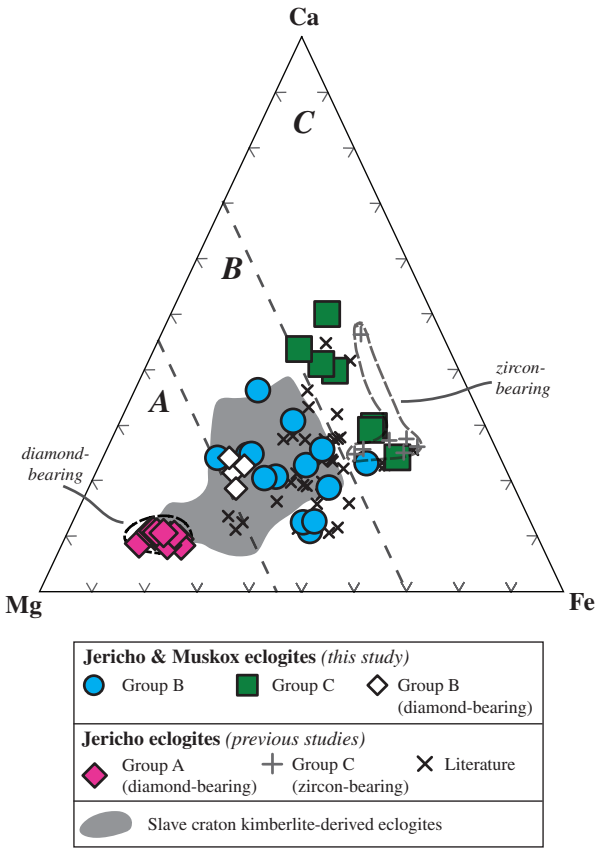

Fig. 2. Ternary diagram showing the Ca–Mg–Fe compositions of garnet from Jericho and Muskox eclogite xenoliths. Group B diamond eclogites include two xenoliths from the Muskox kimberlite (15 km SW from the Jericho kimberlite). Shown for comparison are Jericho Group A diamond-bearing eclogites from Smart *et al.* (2009, 2011), Jericho zircon-bearing eclogites from Heaman *et al.* (2006), and previously published Jericho eclogites from Kopylova *et al.* (1999a) and De Stefano *et al.* (2009). The field of 'Slave eclogites' includes garnet from eclogite xenoliths from the Diavik kimberlite (Aulbach *et al.*, 2007; Schmidberger *et al.*, 2007) located in the central Slave craton and Voyageur kimberlite (Smart *et al.*, in preparation) located in the northern Slave craton. The geochemical group A–B–C compositional divisions are from Coleman *et al.* (1965).

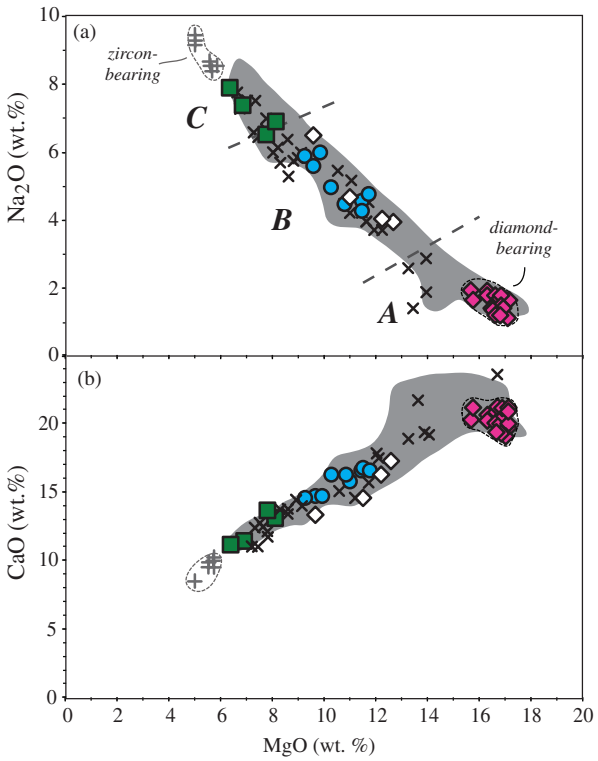

Fig. 3. Composition of clinopyroxenes from Jericho and Muskox eclogite xenoliths. Symbols and comparative fields are the same as in Fig. 2. (a) Na_2O (wt %) and (b) CaO (wt %) vs MgO (wt %). Group A–B–C divisions are from Taylor & Neal (1989).

and diamond-bearing eclogite garnet are illustrated in Fig. 4a, b and c, respectively. Garnet is depleted in LREE and has either flat or slightly depleted HREE patterns with Lu_N/Gd_N values [subscript N indicates chondrite-normalization with values from McDonough & Sun (1995)] of 0·34–1·26 and HREE contents between four and 50 times chondrite (Lu_N 4·1–34). Garnet from eclogite Jer 6 has a fractionated and enriched HREE pattern ($Lu_N/Gd_N = 3·7$, $Lu_N = 62$). Europium anomalies are also commonly found in garnet, with Eu/Eu* [calculated as $2Eu_N/(Sm_N + Gd_N)$] values ranging from 1·1 to 2·1. Garnet has variable but low Ni contents, from 2·2 to 25 ppm, compared with the average of 43 ppm for non-diamondiferous eclogitic garnets worldwide (Jacob, 2004). Most garnets have very low Ba contents (<0·15 ppm); those with elevated Ba (up to 0·61 ppm) also show enrichments in the LREE that could be attributed to accidental incorporation of kimberlite material in the analysis volume.

In contrast to garnet from the Group B and C eclogites, garnets from the Jericho and Muskox Group B diamond-bearing eclogites (Fig. 4c) have flat to positively sloping middle REE (MREE)–HREE patterns (Lu_N/Gd_N Jericho = 0·4–1; Muskox = 2·5–4·7). Eclogite Jde25 has higher amounts of MREE that form an elevated plateau from Eu to Dy and result in a low Lu_N/Gd_N value of 0·4. However, the diamond-bearing eclogite garnets have lower HREE contents ($Lu_N = 4·9–12$) compared with garnets from the diamond-free eclogites (Lu_N up to 34), and Eu anomalies are small or absent (Eu/Eu* = 0·9–1·3). Some garnets also show enrichment in La_N compared with the other LREE, and these garnets also have high Ba contents (0·81–1·53 ppm), which may be attributed to accidental analysis of infiltrated kimberlite material during laser ablation. Ni contents in garnet from the diamond-bearing eclogites range from 22 to 67 ppm.

Clinopyroxene

The REE patterns for clinopyroxene from the Jericho and Muskox eclogites are shown in Fig. 4d for Group B, 4e for Group C and 4f for the diamond-bearing eclogites. These

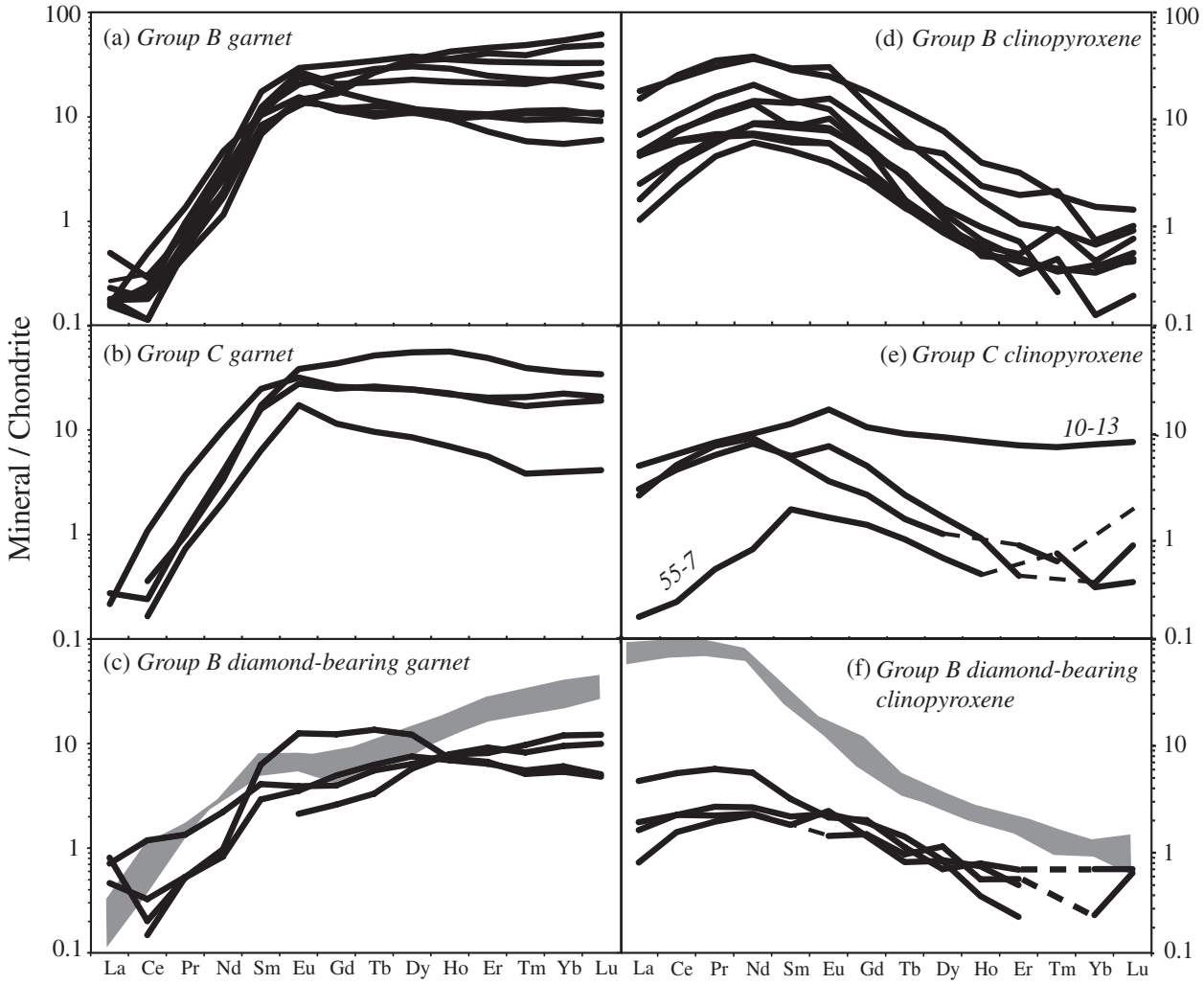

Fig. 4. Chondrite-normalized REE patterns for garnet (a–c) and clinopyroxene (d–f) from Groups B, C and diamond-bearing Group B eclogites, as defined in Figs 2 and 3. Grey fields in (c) and (f) represent the REE pattern for garnet and clinopyroxene from high-MgO Group A Jericho eclogites from Smart *et al.* (2009). Normalization values are from McDonough & Sun (1995).

generally have convex-up patterns with relative depletions in the LREE from La to Ce, a plateau from Nd to Eu, and depletion in the HREE. Two exceptions are clinopyroxene from eclogite 10-13, which has a flat pattern with a peak at Eu, and from eclogite 55-7, which is very LREE depleted. The clinopyroxenes have a range of LREE contents from La_N 1·0 to 18, excluding the very low LREE contents in 55-7 ($La_N = 0·2$). Eu anomalies are also present in the clinopyroxene patterns ($Eu/Eu^* = 0·8–1·5$) and the most pronounced Eu anomalies (1·4–1·5) are found in clinopyroxene in eclogites 10-13 and Jer 2. Sr contents in the clinopyroxene range from 170 to 540 ppm, and strong positive peaks in Sr are observed in primitive mantle normalized trace-element patterns (not shown). The Jericho clinopyroxenes contain 0·03–0·39 ppm Ba, 0·2–1·2 ppm Pb, >0·1 ppm U, and below detection limits of Th. Clinopyroxene from eclogite 35-2 has higher trace-element concentrations than clinopyroxene from the other eclogites, with 1·3 ppm Ba, 680 ppm Sr, 1·2 ppm Pb, and 0·3 ppm U.

Clinopyroxenes from the diamond-bearing eclogites have relatively flat, slightly negatively sloping LREE patterns (Fig. 4f). LREE contents in these clinopyroxenes fall at the lower end of the range observed in diamond-free Jericho eclogites ($La_N = 0·7–4·4$ vs up to 18). Positive Sr anomalies in primitive mantle-normalized multi-element patterns are also observed in clinopyroxenes from diamond-bearing eclogites. However, both Sr (56–83 ppm) and Pb (0·1–0·2 ppm) contents are much lower in the diamond-bearing eclogites than in the diamond-free eclogites.

GEOTHERMOMETRY

Temperatures were calculated at 5 GPa using the Krogh Ravna (2000) calibration of the garnet–clinopyroxene

Fe–Mg exchange thermometer. Because no geobarometer exists for bimineralic eclogites, we used our calculated temperatures to extrapolate pressures from the pressure–temperature array defined for Jericho peridotite xenoliths (Kopylova *et al.*, 1999*b*). Pressures and temperatures were successively iterated using this technique and are given in Table 2. Temperatures for the diamond-free eclogites range between 840 and 1410°C, corresponding to a range in estimated pressures from 4·1 to 6·0 GPa. The choice of an initial pressure of 5 GPa (corresponding approximately to 160–170 km depth) may be excessive for some of the eclogites; however, conducting the iteration with an initial lower pressure (e.g. 4 GPa) produces the same final temperatures and pressures after several iterations. Calculated temperatures for the diamond-bearing eclogites are in the range of 1070–1100°C (Jericho) and 1120–1220°C (Muskox), corresponding to pressures of 4·6–5·0 GPa, and place the diamond-bearing eclogites at the higher end of the temperature range defined by the diamond-free Jericho eclogites. Diamonds from two Jericho eclogites (Jde15, Jde25) have independent temperature estimates from nitrogen aggregation systematics. Assuming diamond formation at 2 Ga synchronous with both Jericho eclogite formation (Schmidberger *et al.*, 2005) and Diavik diamond formation (Aulbach *et al.*, 2009*a*), two diamonds from Jde15 (eclogite temperature of 1040–1080°C), containing 1130–2350 ppm N and with low aggregation (6–10 %B, where %B indicates the proportion of nitrogen aggregated to diamond B centers), yield nitrogen aggregation temperature estimates of 1040–1050°C. Ten diamonds from Jde25 (eclogite temperature 1040–1100°C), containing 1080–1990 ppm N with variable aggregation (12–56 %B) give temperature estimates between 1040 and 1100°C. Thus the nitrogen aggregation diamond-derived temperatures (1040–1100°C) agree with the Fe–Mg exchange eclogite-derived temperatures (1070–1110°C) within the uncertainty of the two techniques.

Two Jericho eclogites give extreme temperatures >1400°C and appear to have equilibrated at conditions deeper than calculated for the magmatic pyroxenites and fertile, porphyroclastic high-T peridotites that are thought to define the base of the Jericho cratonic mantle lithosphere (Kopylova *et al.*, 1999*b*). These geologically unreasonable depths may indicate that the minerals analyzed in these eclogites were not in equilibrium. Alternatively, temperature overestimation could have resulted from using total FeO in the temperature calculation, which, when applied to low-Fe minerals (such as eclogitic omphacite), can produce misleadingly high temperatures (Krogh Ravna, 2000).

CLINOPYROXENE Sr AND Pb ISOTOPE COMPOSITIONS

$^{87}Sr/^{86}Sr$ ratios were determined for clinopyroxene from 15 eclogites (averages and calculated uncertainties for each eclogite are listed in Table 4; full data are given in Supplementary Data Appendix A; supplementary material is available for downloading at http://www.petrology.oxfordjournals.org) and have a range of 0·7032–0·7054 and 131–678 ppm Sr. The Sr isotope compositions reported in Table 4 have been corrected for radiogenic ingrowth of ^{87}Sr since 173 Ma, but because most of the analyzed clinopyroxene grains have very low contents of Rb (below detection to 0·45 ppm), the corrections were very small (<0·0001 change). Whole-rock analyses of the Jericho kimberlite have a range of $^{87}Sr/^{86}Sr$ ratios from 0·7043 to 0·7063 (Kopylova *et al.*, 2009), which overlap with those of the Jericho Group A diamond-bearing eclogites (0·7047–0·7061, Smart *et al.*, 2009). However, 11 of the 15 Jericho eclogites (this study) have clinopyroxene with $^{87}Sr/^{86}Sr$ ratios between 0·7036 and 0·7044 and no correlation between Sr isotope ratios and Sr content is apparent ($r^2 = 0·3$, not shown).

Lead isotope ratios ($^{206}Pb/^{204}Pb$ and $^{207}Pb/^{204}Pb$) were determined for clinopyroxene from 13 eclogites (averages and uncertainties for each eclogite are listed in Table 4; full data are given in Supplementary Data Appendix A) and show a range of 14·68–18·74 and 15·02–15·54, respectively. The Pb isotope data presented here have not been corrected for isotopic ingrowth because $^{238}U/^{204}Pb$ ('μ') values were not measured. However, we assume that our measured Pb isotope values approximate the initial Pb isotope values at the time of eclogite formation (using the 'galena model age' technique) given that the clinopyroxene grains have both very low U contents (below detection to 0·03 ppm) and very low U/Pb ratios (0·01–0·09). However, we stress that the Pb isotope values presented here are maximum values and correction to initial values may shift the isotopic array to less radiogenic values.

In Fig. 5, the Jericho data plot along a broad array from an intercept with the two-stage terrestrial lead evolution curve of Stacey & Kramers (1975) at *c.* 2·2 Ga (defined by the isotopic composition of eclogite Jer 3: $^{206}Pb/^{204}Pb$ 14·02–14·79; $^{207}Pb/^{204}Pb$ 15·08–15·2), towards the more radiogenic isotope compositions of the 173 Ma Jericho kimberlite ($^{206}Pb/^{204}Pb_i = 18·99$; from regression of eclogitic rutile, garnet and kimberlite perovskite; Heaman *et al.*, 2006). As $^{207}Pb/^{204}Pb$ ratios are not available for the Jericho kimberlite, the isotopic composition of the nearby Voyageur kimberlite ($[^{206}Pb/^{204}Pb]_{170\ Ma} = 19·23$; $[^{207}Pb/^{204}Pb]_{170\ Ma} = 15·58$), which is also a Jurassic Group I kimberlite with an age of 170 ± 10 Ma (*in situ* U–Pb dating of perovskite; S. Tappe, personal communication, 2012) is used in Fig. 5 for comparative purposes. The more radiogenic end of the Jericho array is defined by Pb isotope compositions from Jericho Group A diamond-bearing eclogites (dotted ellipses in Fig. 5; $^{206}Pb/^{204}Pb = 18·5–18·7$; $^{207}Pb/^{204}Pb = 15·5–15·7$; Smart *et al.*, 2009), which approach the composition of the Jericho and Voyageur kimberlites.

Table 4: Average Sr and Pb isotope compositions of clinopyroxene from Jericho eclogites determined by ICP-MS

Sample	Class.	$^{87}Sr/^{86}Sr$	2σ	*n*	$^{206}Pb/^{204}Pb$	2σ	$^{207}Pb/^{204}Pb$	2σ	*n*	U/Pb (cpx)
35-2	B/peak.	0·7043	0·00008	7	16·80	0·1	15·29	0·02	8	0·01
1-1	B/peak	0·7054	0·0002	7	17·96	0·15	15·23	0·05	8	0·03
R183	B/peak	0·7052	0·0003	6	18·03	0·09	15·21	0·06	8	0·03
10-13	C/peak	0·7041	0·0003	5	17·07	0·36	15·33	0·13	4	0·03
55-7	C/depl.	0·7040	0·0003	7	15·91	0·48	15·39	0·13	6	b.d.
44-9	A	0·7032	0·0003	8	18·74	0·11	15·54	0·04	4	b.d.
Jd6fn	B/depl	0·7044	0·0001	7	17·01	0·17	15·41	0·07	4	0·07
Jer 1	B/depl	0·7042	0·0004	7	15·83	0·11	15·23	0·1	5	b.d.
Jer 2	B/peak	0·7042	0·0002	7	16·27	0·24	15·02	0·22	5	0·09
Jer 3	C/depl	0·7037	0·0003	9	14·68	0·08	15·13	0·08	5	0·03
Jer 4	B/depl	0·7041	0·0003	8	15·92	0·24	15·23	0·1	5	b.d.
Jer 5	B	0·7032	0·0002	6	16·58	0·05	15·20	0·2	5	0·01
Jer 6	B/depl	0·7036	0·0002	9						
Jer 7	B/peak	0·7042	0·0002	6						
Jer 8	C/depl	0·7036	0·0004	7	16·34	0·18	15·08	0·1	1	0·07
		Coral Standard			NIST SRM 614					
	Measured	0·709115	0·000071	5	17·43	0·10	15·58	0·13	4	
		0·709011	0·000074	7	17·62	0·07	15·59	0·06	4	
	Accepted	0·709098	0·000019		17·833	0·013	15·53	0·007		

Full dataset can be found in Supplementary Data Appendix A. Accepted Sr standard values are from Bizzaro *et al*. (2003); accepted Pb standard values are from Woodhead & Hergt (2001).

Linear regression of the entire eclogite dataset produces a secondary isochron with a calculated age of 1715 + 290/− 320 Ma (2σ, MSWD = 0·8).

OXYGEN ISOTOPE COMPOSITIONS

The oxygen isotope compositions of garnet, clinopyroxene and kyanite mineral separates from 10 of the Jericho eclogites are presented in Table 5. The $\delta^{18}O$ values determined for garnet from both Group B and C eclogites vary between 5·2 and 5·8‰, excluding one kyanite-bearing Group C eclogite (10-13) with higher $\delta^{18}O$ values of 6·3–6·6‰. Kyanite from eclogite 53-11 has an $\delta^{18}O$ value of 6·3‰ and the oxygen isotope fractionation between garnet and kyanite (sample 53-11) is 0·72‰, consistent with isotopic equilibrium (Sharp, 1995). Garnet and clinopyroxene from three Jericho Group A diamond-bearing eclogites from Smart *et al.* (2009) have $\delta^{18}O$ values between 5·3 and 5·5‰, whereas garnet from two Jericho Group B diamond-bearing eclogites has $\delta^{18}O$ values of 6·5–6·6‰. The oxygen isotope composition of garnet from Jericho eclogite Mx8A [a zircon-bearing eclogite from Schmidberger *et al.* (2005) and Heaman *et al.* (2006) with a U–Pb age of 1·9 Ga] has a $\delta^{18}O$ value of 5·6‰.

CALCULATED WHOLE-ROCK COMPOSITIONS

Mantle xenoliths are commonly infiltrated by host kimberlite magmatic fluids or melts, such that bulk xenolith analyses yield contaminated, unrepresentative compositions (e.g. Barth *et al.*, 2001; Schmidberger & Francis, 2001; Jacob, 2004; Aulbach *et al.*, 2007). Therefore, the whole-rock compositions of eclogite xenoliths are generally estimated using modal abundance data and the composition of constituent minerals. However, inaccurate mode estimates owing to small xenolith size, large mineral grains or mineral nugget effects can produce erroneous calculated compositions. For example, coarser-grained (mineral grains exceeding 5 mm) samples are thought to have ±10% uncertainties in modal estimations (Jerde *et al.*, 1993). Calculated major-element whole-rock compositions are particularly mode-dependent (e.g. Smart *et al.*, 2009), which must be taken into consideration when using calculated major-element whole-rock compositions. In contrast, the overall shape of whole-rock trace-element patterns are relatively unaffected by up to 30% variation in mineral modes (Jerde *et al.*, 1993). We have calculated both major- and trace-element whole-rock compositions for the Jericho and Muskox eclogites using both visually estimated and point-counted (using thin sections) modal abundances.

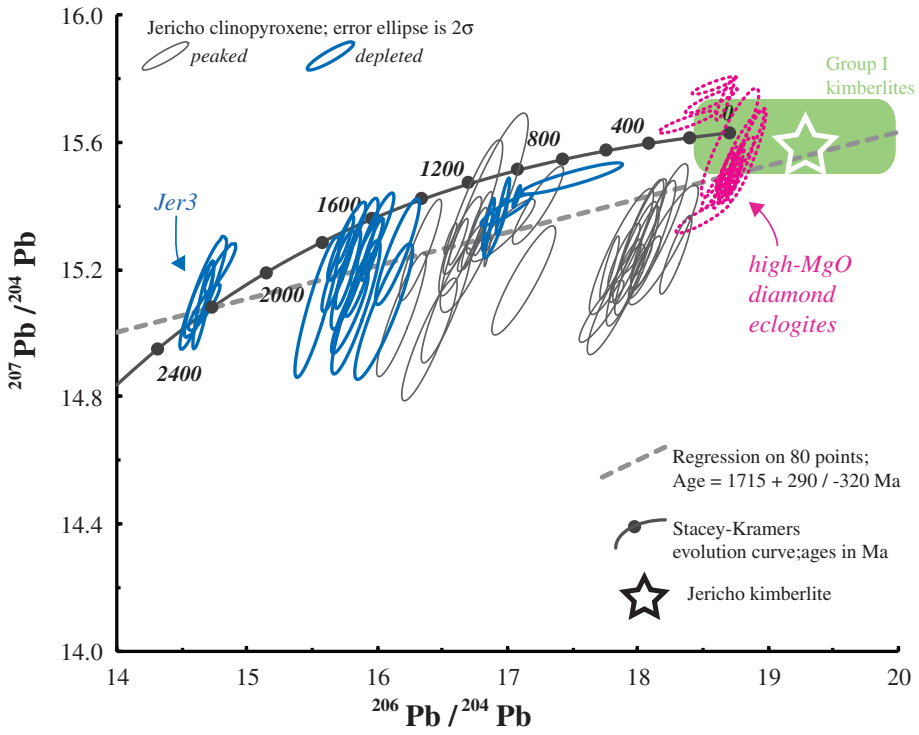

Fig. 5. $^{206}Pb/^{204}$ Pb vs $^{207}Pb/^{204}$ Pb isotope compositions of clinopyroxene from Jericho eclogites analyzed by *in situ* MC-ICP-MS. Each ellipse represents one analysis encompassing the 2σ error. Bold ellipses represent analyses from eclogites exhibiting the depleted trace-element patterns; thin grey ellipses are for the peaked pattern. Eclogite Jer 3 intercepts the Stacey–Kramers curve at *c.* 2·2 Ga. Dotted ellipses represent analyses from high-MgO Jericho diamond eclogites from Smart *et al.* (2009). The two-stage terrestrial Pb evolution curve from Stacey & Kramers (1975) is shown for comparison. Regression of the Jericho clinopyroxene data forms a secondary isochron with an age of 1715 (+290, −320) Ma. The Pb isotopic composition of South African Group I kimberlites (Smith, 1983) is shown for comparison. The approximate Pb isotopic composition of the Jericho kimberlite (white star) is deduced from that of the Jurassic, proximal (50 km) Voyageur kimberlite (~170 Ma, S. Tappe, personal communication, 2012). The Voyageur $^{206}Pb/^{204}Pb$ ratio (19·27) is similar to an initial $^{206}Pb/^{204}Pb$ ratio of 18·99 ± 0·33, derived from a U–Pb plot of Jericho kimberlite perovskite and Jericho eclogite-derived garnet and rutile from Heaman *et al.* (2006), which was interpreted to represent the Pb isotope composition of the Jericho kimberlite magma. The Jericho eclogite clinopyroxene Pb data appear to form a mixing trend between the intersection of the least radiogenic Pb from eclogite Jer 3 with the Stacey–Kramers curve at *c.* 2·2 Ga and the more radiogenic composition of the host kimberlite at *c.* 170 Ma.

Whereas some of the Jericho eclogite samples are small (5 cm in length), the mineral grain diameters are also relatively small (1–3 mm), such that we are confident our estimates are within 10–20% of the actual mode. One exception is sample 44-9, which contains coarser crystals up to 5 mm in diameter. Calculated major-element whole-rock compositions are listed in Table 2 and trace-element compositions in Table 6.

Table 2 shows the compositional range of the calculated bulk-rock Jericho eclogites. The Jericho eclogites have basaltic to picritic compositions, containing 43–50 wt % SiO_2, 5·3–13 wt % MgO and 1·9–4·5 wt % $Na_2O + K_2O$. The Jericho and Muskox diamond-bearing eclogites are also broadly basaltic, but have MgO (11·5–13·7 wt %) and SiO_2 (46·5–48·0 wt %) contents that fall at the upper end of the range shown by the Jericho eclogites. Figure 6 illustrates the MgO vs SiO_2, Al_2O_3, CaO, FeO and Na_2O (wt %) and Ni (ppm) variations in the calculated eclogite bulk-rocks. A negatively sloping trend is observed between MgO and Al_2O_3 in Fig. 6a, whereas MgO and Ni form a positively sloping trend in Fig. 6f. No strong correlations are observed between MgO and CaO, FeO, SiO_2 and Na_2O (Fig. 6b–e). The Jericho eclogite bulk-rocks have broadly similar MgO, Al_2O_3, CaO, Na_2O and Ni contents to modern altered oceanic gabbros (from Bach *et al.*, 2001), but are markedly poorer in SiO_2 and enriched in FeO relative to the gabbros. At comparable MgO contents, the Jericho eclogites have similar CaO, FeO, Na_2O and Ni contents to Archean basalts and picrites, but higher Al_2O_3 and lower SiO_2 contents.

Trace-element classification

The calculated whole-rock trace-element compositions of the Jericho and Muskox eclogites are listed in Table 6 and plotted in Figs 7 and 8. The eclogites of this study have been grouped into three REE pattern types and the averages for each pattern type are shown in Fig. 7a. The first pattern (Fig. 7b) is characterized by slightly positively

Table 5: Oxygen isotope compositions of garnet and clinopyroxene from Jericho eclogites

Sample		Classification	$\delta^{18}O$ (‰)			1σ
35-2	grt	B/peaked	5·73	5·59		±0·1
	cpx					
Mx8A	grt	–	5·64	5·65		±0·1
Jd6fn	grt	B/depleted	5·22	5·36	5·44	±0·1
	cpx					
53-11	grt	C	5·67	5·49		±0·1
	ky		6·3			±0·1
44-9	grt	A	5·64	5·75	5·67	±0·1
	cpx					
55-7	grt	C/depleted	5·57	5·61		±0·18
	cpx					
1-1	grt	B/peaked	5·62	5·54		±0·18
	cpx					
10-13	grt	C/peaked	6·25	6·31	6·55	±0·18
	cpx					
Jde02*	grt		5·30	5·50		±0·15
	cpx		5·45			±0·15
Jde03*	grt		5·47			±0·15
	cpx					
Jde07*	grt		5·49	5·53		±0·15
	cpx					
Jde25*	grt		6·56	6·5		±0·15
	cpx					
Jde15*	grt		6·64	6·61		±0·15
	cpx					
Standards	Measured		Accepted			Reference
Gee Whiz Qtz	12·52 ± 0·14 (1σ) $n = 15$		12·5 ± 0·1 (1σ)			Larson & Sharp (2005)
Gore-3	5·64 ± 0·06 (1σ) $n = 5$		5·74 ± 0·15 (1σ)			UWG-2; Valley *et al.* (1995)

1σ calculated for each day session based on the Gee Whiz Qtz standard. Gore-3 is sampled from the same locality as UWG-2.
*Diamond-bearing samples.

sloped LREE ($La_N/Sm_N = 0·2–0·4$), slightly negatively sloped HREE ($Lu_N/Gd_N = 0·3–0·9$) and distinct positive Eu anomalies ($Eu/Eu^* = 1·3–1·7$). Because the REE appear to 'peak' at Eu, we refer to eclogites displaying this pattern as 'peaked'. In contrast, the second eclogite pattern (Fig. 7c) shows strong depletion in the LREE ($La_N/Sm_N = 0·02–0·2$), flat to slightly positively sloped HREE ($Lu_N/Gd_N = 0·8–0·9$, eclogite Jer 6 = 2·8) and smaller Eu anomalies ($Eu/Eu^* = 0·9–1·3$) compared with the peaked pattern. Eclogites displaying this second pattern are termed 'depleted' based on the strong LREE depletion. Gonzaga *et al.* (2010) recognized these two patterns from worldwide occurrences of eclogite xenoliths. Lastly, all Group B, diamond-bearing eclogites (Fig. 7d) have Lu > La and display concave (Jericho) and positively sloping profiles (Muskox) from La to Lu; hence this final pattern is termed 'sloped'. In general the sloped eclogites display lower REE contents than the peaked or depleted eclogites. Eclogite Jde25 has a plateau in the MREE from Eu to Dy, but in general no Eu anomalies are present in the sloped eclogites ($Eu/Eu^* = 0·9–1·0$).

On primitive-mantle normalized multi-element plots, the three trace-element pattern types also have distinguishing features (Fig. 8a). The peaked and depleted eclogites have generally similar patterns, but as observed in Fig. 7, depleted eclogites exhibit stronger LREE depletion and HREE enrichment than the peaked eclogites (Fig. 8b and c). The sloped eclogites have lower REE abundances, but moderately higher abundances of some of the large ion lithophile elements (LILE; Rb and Ba) and high field strength elements (HFSE; Th, U, Nb, Ta, Zr, Hf and Ti) compared with the other two patterns (Fig. 8d). Strong positive Sr anomalies are observed in all three eclogite patterns, but depletions in the HFSE, observed as sharp negative anomalies in both Ti and Nb, and troughs at Zr–Hf, are only found in the peaked and depleted eclogites. Some HFSE depletion may be due to the omission of rutile from the calculated bulk-rock eclogite, as rutile, although present in some eclogites in trace to minor amounts, was not analyzed for its trace-element content. After incorporation of 0·05–2% rutile into the peaked and depleted whole-rock eclogite compositions [using data from Aulbach *et al.* (2011*a*)], the Ti and Hf depletions are erased, but Zr depletions are still prominent (not shown). Both Ta and Nb concentrations are increased slightly (not shown), but the relative Nb depletion and Ta peak remain in the eclogite pattern. Addition of minor rutile indicates that some of the HFSE anomalies, such as Ti and Hf, may be an artefact of the omission of rutile in the bulk-rock calculation.

This new reconstructed bulk-rock trace-element grouping of the Jericho and Muskox eclogites does not coincide with the garnet-based major-element classification discussed above; rather both Group B and C Jericho eclogites fall into the peaked and depleted groups. However, the peaked eclogites are all Group B except for one Group C eclogite (10-13) and the diamond-bearing eclogites exclusively make up the sloped group.

DISCUSSION

The effect of metasomatism

Mantle eclogites are particularly susceptible to metasomatism because of their protracted residence in the cratonic lithospheric mantle and subsequent entrainment as xenoliths in kimberlite magmas. Metasomatism is generally expressed as either the growth of new minerals (modal

Table 6: Calculated whole-rock trace-element composition of Jericho and Muskox eclogites

Eclogite:	35-2	1-1	R183	Jer 2	Jer 7	10-13	Jd6fn	Jer 1	Jer 4	Jer 6	55-7	Jer 3	Jer 8	Mox001	Mox23	Jde15	Jde25	44-9	Jer 5
Rb	0·20	0·03	0·09	0·03	0·09	0·06	0·03	0·17	0·05	0·23	0·13	0·48	0·06	0·11	0·59	0·14	0·00	0·06	0·03
Ba	0·71	0·14	0·19	0·06	0·08	0·17	0·32	0·17	0·08	0·17	0·09	0·07	0·04	0·34	1·02	0·45	0·09	0·22	0·16
Th	0·07				0·22		0·01		0·11	0·26			0·04	0·28		0·02		0·02	0·10
U	0·02	0·01	0·01	0·02	0·03	0·01	0·03	0·02	0·00	0·05	0·01	0·04	0·02	0·15	0·05	0·03	0·01	0·01	0·02
Nb	0·13	0·05	0·06	0·01	0·05	0·05	0·02	0·06	0·07	0·02	0·05	0·01	0·01	0·35	0·20	0·15	0·22	0·20	0·01
Ta	0·09	0·03	0·02	0·04	0·03	0·03	0·02	0·02	0·09	0·03	0·01	0·03	0·00	0·05	0·03	0·04	0·06	0·00	0·00
La	1·74	0·66	0·63	0·45	0·81	0·39	0·29	0·14	0·17	0·42	0·05	0·25	0·16	0·52	0·23	0·27	0·09	1·54	3·17
Ce	5·74	2·24	2·17	1·90	3·16	1·33	1·26	0·81	0·84	1·83	0·14	1·54	0·80	1·72	0·63	0·70	0·48	4·75	13·8
Pr	1·18	0·41	0·39	0·44	0·75	0·30	0·34	0·26	0·23	0·43	0·08	0·47	0·20	0·29	0·11	0·14	0·11	0·82	2·91
Pb	0·47	0·29	0·24	0·18	0·40	0·15	0·18	0·33	0·24	0·55	0·14	0·32	0·19	0·17	0·13	0·09	0·00	0·14	1·90
Sr	271	126	121	92·7	200	64·1	106	101	109	215	68·7	97·1	51·6	33·8	27·0	40·0	28·3	65·6	659
Nd	7·26	2·24	2·16	3·24	5·06	2·09	2·76	2·36	1·96	2·90	1·23	4·29	2·00	1·57	0·62	0·75	0·70	4·25	15·6
Sm	2·82	1·03	0·97	1·41	1·62	1·21	1·87	1·12	1·58	1·41	1·51	2·51	2·11	0·54	0·00	0·37	0·59	1·13	3·85
Zr	7·62	10·2	9·95	5·63	5·83	5·51	5·52	9·22	6·91	7·55	11·0	21·6	9·76	9·94	2·44	7·41	13·1	21·4	9·34
Hf	0·47	0·43	0·40	0·23	0·28	0·21	0·36	0·28	0·33	0·45	0·28	0·56	0·42	0·28	0·17	0·37	0·54	0·97	0·73
Eu	1·58	0·49	0·49	1·02	0·74	0·94	1·03	0·53	0·90	0·83	0·97	1·14	1·72	0·18	0·10	0·16	0·42	0·38	1·30
Ti	697	937	948	367	307	789	602	553	437	511	810	1070	536	1467	1038	2225	1985	100	449
Gd	3·49	1·35	1·32	2·49	1·75	2·23	3·63	1·39	3·52	2·68	3·06	3·29	6·68	0·62	0·42	0·67	1·35	1·49	3·46
Tb	0·55	0·22	0·21	0·33	0·24	0·34	0·67	0·21	0·71	0·66	0·58	0·56	1·42	0·13	0·08	0·14	0·26	0·28	0·46
Dy	3·65	1·33	1·30	1·86	1·47	2·10	4·82	1·47	4·98	5·66	3·65	3·69	10·3	1·01	0·95	1·02	1·59	2·08	2·45
Y	19·0	6·58	6·35	6·86	7·21	10·0	20·7	6·64	22·3	34·2	15·8	15·8	56·3	6·59	6·18	5·26	7·42	8·82	9·41
Ho	0·74	0·27	0·26	0·31	0·31	0·40	0·98	0·28	1·04	1·43	0·74	0·72	2·31	0·27	0·27	0·21	0·21	0·43	0·37
Er	2·09	0·69	0·67	0·71	0·88	0·98	2·74	0·84	2·61	4·51	1·82	2·01	5·86	0·92	0·81	0·55	0·55	1·15	1·07
Tm	0·31	0·11	0·1	0·09	0·14	0·12	0·41	0·14	0·37	0·74	0·26	0·31	0·73	0·12	0·16	0·08	0·06	0·16	0·14
Yb	2·30	0·68	0·64	0·53	0·96	0·83	2·67	0·88	2·31	5·26	1·77	2·16	4·34	0·96	1·17	0·49	0·43	0·96	0·95
Lu	0·39	0·10	0·09	0·10	0·14	0·13	0·40	0·14	0·32	0·92	0·29	0·31	0·63	0·15	0·19	0·06	0·06	0·14	0·15
Eu/Eu*	1·5	1·3	1·3	1·7	1·3	1·7	1·2	1·3	1·1	1·3	1·3	1·2	1·3	0·9	1·7	1·0	1·4	0·9	1·1
Sr/Sr*	2·6	3·7	3·7	2·2	2·9	2·3	3·0	3·5	4·5	5·4	5·3	1·8	2·2	1·4	3·0	3·5	2·9	1·0	2·8
Class.	Peak	Peak	Peak	Peak	Peak	Peak	Depl	Depl	Depl	Depl	Depl	Depl	Depl	Slope	Slope	Slope	Slope	Pyx	Pyx

$Eu^* = 2Eu_N/(Gd_N + Sm_N)$; $Sr^* = 2Sr_{PM}/(Pr_{PM} + Nd_{PM})$. Subscripts N and PM indicate normalization to chondrite and primitive mantle respectively from McDonough & Sun (1995). Class., classification of eclogites according to whole-rock chondrite-normalized REE pattern (see Figs 7 and 8 and text).

metasomatism) and/or trace-element enrichment without new mineral growth (cryptic metasomatism; Dawson, 1984). It is critical to evaluate the potential effects of metasomatism in xenolith studies so that the petrogenetic history of the pre-metasomatic protolith may be determined.

The Jericho and Muskox eclogites of this study do not show strong evidence of modal metasomatism, and although secondary veins of fine-grained phlogopite, calcite and apatite are common, these are regarded as products of kimberlite infiltration. In comparison, diamond found in the Jericho and Muskox eclogites is clearly a secondary mineral and it is often surrounded by altered clinopyroxene and garnet. It is possible that diamond growth was accompanied by cryptic metasomatism in these eclogites; however, comparison of the diamond-bearing eclogites of this study and the high-MgO diamond-bearing eclogites from Smart *et al.* (2009) in Figs 7d and 8d demonstrates that the diamond-bearing eclogites reported here do not display the extreme LREE enrichment found in the high-MgO diamond-bearing eclogites, and thus have not undergone significant metasomatic enrichment. Therefore, excluding the diamond-bearing eclogites, clear evidence for modal metasomatism is absent in the Jericho eclogites.

In contrast, constraining the effects of cryptic metasomatism in eclogite xenoliths is more difficult. Garnet and clinopyroxene in eclogite xenoliths exhibiting obvious signs of modal metasomatism (e.g. phlogopite-, diamond- and zircon-bearing eclogites; see Heaman *et al.*, 2002, 2006; Jacob *et al.*, 2009; Smart *et al.*, 2009; Gréau *et al.*, 2011) sometimes contain evidence of cryptic metasomatism, observed as higher concentrations of incompatible

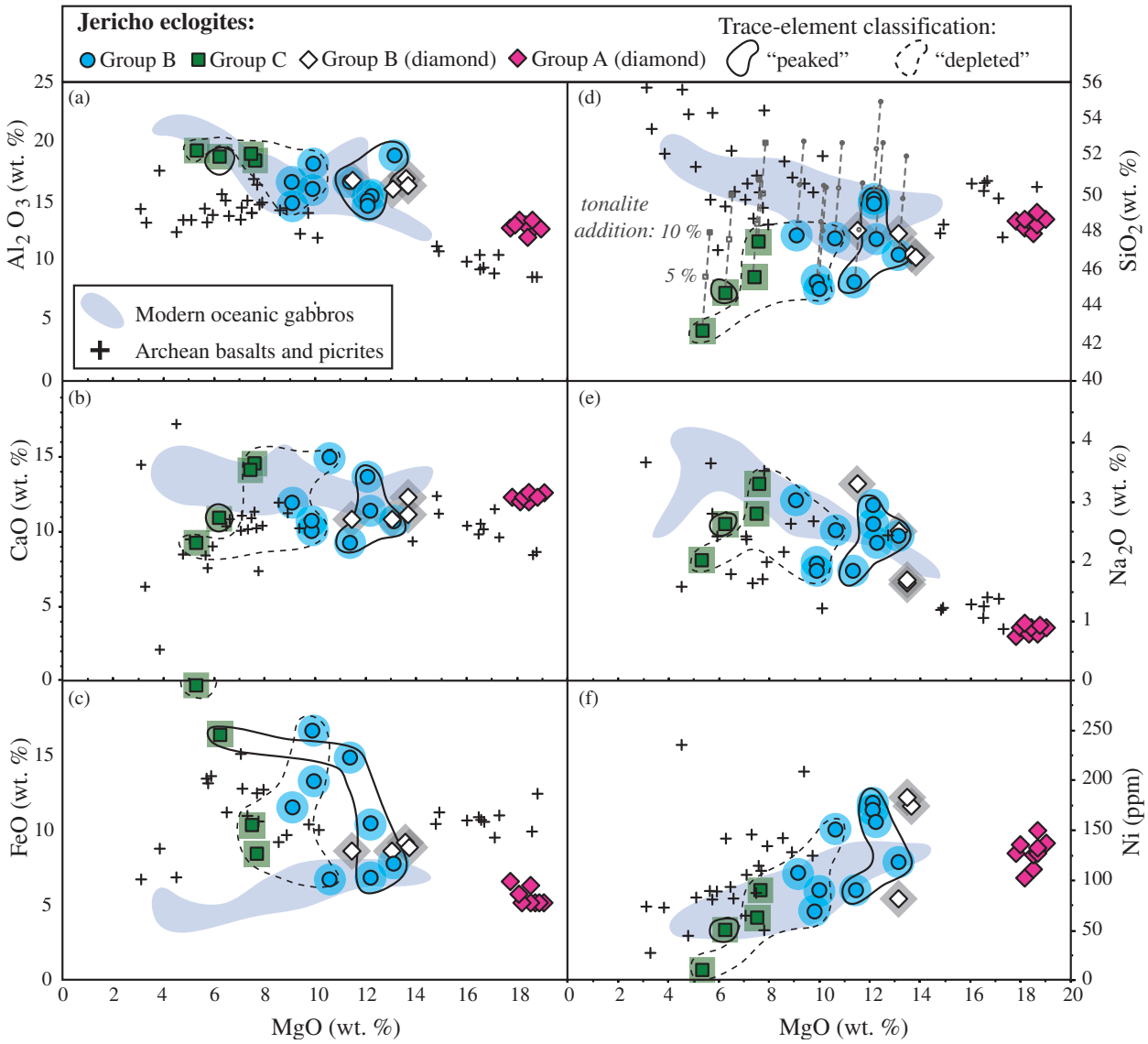

Fig. 6. Variation diagrams showing the calculated whole-rock compositions of the Jericho and Muskox eclogites: (a) Al_2O_3 vs MgO (wt %); (b) CaO vs MgO (wt %); (c) FeO vs MgO (wt %); (d) SiO_2 vs MgO (wt %); (e) Na_2O vs MgO (wt %); (f) Ni (ppm) vs MgO (wt %). Eclogite symbols are from the Group A–B–C classification shown in Fig. 2 and the larger shaded area for each symbol represents variation of the mineral modal abundances by 10%. The Jericho and Muskox eclogites are further grouped by continuous and dashed lines into the trace-element patterns introduced in the text and shown in Fig. 7. In (d), 5–10% tonalite composition (from Rapp & Watson, 1995) is added to each eclogite composition and is shown by the grey dashed lines. Field of modern oceanic gabbros is from Bach *et al.* (2001); Archean basalts, picrites and komatiites are from Rollinson (1999), Yamashita *et al.* (2000) and Polat *et al.* (2007, 2008).

elements (e.g. Th, U, Ba, Sr, Zr, Hf and the LREE). Comparison of incompatible element contents in minerals from eclogites with clear evidence of modal metasomatism and the Jericho eclogites of this study (Fig. 9) demonstrates that garnet and clinopyroxene from modally metasomatized eclogites are clearly more enriched in incompatible elements (represented by Zr and Ce). In Fig. 10, we compare the eclogites of this study with the metasomatized zircon-bearing high-FeO and diamond-bearing high-MgO eclogites from the Jericho kimberlite (Heaman *et al.*, 2002; Smart *et al.*, 2009). Both the high-MgO diamond-bearing and zircon-bearing eclogite suites have higher concentrations of REE from La to Sm, whereas the zircon-bearing eclogites have much higher concentrations of the LILE and HFSE, up to 1000 times primitive mantle. It should be noted that the data for the zircon-bearing eclogites from Heaman *et al.* (2002) are from bulk-rock eclogite analyses, which is probably responsible for the extreme trace-element concentrations observed in these eclogites. From this comparison, it appears the Jericho eclogites of the

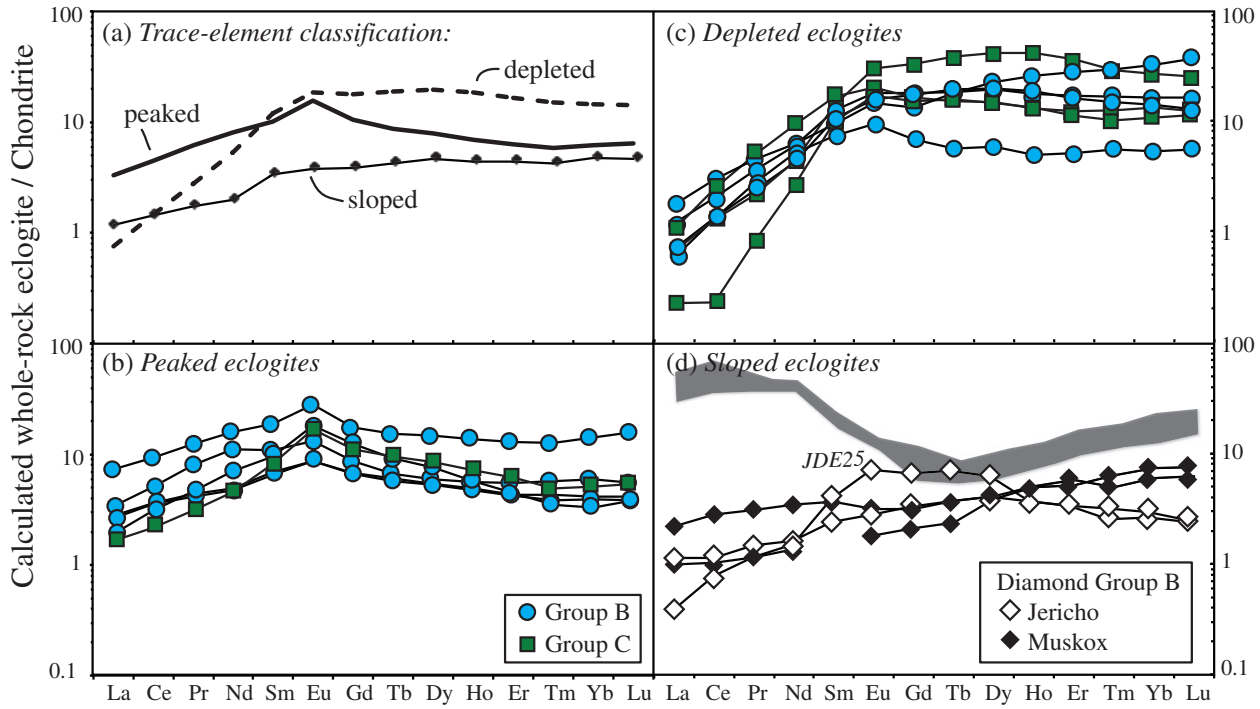

Fig. 7. Calculated whole-rock REE compositions of the Jericho and Muskox eclogite xenoliths. (a) Representative patterns for the three new trace-element pattern types introduced for the Jericho and Muskox eclogites. (b) Peaked eclogites have negatively sloping, depleted LREE and mildly depleted to flat HREE patterns with distinctive positive Eu anomalies (Eu/Eu* = 1·3–1·7). (c) Depleted eclogites have overall higher contents of HREE, stronger depletions in the LREE and smaller Eu anomalies (Eu/Eu* = 0·9–1·3) compared with the peaked eclogites. (d) Sloped eclogites have overall positive slopes in the REE, and are slightly depleted in LREE compared with the HREE. All Group B diamond-bearing eclogites fall into the sloped group. Symbols in (b)–(d) reflect the garnet composition classification from Fig. 2. Shaded field in (d) represents the composition of Jericho high-MgO diamond-bearing eclogites from Smart *et al.* (2009). Chondrite normalization values are from McDonough & Sun (1995).

present study have not been strongly affected by metasomatic processes and we can confidently use the eclogite bulk-rock geochemical data to assess the potential eclogite protoliths and their petrogenetic histories.

Crustal vs mantle eclogites

Kimberlite-hosted mantle-derived eclogite xenoliths commonly have basaltic to gabbroic compositions that overlap those of Archean basalts, komatiites and modern oceanic gabbros (e.g. Barth *et al.*, 2001; Jacob, 2004). These compositional similarities between eclogites and oceanic rocks are also shown by the Jericho and Muskox eclogites of this study (Fig. 6). The broadly basaltic composition of eclogite xenoliths has caused much debate about their origin; they have been hypothesized to form either in the upper mantle as magmatic cumulates crystallized from peridotite-derived basaltic magmas (e.g. O'Hara & Yoder, 1967; Griffin & O'Reilly, 2007), or in the oceanic lithosphere as basalts or gabbros, before being recycled into the cratonic lithospheric mantle (e.g. Helmstaedt & Doig, 1975; Jagoutz *et al.*, 1984; Jacob *et al.*, 1994; Barth *et al.*, 2001). However, although a bulk-rock basaltic composition alone cannot discriminate between a 'shallow' oceanic lithosphere or a 'deep' mantle magmatic origin for eclogites, their trace-element and oxygen isotope compositions can provide better constraints on their origin(s). At present there is no definitive evidence for the formation of eclogites as mantle cumulates (e.g. Jacob, 2004), but compelling evidence for a recycled oceanic crust origin is provided by the range of oxygen isotope compositions of mantle eclogites, which overlaps with both seawater-altered, modern-day oceanic crust (Muehlenbachs and Clayton, 1972; Alt *et al.*, 1989) and oceanic crust preserved in ophiolite complexes (Gregory & Taylor, 1981), and deviates significantly from the average mantle value of 5·5 ± 0·4‰ (Mattey *et al.*, 1994). Given the limited fractionation of oxygen isotopes at high temperatures at mantle conditions (Clayton *et al.*, 1975; Eiler, 2001), any deviation of eclogite oxygen isotope compositions outside the mantle average is probably due to protolith interaction with seawater near the Earth's surface (Muehlenbachs and Clayton, 1972).

Garnets from the Jericho eclogites have oxygen isotope compositions ranging from 5·3 to 6·6‰; however, only three of the nine eclogites analyzed for their oxygen isotope composition have garnet $\delta^{18}O$ values outside the mantle range of 5·5 ± 0·4‰. Garnets from these three

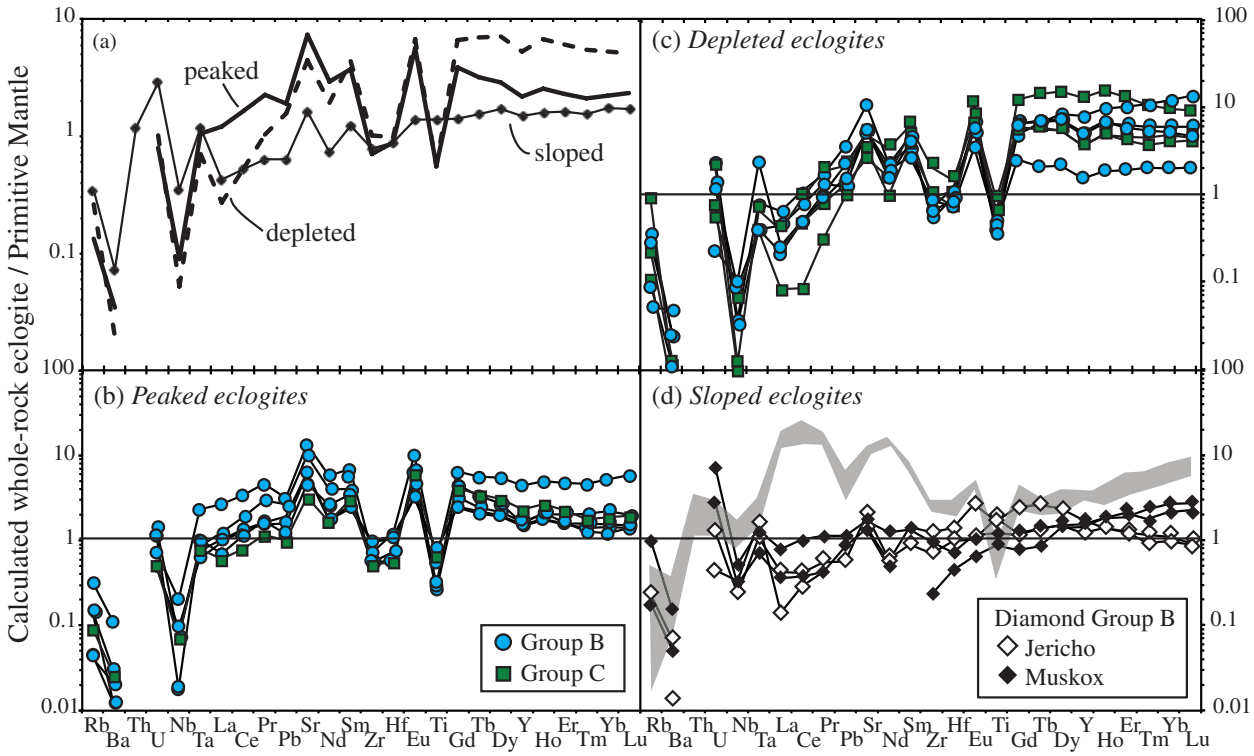

Fig. 8. (a) Calculated whole-rock multi-element patterns for the three eclogite trace-element types from Fig. 7; (b) peaked; (c) depleted; (d) sloped. Shaded field in (d) represents the composition of Jericho high-MgO diamond-bearing eclogites from Smart *et al.* (2009). Primitive mantle values are from McDonough & Sun (1995).

samples have $\delta^{18}O$ values >6‰ and comprise one peaked (10-13) and two sloped eclogites (Jde15, Jde25). Although most of the measured eclogites have 'mantle-like' oxygen isotope compositions, this does not preclude an oceanic crustal protolith for these eclogites (e.g. Schmickler *et al.*, 2004; Smart *et al.*, 2012). Oxygen isotope depth profiles through the oceanic crust show that the upper part of the sheeted dyke layer in the oceanic crustal column has $\delta^{18}O$ values close to 5·5‰ (Alt *et al.*, 1989), despite the fact that these rocks have undergone a significant amount of seawater alteration. The occurrence of mantle-like $\delta^{18}O$ values in the upper sheeted dykes reflects the fact that this depth marks the transition from lower temperature seawater–rock interactions in the shallow pillow basalts ($\delta^{18}O > 6‰$), to higher-temperature water–rock interactions in the lower sheeted dykes and upper gabbros ($\delta^{18}O < 5‰$). Furthermore, some deeper sections of the oceanic crust (e.g. middle to lower gabbros) may escape seawater alteration altogether and thus preserve mantle-like oxygen isotope compositions (e.g. Gregory & Taylor, 1981; Hart *et al.*, 1999). Despite the predominant 'mantle' signature of the oxygen isotope compositions, the Jericho eclogites have trace-element characteristics that are indicative of protolith crystallization at low pressures. These characteristics are examined in the following discussion.

Peaked and depleted eclogites

Protolith formation as oceanic gabbros

The Jericho and Muskox eclogites have variable compositions ranging from more Ni-rich, picritic compositions with 13 wt % MgO, to more Al_2O_3- and Na_2O-rich, basaltic compositions with 5·3 wt % MgO and low Ni contents (Fig. 6a, e and f). The trace-element patterns defined in this study for the Jericho eclogites broadly correspond to the major-element groups. Specifically, the peaked (and sloped) eclogites correspond to the more MgO-rich picrite group, and the depleted eclogites to the Al-rich basaltic group (Fig. 11). The well-defined trend between MgO vs Al_2O_3 displayed by these eclogites is very similar to magmatic differentiation trends defined by both natural (Cox, 1980; Eggins, 1993; Benoit *et al.*, 1996) and experimental (Baker & Stolper, 1994) picrites and basalts, which have been superimposed on Fig. 11. The similarity between the differentiation and eclogite trends suggests that the eclogite compositional variation may be related to sampling of oceanic rocks that underwent variable amounts of crystal fractionation. It is not possible to determine the exact mineralogy of the eclogite protoliths; nevertheless, similarities to the gabbroic cumulates in ophiolites (Ni 130–360 ppm; MgO 4·5–12·5 wt %; Benoit *et al.*, 1996), as well as the overall low Ni contents (<10–180 ppm) at low to moderate

MgO contents (5·3–13·7 wt %) indicate that olivine was probably not an abundant mineral phase (e.g. Jacob & Foley, 1999), and the eclogites were probably plagioclase- and clinopyroxene-rich gabbroic rocks.

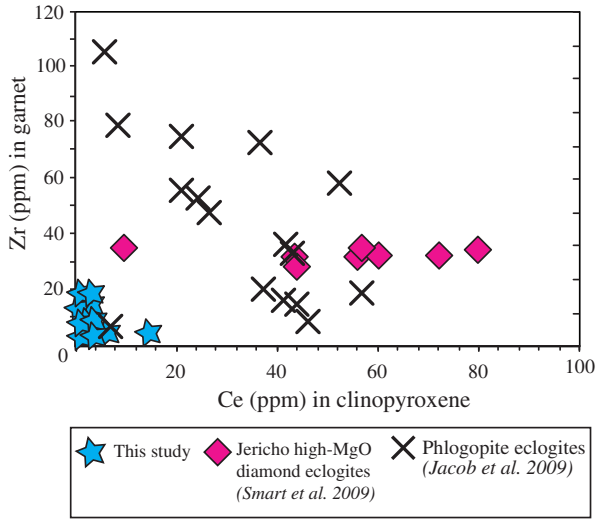

Fig. 9. Evaluation of the effects of metasomatism on the Jericho and Muskox eclogites based on garnet Zr (ppm) and clinopyroxene Ce (ppm) contents. Compared with garnet and clinopyroxene from modally metasomatized eclogite suites that have associated evidence of cryptic metasomatism (e.g. phlogopite eclogites from Kimberley, Jacob *et al.*, 2009; phlogopite + diamond eclogites from Jericho, Smart *et al.*, 2009), the Jericho and Muskox eclogites of this study have very low contents of incompatible elements.

One aspect that is problematic for this hypothesis is the high FeO content (>13 wt %) found in several calculated eclogite compositions (Fig. 6c). There is a positive correlation between FeO and Y content ($r^2 = 0{\cdot}6$, not shown) and eclogites with the highest FeO (up to 21·8 wt %) and Y (up to 56 ppm) contents are also the most garnet rich (eclogites 35-2, 10-13, Jer 4, Jer 6 and Jer 8). However, adjustment of the garnet:clinopyroxene modes to 50:50 does not diminish the trends and absolute FeO contents remain high (up to 17·0 wt %). Whereas these eclogites do not overlap with the natural gabbro field shown in Fig. 6, some of the Archean basalts plotted do have higher FeO contents, up to 15 wt %. Thus the elevated FeO contents, although still enigmatic, may be explained by either derivation from a high-FeO precursor or accumulation of almandine-rich garnet during eclogitization.

The presence of Eu and Sr anomalies in the peaked and depleted eclogites could suggest that plagioclase accumulation occurred in the protoliths. Comparison of these two eclogite groups with both modern oceanic gabbros (Bach *et al.*, 2001) and gabbroic cumulates from the Oman ophiolite (Benoit *et al.*, 1996) in Fig. 12 demonstrates the strong similarities between these lithological groups. Both the oceanic gabbros and the Jericho peaked and depleted eclogites exhibit positive Eu, Sr and Pb anomalies and negative Zr anomalies, as well as flat HREE patterns (Figs 7 and 8).

Therefore, we suggest that the peaked and depleted Jericho eclogites represent gabbroic cumulates formed by variable fractionation of plagioclase, clinopyroxene and

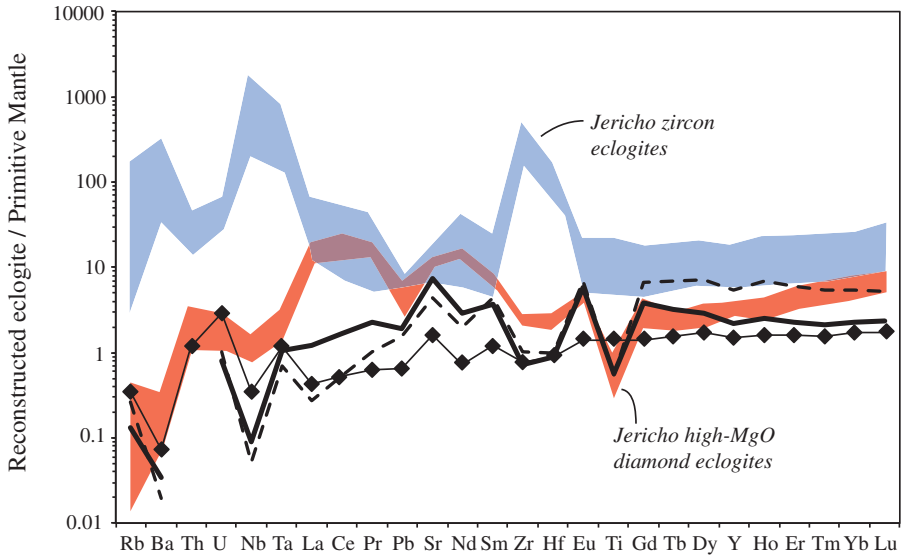

Fig. 10. Comparison of the three eclogite patterns from this study (symbols as in Fig. 8) with the high-MgO diamond-bearing eclogites and zircon-bearing eclogites from the Jericho kimberlite that contain evidence of modal and cryptic metasomatism. The high-MgO diamond-bearing eclogites (Smart *et al.*, 2009) have much higher contents of REE from La to Sm, and also of Nb, Pb, Zr and Hf compared with the Jericho eclogites of this study. Zircon-bearing eclogites (Heaman *et al.*, 2002) have overall much higher trace-element contents than the eclogites studied here and also display extremely high HFSE contents. Primitive-mantle normalization values are from McDonough & Sun (1995).

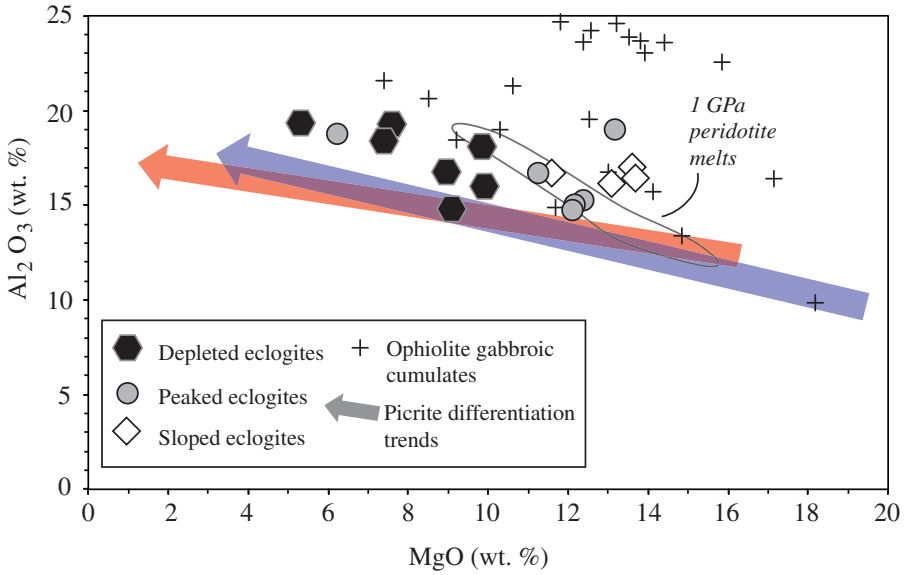

Fig. 11. Calculated bulk-rock eclogite compositions showing a diffuse negative trend in Al_2O_3 vs MgO (wt %) space that parallels picritic melt differentiation trends. Mafic cumulates from the Oman ophiolite are from Benoit *et al.* (1996). Picrite differentiation trends are from Eggins (1993) and Alonso-Perez (2006). Field of experimental melts of peridotite at 1 GPa is from Baker & Stolper (1994).

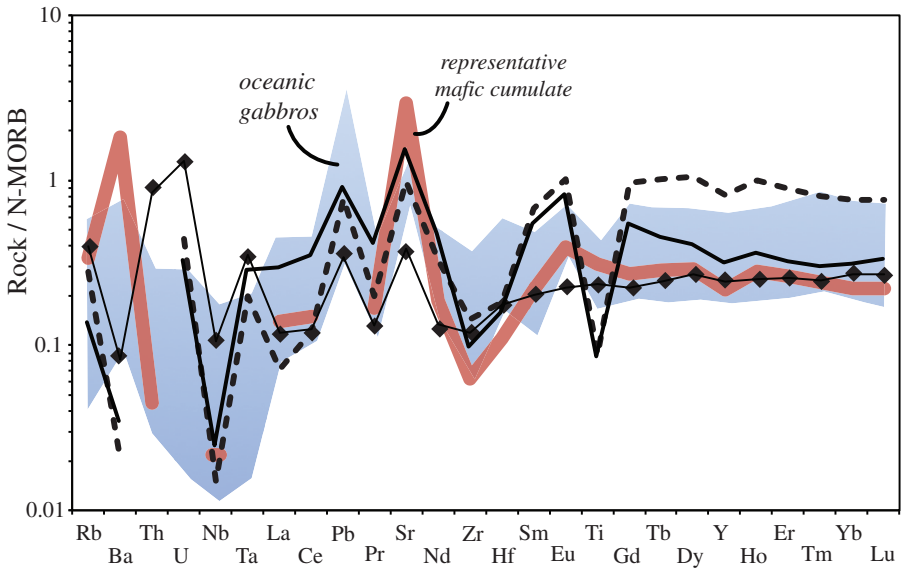

Fig. 12. MORB-normalized trace-element patterns of the peaked, depleted and sloped Jericho and Muskox eclogites with oceanic gabbros (Bach *et al.*, 2001) and a representative olivine gabbro cumulate from the Oman ophiolite (Benoit *et al.*, 1996). Symbols for eclogites are as in Fig. 8. N-MORB normalizing values are from Sun & McDonough (1989).

olivine from evolving basaltic–picritic magmas during formation of ancient oceanic crust. Trace-element modeling of a gabbroic cumulate crystallized from a partial melt of depleted MORB mantle (model details are described in the caption to Fig. 13) shows that the resulting REE pattern has a positive Eu anomaly of 1·8, flat HREE and a slight depletion in the LREE (Fig. 13a). The model gabbro REE pattern resembles both the peaked and depleted eclogites (Fig. 13a), but is lacking some of the more pronounced LREE depletion observed in the depleted eclogites. The REE pattern of the peaked eclogites is strikingly similar to that of modern oceanic and ophiolitic gabbros (Fig. 13a); in comparison, the depleted eclogites have lower LREE and higher HREE contents. This depletion in the most incompatible elements, in combination with the lower SiO_2 contents observed in the depleted eclogites

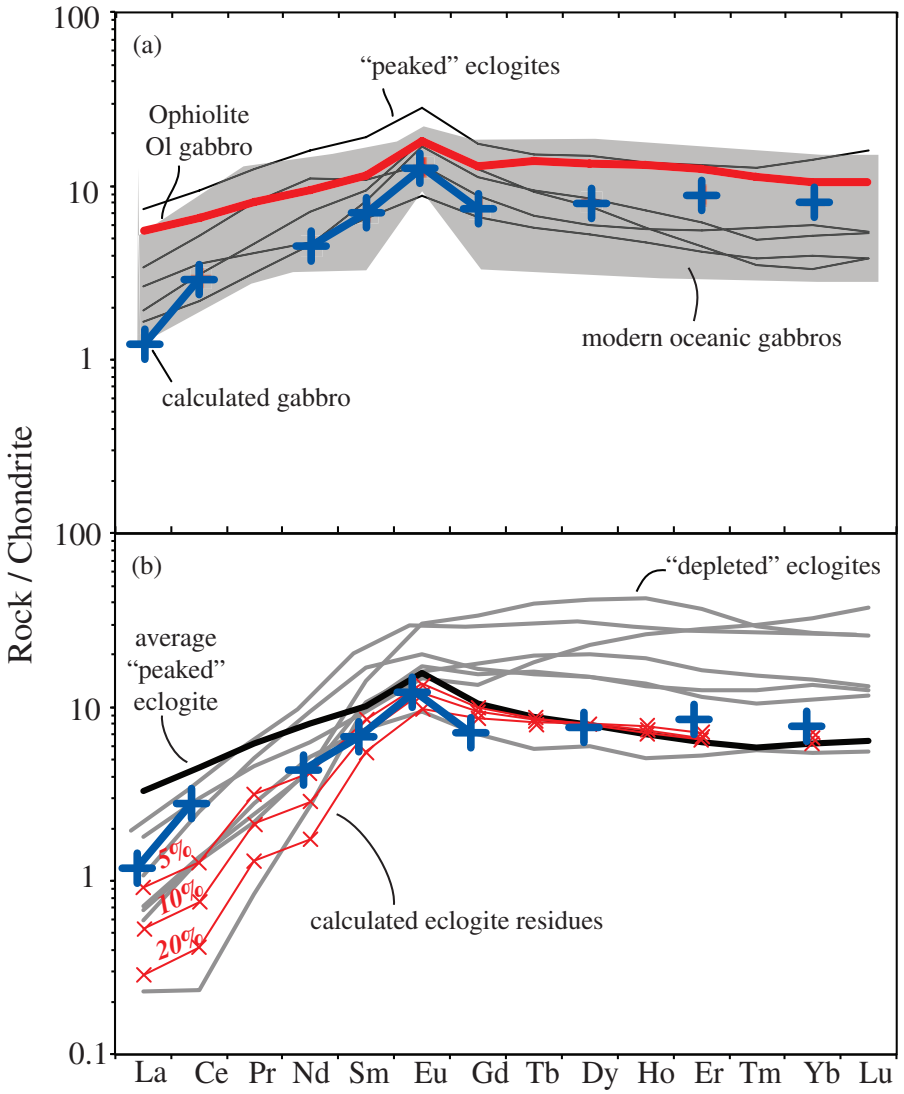

Fig. 13. Trace-element modeling of the petrogenesis of the Jericho peaked and depleted eclogites. (a) Comparison of peaked eclogites with modeled gabbro. The model gabbro composition was calculated to have formed from a 6% fractional partial melt of depleted MORB mantle (DMM) [starting composition and fraction of melting from Workman & Hart (2005)] using the partition coefficients of Kelemen *et al.* (1993). The gabbro composition was calculated assuming 90% fractional crystallization of this melt using the partition coefficients for plagioclase, pyroxenes and olivine from Norman *et al.* (2005). The modal abundance of plagioclase, clinopyroxene, orthopyroxene and olivine (53%, 20%, 0%, 27%) used for the calculated gabbro was determined from the average CIPW norms calculated for the whole-rock compositions of peaked Jericho eclogites. Field of oceanic gabbros is from Bach *et al.* (2001) and representative ophiolite olivine gabbro is from Benoit *et al.* (1996). (b) Jericho depleted eclogites are modeled as residual peaked eclogites after partial melt extraction at high pressure. Incremental 5, 10 and 20% batch partial melts were extracted from the average peaked Jericho eclogite using partition coefficients for gabbroic-protolith eclogite/melt from Yaxley & Sobolev (2007) and a mode of 50% garnet and 50% clinopyroxene. Chondrite normalization values are from McDonough & Sun (1995).

(Fig. 6e), is evidence for removal of a partial melt from these eclogites.

Effect of melt depletion

Low SiO_2 for a given MgO content is often observed in eclogite xenoliths when compared with both oceanic crust and Phanerozoic crustal eclogites (Pearson *et al.*, 2003), and is commonly ascribed to partial melt extraction (e.g. Ireland *et al.*, 1994; Jacob & Foley, 1999). Partial melting of oceanic crust in Archean subduction zones has often been cited as the mechanism for tonalite–trondjhemite–granodiorite (TTG) production and cratonic crust growth (Ireland *et al.*, 1994), which left behind eclogite residues that were entrained in the cratonic mantle lithosphere. Jacob & Foley (1999) demonstrated that addition of a hypothetical eclogite melt product (e.g. tonalite) can

'restore' the SiO_2 composition of mantle eclogite xenoliths back to basaltic compositions. Here, we apply the same principle, and show that addition of 5–10% tonalitic melt to the calculated depleted eclogite compositions is sufficient to reach the SiO_2 contents of Archean basalts or modern gabbros (dashed lines in Fig. 6e). Trace-element modeling of 5–20% bulk partial melt extraction from the peaked eclogites, shown in Fig. 13b (details of the modeling are given in the figure caption), produces the appropriate range of LREE depletion displayed by the depleted eclogites. Thus, variable amounts of partial melt extraction from the peaked group of eclogites appear to be responsible for the composition of the depleted eclogites.

Sloped eclogites

Protolith formation as second-stage melts

In contrast to the gabbroic nature of the Jericho peaked and depleted eclogites, the sloped eclogites lack Eu and Zr anomalies, display both concave-up REE (Jericho) and fractionated HREE (Muskox) patterns (Fig. 7d), and have relatively smaller positive Sr anomalies (Fig. 10). Additionally, the sloped eclogites are compositionally more uniform and appear to be more 'primitive', having elevated Mg-numbers of 75–76 and overall lower contents of REE (Figs 7a and 8a). Combined with the elevated $\delta^{18}O$ values of 6·5–6·6‰ in these eclogites, we suggest an origin as seawater-altered basaltic–picritic lavas rather than plagioclase-rich gabbros. However, the REE patterns of the Jericho and Muskox sloped eclogites do not resemble typical normal mid-ocean ridge basalt (N-MORB) or enriched (E-)MORB patterns; instead, the overall lower trace-element contents and higher Mg-numbers imply that the magma source for these eclogites was similarly depleted. Low-Mg and high-Ca eclogites from the Lac de Gras kimberlites, 100 km south of Jericho, have trace-element patterns that resemble those of the Muskox and Jericho sloped eclogites, respectively. The low-Mg eclogites of Diavik (Aulbach *et al.*, 2007) and the Muskox eclogites of this study have similar positively sloping HREE patterns and subchondritic Zr/Hf values, features that Aulbach *et al.* (2007) noted as similar to melts formed from previously depleted sources, such as boninites (e.g. Wyman, 1999; Polat *et al.*, 2002; Smithies *et al.*, 2004). The resemblance between the Muskox sloped eclogites and boninites is demonstrated in Fig. 14, and the higher MgO contents in these eclogites support derivation from previously depleted sources.

In contrast, the Jericho sloped eclogites with concave-up REE patterns and a strong MREE plateau (see Jde25) resemble the high-Ca and diamond-bearing HREE-enriched eclogites from the Lac de Gras area (Aulbach *et al.*, 2007, 2011*b*). The Lac de Gras eclogite groups were proposed to form by fluid-mediated eclogitization of a subducting slab, driven by the influx of massive amounts of subduction fluids related to serpentinite dehydration in the deeper mantle sections of the slab (Aulbach *et al.*, 2011*b*). Considering the similar concave REE pattern with an MREE plateau, a subduction-fluid mediated origin may also be acceptable for the Jericho sloped eclogites. Diamond formation is intimately associated with the serpentinite-fluid eclogitization in the Lac de Gras eclogites (Aulbach *et al.*, 2011*b*), and an oceanic mantle lithosphere-derived fluid may also serve to explain the presence of diamond with broadly mantle-like $\delta^{13}C$ values between −3·5 and −5·3‰ (Smart *et al.*, 2011) in the Jericho sloped eclogites.

Isotopic composition and possible age of the Jericho eclogites

Pb isotope age constraints

The geochemical data suggest that, despite some petrological differences, all three Jericho eclogite groups probably had oceanic lithosphere protoliths. In the Slave craton there are two proposed subduction events that may have resulted in the incorporation of oceanic crust into the lithospheric mantle: (1) subduction associated with juvenile terrane accretion and craton amalgamation at *c.* 2·7–2·6 Ga (Davis *et al.*, 2003); (2) collision of the Hottah terrane and development of the Great Bear Magmatic arc as part of the Wopmay orogeny at *c.* 1·8–2·1 Ga (Hildebrand *et al.*, 1987; Cook, 2011). If the Jericho Pb isotope data array (Fig. 5) represents a secondary isochron, then the slope of that array yields a Paleoproterozoic age of $1{\cdot}7 \pm 0{\cdot}3$ Ga, which, within error, is consistent with the age of the Wopmay orogeny, and may represent the timing of eclogitization during subduction of oceanic crust at the western margin of the Slave craton. However, another possibility is that the Pb isotope array shown in Fig. 5 represents mixing of Pb between the eclogite protolith and the host kimberlite. Isotopic mixing arrays between 'protolith' and host kimberlite are commonly used to explain isotopic variations in mantle samples (e.g. Schmidberger *et al.*, 2007; Tappe *et al.*, 2011; Hunt *et al.*, 2012); however, in such cases, elemental and isotopic ratio correlations are often observed. There is no correlation of Pb content with $^{206}Pb/^{204}Pb$ ratios in the Jericho clinopyroxenes ($r^2 = 0{\cdot}09$, not shown) but it is possible that the Pb systematics of the Jericho eclogites may have been disturbed by secondary processes.

Diffusion of Pb isotopes in clinopyroxene is relatively slow even at elevated temperatures, such that original compositions can be retained by 1 mm grains of clinopyroxene at moderate cratonic mantle temperatures of 900°C for 10 Myr timescales, although this has been shown to be highly dependent on clinopyroxene composition and oxygen fugacity (Cherniak, 2001). Most of the Jericho eclogites record a range of equilibration temperatures from 850 to 1250°C and contain 1–3 mm clinopyroxene

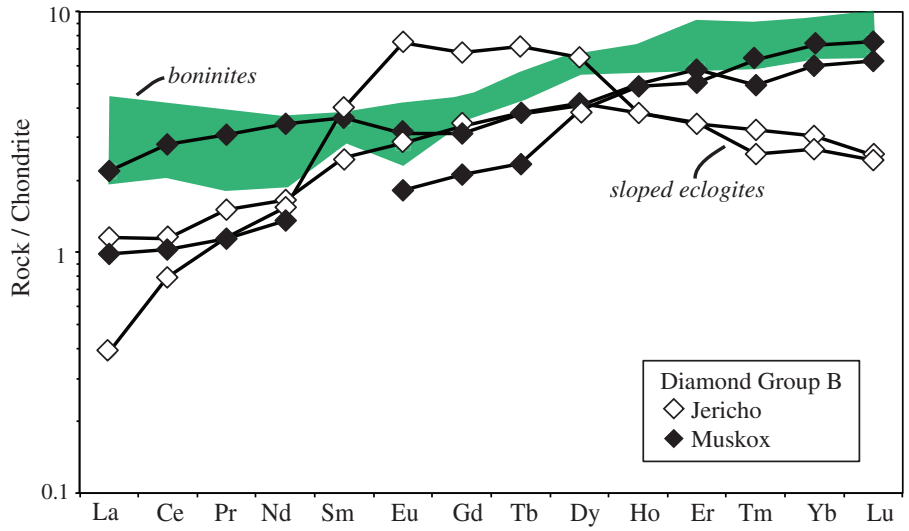

Fig. 14. Comparison of the Jericho and Muskox sloped eclogites with Archean and modern boninite lavas (Polat *et al.*, 2002; König *et al.*, 2008). Chondrite normalization values are from McDonough & Sun (1995).

grains. If contact with any metasomatic agents (e.g. the host kimberlite before eruption) or exchange with high-μ lithologies occurred only on short timescales, then it is possible that the clinopyroxene grains could retain their near-primary Pb isotope composition. Coupled with the low U/Pb values in the Jericho clinopyroxene and assuming the Pb isotope compositions were 'frozen in' the clinopyroxene shortly after eclogitization of the subducting slab (owing to slab melting; see below), we argue that the Pb isotope compositions of the clinopyroxene closely represent that of the protolith.

To determine a common Pb model age for the Jericho eclogites, we applied the Stacey & Kramers (1975) two-stage Pb evolution model. This model is a reasonable approximation of the Pb isotopic evolution in the upper mantle (Stacey & Kramers, 1975), which in turn is an appropriate model reservoir for extraction of the Jericho oceanic lithosphere protoliths. Eclogite Jer 3 intersects the Stacey–Kramers curve at *c.* 2·2 Ga, and provides good evidence for Paleoproterozoic formation of the Jericho protoliths. However, it must be stressed that the 2·2 Ga model age is a minimum age. It is possible that at some point during eclogite petrogenesis, clinopyroxene could have evolved at a high-μ value such that the least radiogenic isotopic composition preserved in the Jericho clinopyroxene ($^{206}Pb/^{204}Pb = 14{\cdot}7$) is not representative of the initial isotopic ratio as assumed above. This speculation is significant in that it would imply pre 2·2 Ga (Archean?) eclogite formation and preservation in the northern Slave craton. However, Archean eclogite formation is not considered likely as there is no independent line of evidence for older eclogite formation, and the Pb model ages determined here overlap well with Hf model ages of 2·1 ±0·1 and 2·3 ± 0·1 Ga determined from zircons extracted from the Jericho high-FeO eclogites (Schmidberger *et al.*, 2005).

The minimum model age of 2·2 Ga is ~100–300 Myr older than the known subduction events associated with formation of the *c.* 2·1–1·9 Ga Hottah arc terrane or *c.* 1·87–1·84 Ga Great Bear Magmatic zone in the Wopmay orogeny (Cook, 2011). The age discrepancy may be attributed to the time difference between stages of a Wilson cycle; for example, formation of the protolith oceanic crust, eclogitization and incorporation into the cratonic mantle lithosphere during subduction (e.g. Shirey & Richardson, 2011). Furthermore, if we consider the isotopic composition of clinopyroxene from Jer 3 to represent that of the Paleoproterozoic protolith oceanic crust (and, by proxy, the mantle source), then we must account for in-growth of radiogenic Pb between oceanic crust formation and clinopyroxene growth during eclogitization. Considering extraction of oceanic crust from the depleted mantle at *c.* 2·2 Ga, possibly followed by seawater alteration in which hydrothermal alteration preferentially strips Pb over U, increasing both the U/Pb (and thus the μ-value) of the altered crust (Chauvel *et al.*, 1992), the oceanic crust would have *c.* 200 Myr of radiogenic Pb in-growth prior to eclogitization. Fluid and/or partial melt extraction that accompanied subduction would preferentially remove U relative to Pb (Klemme *et al.*, 2002), lowering both the bulk-rock eclogite and thus clinopyroxene U/Pb (<0·15 and <0·07, respectively, for the Jericho eclogites), and thus significantly slow down isotopic in-growth, effectively freezing in the Pb isotopic ratios.

Assuming μ values for 'normal' oceanic crust (μ = 8) and HIMU-type oceanic crust (μ = 22), the $^{206}Pb/^{204}Pb$ value increases between 0·25 and 0·7. This small change is

almost encompassed by the large error ellipses on the clinopyroxene Pb data in Fig. 5, and thus does not affect the overall interpretation that the Jericho eclogites have Paleoproterozoic formation ages. Applying the common Pb model age method to the Jericho eclogites requires that the smearing of the remaining Jericho Pb data towards more radiogenic isotope compositions may be due to mixing of Pb between Paleoproterozoic mantle and Phanerozoic kimberlite sources, and therefore the *c.* 1·7 Ga age calculated from the Pb secondary isochron may be meaningless. Regardless of whether the 1·7 ± 0·3 Ga secondary isochron or the 2·2 Ga minimum model age is preferred for the Jericho eclogites, the overall interpretation that the Jericho eclogites formed in the Paleoproterozoic remains unchanged.

Two other eclogite suites from the Slave craton provide geochronological evidence that may capture different stages of Wilson cycle processes. Eclogites from the Diavik kimberlite (Schmidberger *et al.*, 2007) have older Pb model ages (2·4–2·3 and 2·1 Ga) but a younger Lu–Hf errorchron age (2·1 ± 0·3 Ga), whereas zircon-bearing eclogites also from Jericho (Schmidberger *et al.*, 2005) have Hf model ages between 2·1 and 2·3 Ga and U–Pb ages of 1·9 Ga. In both these studies, the older model ages are interpreted to mark oceanic crust (protolith) formation whereas the younger ages mark subduction and eclogitization of the oceanic crust *c.* 200 Myr later. As demonstrated above, 200 Myr of isotopic in-growth does not substantially change the Pb isotope ratios and age interpretations.

Insights from Sr isotopes

Further insight into potential isotope mixing processes is gained from the Sr isotope systematics of the Jericho eclogites. The $^{87}Sr/^{86}Sr$ compositions of the eclogite clinopyroxene range between 0·7032 and 0·7052, but a large proportion of the data are *c.* 0·7040. If protolith formation is assumed to have occurred at *c.* 2·2 Ga, then it is reasonable to assume that the eclogite clinopyroxene may preserve the Sr isotopic compositions of Paleoproterozoic oceanic lithosphere, given that the radiogenic in-growth of Sr isotopes during the 200 Myr between oceanic crust extraction from the upper mantle and eclogitization during subduction will change the $^{87}Sr/^{86}Sr$ values by only 0·0002 (using Rb/Sr ratios of unaltered and seawater-altered oceanic crust; Bach *et al.*, 2001). Using the parameters given by Workman & Hart (2005), the $^{87}Sr/^{86}Sr$ ratio of oceanic crust extracted from depleted MORB mantle at *c.* 2 Ga is *c.* 0·7010, which is clearly much lower than the values observed in the Jericho eclogites. The oxygen isotope compositions of some Jericho eclogites indicate that seawater alteration may have affected some protoliths, and it is possible that this alteration could have caused the protoliths to assume the Sr isotopic composition of Paleoproterozoic seawater (0·7040 at *c.* 2 Ga; Veizer & Compston, 1976) in a similar fashion to the *c.* 2 Ga eclogites from the Diavik kimberlite (Schmidberger *et al.*, 2007). However, there are still some Jericho eclogite clinopyroxenes with $^{87}Sr/^{86}Sr$ values significantly higher than 0·7040 that cannot reasonably be explained by this process. Mixing with a more radiogenic metasomatic component, comparable with the Jericho kimberlite, may explain some of the variation in both the Sr and Pb isotopic compositions of the Jericho eclogites. It is interesting that clinopyroxenes from the peaked eclogites largely have more radiogenic Sr isotope compositions compared with the depleted eclogites, and the same pattern is also be observed in the Pb isotope compositions (Fig. 5). This may suggest that the peaked eclogite group was affected to a greater extent by later metasomatic events.

The effect of kimberlite-related metasomatism

Figure 15 explores Sr–Pb isotope mixing relationships between (seawater-altered) Paleoproterozoic oceanic crust and potential metasomatic components. The mixing models require several components, including 'pristine' 2·2 Ga oceanic crust, seawater-altered *c.* 2 Ga oceanic crust, and a metasomatic agent, which we interpret to be the host Jericho kimberlite, or a similar 'pre-kimberlitic' fluid or melt (see Kopylova *et al.*, 2009). All model values and sources are detailed in Table 7 and the captions to Figs 5 and 15. The Sr and Pb isotopic compositions of the Jericho clinopyroxenes define a diffuse, positively sloped array between relatively unradiogenic and more radiogenic Sr and Pb end-members (Fig. 15). Mixing between unaltered 2·2 Ga oceanic crust and the kimberlite-like metasomatic agents produces a mixing curve that does not correspond to the eclogite clinopyroxene because of the low $^{87}Sr/^{86}Sr$ of the oceanic crust. However, if a seawater-altered protolith is used (with more radiogenic initial Sr and a slightly more radiogenic Pb isotopic composition), mixing with the kimberlite produces mixing curves that approximate the array shown by the Jericho eclogites. From Fig. 15, regardless of whether the $^{206}Pb/^{204}Pb$ ratios for unaltered or altered oceanic crust are used, it appears that <1 to 5% mixing of the kimberlitic metasomatic agent (with the higher $^{87}Sr/^{86}Sr$ ratio) provides the best approximation of the eclogite data. In general, the depleted eclogites require less than 1% kimberlite mixing, whereas the peaked eclogites require more kimberlite metasomatism, up to 5%. Several of the diamond-bearing high-MgO eclogites (diamonds in Fig. 15) from Smart *et al.* (2009), however, appear to require much higher amounts of the metasomatic agent (>20%) to produce the more radiogenic compositions. However, addition of >20% kimberlite would produce decidedly non-basaltic compositions, and as such, Smart *et al.* (2009) attributed the radiogenic isotopic composition of the high-MgO diamond-bearing eclogites to an early LREE-enriched metasomatic event, possibly associated with diamond formation.

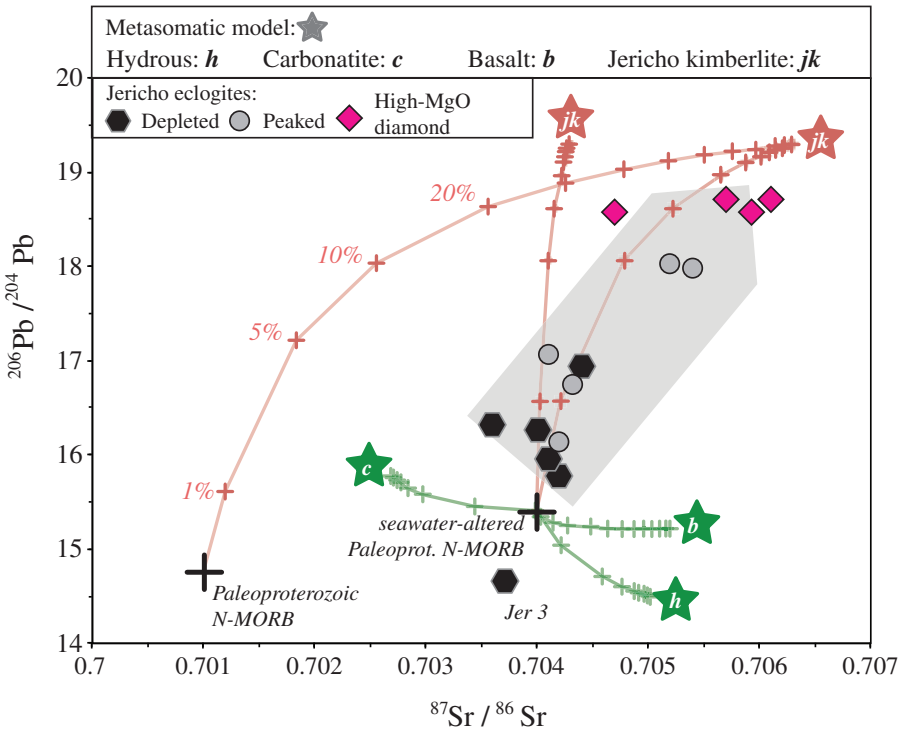

Fig. 15. Relationship between the Sr and Pb isotope compositions of clinopyroxene from the Jericho eclogites. The effects of potential metasomatic overprinting of the hypothesized oceanic crust protolith by either the Jurassic host Jericho kimberlite and/or various agents associated with the Mesoproterozoic Mackenzie Igneous Event are considered. All mixing lines represent increments of 1 and 5%, followed by 10%, 20%, and higher proportions of the metasomatic agent; representative mixing increments are indicated for the mixing curve between Paleoproterozoic N-MORB with Jericho kimberlite. It should be noted that sample 44-9 is not plotted. All parameters used in the isotopic modeling are discussed in the text and listed in Table 7.

Table 7: Parameters for isotopic mixing models in Fig. 15

	2·2 Ga oceanic crust		173 Ma Jericho kimberlite		1·27 Ga Mackenzie Event		
	Unaltered	Seawater altered	Radiogenic	Unradiogenic	Basalt	Lamproite/Hydrous	Carbonatite
$^{87}Sr/^{86}Sr$	0·7010[a]	0·7040[d]	0·7063[g]	0·7043[g]	0·7052[j]	0·705[k]	0·7025[l]
Sr (ppm)	150[b]	55[e]	560[h]	560[h]	146[j]	1500[k]	4200[l]
$^{206}Pb/^{204}Pb$	14·74[c]	15·40[f]	19·30[i]	19·30[i]	15·21[j]	14·50[k]	16·10[m]
Pb (ppm)	0·34[b]	0·19[e]	8[h]	8[h]	7[j]	12[k]	3·5[m]

[a]Calculated from Workman & Hart (2005), assuming derivation from depleted MORB mantle.
[b]From Bach *et al.* (2001).
[c]Calculated from Stacey & Kramers (1975) at 2·2 Ga.
[d]Estimated from Veizer & Compston (1976) at *c.* 2 Ga.
[e]Eclogitic residue after 10% batch melt extraction from [b], partition coefficients from Klemme *et al.* (2002).
[f]Isotopic composition of [c] evolved for 200 Myr at $\mu = 22$ to represent evolution of altered oceanic crust with high U/Pb; details are given in the discussion.
[g]Minimum and maximum values of Jericho whole-rock kimberlite; taken from Kopylova *et al.* (2009).
[h]Average from Price *et al.* (2000).
[i]Initial value for proximal 170 Ma Voyageur kimberlite from S. Tappe (personal communication, 2012); rationale is given in text.
[j]Average values of the Muskox intrusion taken from Purves (2007).
[k]Average values from 1·37 Ga olivine lamproite located in the North Atlantic craton of eastern Canada (Tappe *et al.*, 2007).
[l]Taken from 1170 Ma North American carbonatites (Bell & Blenkinsop, 1989).
[m]Taken from 1170 Ma North American carbonatite (Kwon *et al.*, 1989).

Potential Mesoproterozoic metasomatic event

Age information derived from eclogitic diamond inclusions and eclogite xenoliths from Slave craton kimberlites shows peaks in the Paleoproterozoic, at *c.* 2 Ga (Schmidberger *et al.*, 2005, 2007; Aulbach *et al.*, 2009*a*), whereas peridotitic diamond inclusions show peaks in the Neo- and Mesoarchean at *c.* 2·7–3 Ga (e.g. Irvine *et al.*, 2003; Aulbach *et al.*, 2009*b*) and, significantly, ages >3 Ga are rare (e.g. Westerlund *et al.*, 2006; Aulbach *et al.*, 2009*b*). In contrast, peridotite and zircon-bearing eclogite xenoliths from the Jericho kimberlite display a noteworthy abundance of Mesoproterozoic 1·3 Ga model ages (Irvine *et al.*, 2003; Heaman *et al.*, 2006), which have been attributed to modification of the northern Slave cratonic mantle by the 1·27 Ga Mackenzie Large Igneous Event (Le Cheminant & Heaman, 1989). The abundance of Mackenzie ages from Jericho mantle material compared with the effective absence from the central Slave mantle is probably due to the proximity of Jericho to the focal point of the Mackenzie intrusions in the northernmost Slave craton. The Mackenzie event involved large-scale mafic magmatism for which a mantle plume at the base of the lithosphere is thought to be the impetus (Le Cheminant & Heaman, 1989). The presence of a thermal anomaly at the base of the northern Slave cratonic mantle may have also caused volatile-driven incipient melting and the generation of low-volume, silica-poor, volatile-rich melts, such as carbonatite- or lamproite/kimberlite-like melts (e.g. Dalton & Presnall, 1998; Wallace & Green, 1988; Ernst & Bell, 2010) that would be extremely reactive with the cratonic mantle (e.g. Tappe *et al.*, 2012). The impact of such metasomatic events on cratonic mantle has been well studied in peridotite systems (e.g. Rudnick *et al.*, 1993; Klemme *et al.*, 1995), whereas less is known about the different effects in the eclogitic system (e.g. Jacob *et al.*, 2009). The Jericho eclogites of this study contain secondary veins of calcite, apatite and phlogopite, which are probably the product of kimberlite infiltration. In contrast, both the high-MgO diamond-bearing and zircon-bearing eclogites from Jericho contain macrocystal phlogopite that is attributed to carbonatite-driven metasomatism (Smart *et al.*, 2009). Combined with Sm–Nd isotopic evidence from the zircon-bearing eclogites, this metasomatism has been hypothesized to be associated with the Mesoproterozoic Mackenzie event (Heaman *et al.*, 2006). Thus, although there is no resolvable isotopic evidence that clearly indicates Mackenzie-age metasomatism in the Jericho eclogites of this study (i.e. no 1·3 Ga Pb model ages are observed), and kimberlite–eclogite mixing can account for the eclogite Sr–Pb isotope systematics, no relationships exist between Sr and Pb concentrations and isotopic ratios ($^{87}Sr/^{86}Sr$ and Sr, $r^2 = 0{\cdot}33$; $^{206}Pb/^{204}Pb$ and Pb, $r^2 = 0{\cdot}09$). Although it may be over-optimistic to expect clear geochemical correlations in mantle-derived samples, the complete lack of any relationship could indicate that the eclogite system was disturbed by multiple metasomatic events during their storage in the Slave cratonic mantle.

The potential isotopic effect(s) of a 1·3 Ga Mackenzie-driven metasomatic event are estimated in Fig. 15. The nature of this metasomatic event is difficult to constrain, and as such we have adapted three separate approaches. The first approach (Basaltic model) assumes that the Jericho cratonic mantle lithosphere was affected by the same mafic melts as now manifested in the Slave crust as widespread flood basalts, mafic dikes and the Muskox layered intrusion. The increasing Y, Zr, Ti and FeO contents with depth observed in Jericho peridotite xenoliths are consistent with melt (basaltic)-metasomatism (Griffin *et al.*, 2004*b*). Constraints for this Basaltic model are taken from the Muskox layered intrusion from the northern Slave (Purves, 2007). The second (Hydrous model) and third (Carbonatite model) approaches are based on the assumption that low-volume, volatile-rich melts, which are more likely to be generated at plume peripheries (e.g. Wyllie, 1988), would be a better approximation of the thermal and melting regime present in the 1·3 Ga Jericho cratonic mantle lithosphere. Hydrous melting of peridotite produces lamproitic-type melts (e.g. Foley, 1993), whereas carbon-fluxed melting of peridotite produces carbonatite-like melts (e.g. Wallace & Green, 1988). Evidence for the influx of hydrous melts may be inferred from the presence of phlogopite and MARID-like geochemical signatures in Slave mantle xenoliths (Aulbach *et al.*, 2007; Smart *et al.*, 2009), whereas evidence of carbonatite-driven metasomatism is provided by carbonatite-like inclusions in kimberlite-derived megacrysts and diamonds from central Slave kimberlites (van Achterberg *et al.*, 2002; Klein-BenDavid *et al.*, 2007). For both the Hydrous and Carbonatite models, the metasomatic agents are estimated from Canadian Mesoproterozoic lamproites (Tappe *et al.*, 2007) and carbonatites (Bell & Blenkinsop, 1989; Kwon *et al.*, 1989). Details of the geochemical and isotopic composition of the models are found in Table 7 and the caption of Fig. 15.

Figure 15 shows the estimated effects of a Mackenzie-related metasomatic event. Mixing of the protolith with either basaltic melts (Basalt model) or low-volume, hydrous melts (Hydrous model) produces arrays with relatively unradiogenic $^{206}Pb/^{204}Pb$ values that do not correspond to the isotopic compositions of the Jericho eclogites. These metasomatic agents are further dismissed because the Jericho eclogites do not preserve any strong features of basaltic melt-metasomatism; specifically, the garnet has low TiO_2 contents (<0·15 wt %) and lacks strong enrichments in Zr (<20 ppm) (Fig. 9; e.g. Griffin *et al.*, 2004*a*). By comparison, mixing of the protolith with the model carbonatite produces arrays with less radiogenic $^{87}Sr/^{86}Sr$ values than observed in the Jericho eclogites.

Therefore, straightforward mixing of an oceanic crustal protolith in any of the Mesoproterozoic metasomatic models does not produce the observed Sr–Pb isotope systematics of the Jericho eclogites. Although the protoliths of the mantle xenoliths have long residence times in the cratonic mantle, and the probability is high that those protoliths have been affected by more than one metasomatic event (e.g. three-component mixing in Fig. 15), it appears that in the case of the Jericho eclogites the simplest explanation for the isotopic data involves metasomatism of the Paleoproterozoic oceanic protoliths by an agent similar to the host Jericho kimberlite (shaded arrow in Fig. 15).

Relationship to tectonomagmatic events in the Slave craton

Cratons such as the Kaapvaal craton in southern Africa and the North Atlantic craton in West Greenland–northeastern Canada preserve excellent links between Archean crustal growth, subduction events and the formation of eclogites (± diamonds) in the cratonic mantle (e.g. Shirey *et al.*, 2004; Wittig *et al.*, 2010; Tappe *et al.*, 2011). However, Neoarchean eclogitic mantle material, which is documented ubiquitously from the Kaapvaal craton, is thus far completely absent from the Slave craton in NW Canada. Instead, abundant Paleoproterozoic, *c.* 1·8–2·2 Ga eclogite xenoliths and eclogite-type diamond inclusions are known from kimberlites from both the central and northern part of the Slave craton (e.g. this study; Schmidberger *et al.*, 2005, 2007; Aulbach *et al.*, 2009*a*, 2009*b*). The apparent absence of older eclogitic material from the Slave craton is interesting in light of the evidence for a Neoarchean craton amalgamation event (Davis *et al.*, 2003) that could have emplaced eclogitic material into the cratonic mantle and perhaps contributed to diamond formation at this time (e.g. Smart *et al.*, 2011). Because glimpses of Neoarchean magmatic events are recorded in Slave peridotite xenoliths and P-type diamond inclusions (e.g. Irvine *et al.*, 2003; Aulbach *et al.*, 2009*b*), the apparent absence of a Neoarchean eclogitic record may be due to purging of the older, dense eclogites from the cratonic mantle root (e.g. Pearson & Wittig, 2008; Tappe *et al.*, 2011) or to the heterogeneous sampling patterns of kimberlites (Aulbach *et al.*, 2009*a*). Nevertheless, subduction associated with the Paleoproterozoic Wopmay orogeny appears to have been an active contributor of significant amounts of basaltic and volatile (e.g. carbon) components to the Slave cratonic mantle, which is manifested in the occurrence of *c.* 2 Ga eclogite xenoliths and diamond inclusions (this study; Schmidberger *et al.*, 2005, 2007; Aulbach *et al.*, 2009*a*; Smart *et al.*, 2011). Furthermore, evidence for Mesoproterozoic metasomatism of the Slave cratonic root that is associated with the Mackenzie Large Igneous Event is recorded in the northern Slave mantle lithosphere, where *c.* 1·3 Ga model ages have been obtained for some Jericho peridotite xenoliths (Irvine *et al.*, 2003) and eclogite xenoliths (Heaman *et al.*, 2006). This Mesoproterozoic overprint, although not clearly recorded in the eclogites of this study, may nevertheless have contributed to cryptic Sr and Pb isotopic modifications. The integrated studies of Jericho mantle materials clearly suggest that major crustal events that affected the post-Archean Slave craton also significantly affected the Slave mantle lithosphere. Although the Slave cratonic mantle appears to have either lost or concealed a significant part of its Archean eclogite memory, it provides strong evidence for the operation of Paleoproterozoic subduction-driven modification processes that occurred during the assembly of the Laurentia supercraton (Hoffman, 1989).

ACKNOWLEDGEMENTS

We thank Tahera Diamond Corporation and M. Kopylova for provision of the eclogite samples. K.A.S. thanks S. Tappe for the highly beneficial discussions and insight into the isotopic composition of the Voyageur kimberlite. The authors are indebted to S. Aulbach, G. Yaxley and an anonymous reviewer for constructive reviews and M. Wilson for seamless editorial handling. We thank S. Matveev for his assistance with the EMPA analyses at UA, and V. Altudorei for his support with the oxygen isotope analyses at UNM.

FUNDING

K.A.S. acknowledges an NSERC PGS-D scholarship and an A. von Humboldt Post-Doctoral Fellowship. This work was supported by funding provided by National Science and Engineering Research Council of Canada (NSERC) Discovery grants to T.C. and L.M.H.

SUPPLEMENTARY DATA

Supplementary data for this paper are available at *Journal of Petrology* online.

REFERENCES

Alonso-Perez, R. (2006). The role of garnet in the evolution of hydrous, calc-alkaline magmas: An experimental study at 0·8–1·5 GPa, PhD thesis, Swiss Federal Institute of Technology, Zurich.

Alt, J. C., Anderson, T. F., Bonnell, L. & Muehlenbachs, K. (1989). Mineralogy, chemistry, and stable isotopic composition of hydrothermally altered sheeted dikes: ODP hole 504B, Leg 111. In: Becker, K. & Sakai, H. *et al.* (eds) *Proceedings of the Oceanic Drilling Program, Scientific Results, 111.* Ocean Drilling Program, pp. 27–40.

Aulbach, S. (2012). Craton nucleation and formation of thick lithospheric roots. *Lithos* **149**, 16–30.

Aulbach, S., Pearson, N. J., O'Reilly, S. Y. & Doyle, B. J. (2007). Origins of xenolithic eclogites and pyroxenites from the central Slave Craton, Canada. *Journal of Petrology* **48**, 1843–1873.

Aulbach, S., Stachel, T., Creaser, R. A., Heaman, L. M., Shirey, S. B., Muehlenbachs, K., Eichenberg, D. & Harris, J. W. (2009*a*). Sulphide survival and diamond genesis during formation and

evolution of Archaean subcontinental lithosphere: A comparison between the Slave and Kaapvaal cratons. *Lithos* **112S**, 747–757.

Aulbach, S., Creaser, R. A., Pearson, N. J., Simonetti, S. S., Heaman, L. M., Griffin, W. L. & Stachel, T. (2009*b*). Sulfide and whole rock Re–Os systematics of eclogite and pyroxenite xenoliths from the Slave Craton, Canada. *Earth and Planetary Science Letters* **283**, 48–58.

Aulbach, S., O'Reilly, S. Y. & Pearson, N. J. (2011*a*). Constraints from eclogite and MARID xenoliths on origins of mantle Zr/Hf–Nb/Ta variability. *Contributions to Mineralogy and Petrology* **162**, 1047–1062.

Aulbach, S., Stachel, T., Heaman, L. M. & Carlson, J. A. (2011*b*). Microxenoliths from the Slave craton: Archives of diamond formation along fluid conduits. *Lithos* **126**, 419–434.

Bach, W., Alt, J. C., Niu, Y., Humphris, S. E., Erzinger, J. & Dick, H. J. B. (2001). The geochemical consequences of late-stage low-grade alteration of lower ocean crust at the SW Indian Ridge: Results from ODP Hole 735B (Leg 176). *Geochimica et Cosmochimica Acta* **65**, 3267–3287.

Baker, M. B. & Stolper, E. M. (1994). Determining the composition of high-pressure mantle melts using diamond aggregates. *Geochimica et Cosmochimica Acta* **58**, 2811–2827.

Barth, M. G., Rudnick, R. L., Horn, I., McDonough, W. F., Spicuzza, M. J., Valley, J. W. & Haggerty, S. E. (2001). Geochemistry of xenolithic eclogites from West Africa, Part I: A link between low MgO eclogites and Archean crust formation. *Geochimica et Cosmochimica Acta* **65**, 1499–1527.

Bell, K. & Blenkinsop, J. (1989). Neodymium and strontium isotope geochemistry of carbonatites. In: Bell, K. (ed.) *Carbonatites: Genesis and Evolution*. Unwin Hyman: London, pp. 278–300.

Benoit, M., Polvé, M. & Ceuleneer, G. (1996). Trace element and isotopic characterization of mafic cumulates in a fossil mantle diapir (Oman ophiolite). *Chemical Geology* **134**, 199–214.

Bizzarro, M., Simonetti, A., Stevenson, R. K. & Kursziaukis, S. (2003). *In situ* $^{87}Sr/^{86}Sr$ investigation of igneous apatites and carbonates using laser ablation MC-ICP-MS. *Geochimica et Cosmochimica Acta* **67**, 289–302.

Bleeker, W. (2003). The late Archean record: a puzzle in *ca.* 35 pieces. *Lithos* **71**, 99–134.

Bleeker, W. & Hall, B. (2007). The Slave Craton: geology and metallogenic evolution. In: Goodfellow, W. D. (ed.) *Mineral Deposits of Canada: A Synthesis of Major Deposit-Types, District Metallogeny, the Evolution of Geological Provinces, and Exploration Methods. GAC Mineral Deposits Division, Special Publication* **5**, 849–879.

Bleeker, W., Ketchum, J. & Davis, W. (1999). The Central Slave Basement Complex, Part II: age and tectonic significance of high-strain zones along the basement–cover contact. *Canadian Journal of Earth Sciences* **36**, 1111–1130.

Carlson, R. W., Pearson, D. G. & James, D. E. (2005). Physical, chemical and chronological characteristics of continental mantle. *Reviews of Geophysics* **43**, RG1001.

Chauvel, C., Hofmann, A. W. & Vidal, P. (1992). HIMU-EM: The French Polynesian connection. *Earth and Planetary Science Letters* **110**, 99–119.

Cherniak, D. J. (2001). Pb diffusion in Cr diopside, augite, and enstatite, and consideration of the dependence of cation diffusion in pyroxene on oxygen fugacity. *Chemical Geology* **177**, 381–397.

Clayton, R. N., Goldsmith, J. R., Karel, V. J., Mayeda, T. K. & Newton, R. C. (1975). Limits on the effect of pressure on isotopic fractionation. *Geochimica et Cosmochimica Acta* **39**, 1197–1201.

Coleman, R. G., Lee, E. D., Beatty, L. B. & Brannock, W. W. (1965). Eclogites and eclogites: their differences and similarities. *Geological Society of America Bulletin* **76**, 483–508.

Cook, F. A. (2011). Multiple arc development in the Paleoproterozoic Wopmay Orogen, northwestern Canada. In: Brown, D. & Ryan, P. D. (eds) *Arc–Continent Collision, Frontiers in Earth Sciences*. Springer: Berlin, pp. 403–428.

Cook, F. A., van der Velden, A. J. & Hall, K. W. (1999). Frozen subduction in Canada's Northwest Territories: Lithoprobe deep lithospheric reflection profiling of the western Canadian Shield. *Tectonics* **18**, 1–24.

Cox, K. G. (1980). A model for flood basalt vulcanism. *Journal of Petrology* **21**, 629–650.

Creaser, R. A., Grutter, H., Carlson, J. & Crawford, B. (2004). Macrocrystal phlogopite Rb–Sr dates for the Ekati property kimberlites, Slave Province, Canada: evidence for multiple intrusive episodes in the Paleocene and Eocene. *Lithos* **76**, 399–414.

Dalton, J. A. & Presnall, D. C. (1998). The continuum of primary carbonatitic–kimberlitic melt compositions in equilibrium with lherzolite: data from the system $CaO–MgO–Al_2O_3–SiO_2–CO_2$ at 6 GPa. *Journal of Petrology* **39**, 1953–1964.

Davis, W. J., Jones, A. G., Bleeker, W. & Grütter, H. (2003). Lithosphere development in the Slave craton: a linked crustal and mantle perspective. *Lithos* **71**, 575–589.

Dawson, J. B. (1984). Contrasting types of upper-mantle metasomatism. In: Kornprobst, J. (ed.) *Kimberlites II—The Mantle and Crust–Mantle Relationships*. Elsevier, pp. 289–294.

De Stefano, A., Kopylova, M. G., Cartigny, P. & Afanasiev, V. (2009). Diamonds and eclogites of the Jericho kimberlite (Northern Canada). *Contributions to Mineralogy and Petrology* **158**, 295–315.

Dhuime, B., Hawkesworth, C. J., Cawood, P. A. & Storey, C. D. (2012). A change in the geodynamics of continental growth 3 billion years ago. *Science* **335**, 1334–1336.

Eggins, S. M. (1993). Origin and differentiation of picritic arc magmas, Ambae (Aoba), Vanuatu. *Contributions to Mineralogy and Petrology* **114**, 79–100.

Eiler, J. M. (2001). Oxygen isotope variations of basaltic lavas and upper mantle rocks. In: Valley, J. W. & Cole, D. R. (eds) *Stable Isotope Geochemistry. Mineralogical Society of America and Geochemical Society, Reviews in Mineralogy and Geochemistry* **43**, 319–364.

Ellis, D. J. & Green, D. H. (1979). An experimental study of the effect of Ca upon garnet–clinopyroxene Fe–Mg exchange equilibria. *Contributions to Mineralogy and Petrology* **71**, 13–22.

Ernst, R. E. & Bell, K. (2010). Large Igneous Provinces (LIPs) and carbonatites. *Mineralogy and Petrology* **98**, 55–76.

Foley, S. F. (1993). An experimental study of olivine lamproite: First results from the diamond stability field. *Geochimica et Cosmochimica Acta* **57**, 483–489.

Gonzaga, R. G., Lowry, D., Jacob, D. E., LeRoex, A. & Menzies, M. A. (2010). Eclogites and garnet pyroxenites: Similarities and differences. *Journal of Volcanology and Geothermal Research* **190**, 235–247.

Gréau, Y., Huang, J.-X., Griffin, W. L., Renac, C., Alard, O. & O'Reilly, S. Y. (2011). Type I eclogites from Roberts Victor kimberlites: Products of extensive mantle metasomatism. *Geochimica et Cosmochimica Acta* **75**, 6927–6954.

Gregory, R. T. & Taylor, H. P. (1981). An oxygen isotope profile in a section of Cretaceous oceanic crust, Samail Ophiolite, Oman: evidence for $\delta^{18}O$ buffering of the oceans by deep (>5 km) seawater–hydrothermal circulation at mid-ocean ridges. *Journal of Geophysical Research* **86B**, 2737–2755.

Griffin, W. L. & O'Reilly, S. Y. (2007). Cratonic lithospheric mantle: Is anything subducted? *Episodes* **30**, 43–53.

Griffin, W. L., Doyle, B. J., Ryan, C. G., Pearson, N. J., O'Reilly, S. Y., Natapov, L., Kivi, K., Kretschmar, U. & Ward, J. (1999). Lithospheric structure and mantle terranes: Slave Craton, Canada. In: Gurney, J. J., Gurney, J. L., Pascoe, M. D. & Richardson, S. H. (eds) *Proceedings of the 7th International Kimberlite Conference. J. B. Dawson Volume*. Cape Town: Red Roof Design, pp. 299–306.

Griffin, W. L., O'Reilly, S. Y., Abe, N., Aulbach, S., Davies, R. M., Pearson, N. J., Doyle, B. J. & Kivi, K. (2003). The origin and evolution of Archean lithospheric mantle. *Precambrian Research* **127**, 19–41.

Griffin, W. L., Graham, S., O'Reilly, S. Y. & Pearson, N. J. (2004*a*). Lithosphere evolution beneath the Kaapvaal Craton: Re–Os systematics of sulfides in mantle-derived peridotites. *Chemical Geology* **208**, 89–118.

Griffin, W. L., O'Reilly, S. Y., Doyle, B. J., Pearson, N. J., Coopersmith, H., Kivi, K., Malkovets, V. & Pokhilenko, N. (2004*b*). Lithosphere mapping beneath the North American plate. *Lithos* **77**, 873–922.

Grütter, H. S., Apter, D. B. & Kong, J. (1999). Crust–mantle coupling: Evidence from mantle-derived xenocrystic garnets. In: Gurney, J. J., Gurney, J. L., Pascoe, M. D. & Richardson, S. H. (eds) *Proceedings of the 7th International Kimberlite Conference. J. B. Dawson Volume*. Red Roof Design, pp. 307–313.

Hart, S. R., Blusztain, J., Dick, H. J. B., Meyer, P. S. & Muehlenbachs, K. (1999). The fingerprint of seawater circulation in a 500-meter section of ocean crust gabbros. *Geochimica et Cosmochimica Acta* **63**, 4059–4080.

Hawkesworth, C. J. & Kemp, A. I. S. (2006). Evolution of the continental crust. *Nature* **443**, 811–817.

Hayman, P. C. & Cas, R. A. F. (2011). Criteria for interpreting kimberlite as coherent: insights from the Muskox and Jericho kimberlites. *Bulletin of Volcanology* **73**, 1005–1027.

Heaman, L. M., Creaser, R. A. & Cookenboo, H. O. (2002). Extreme enrichment of high field strength elements in Jericho eclogite xenoliths: A cryptic record of Paleoproterozoic subduction, partial melting, and metasomatism beneath the Slave craton, Canada. *Geology* **30**, 507–510.

Heaman, L. M., Creaser, R. A., Cookenboo, H. O. & Chacko, T. (2006). Multi-stage modification of the Northern Slave mantle lithosphere: evidence from zircon- and diamond-bearing eclogite xenoliths entrained in Jericho kimberlite, Canada. *Journal of Petrology* **47**, 821–858.

Helmstaedt, H. & Doig, R. (1975). Eclogite nodules from kimberlite pipes in the Colorado Plateau—samples of subducted Franciscan type oceanic lithosphere. *Physics and Chemistry of the Earth* **9**, 95–111.

Helmstaedt, H. & Schulze, D. J. (1989). Southern African kimberlites and their mantle sample: implications for Archean tectonics and lithosphere evolution. In: Ross, J., Jaques, A. L., Ferguson, J., Green, D. H., O'Reilly, S. Y., Danchin, R. V. & Janse, A.J. A. (eds) *Kimberlites and Related Rocks, Vol. 1. Geological Society of Australia, Special Publication* **14**, 358–368.

Herzberg, C. & Rudnick, R. (2012). Formation of cratonic lithosphere: An integrated thermal and petrological model. *Lithos* **149**, 4–15.

Hildebrand, R., Hofmann, P. F. & Bowring, S. A. (1987). Tectonomagmatic evolution of the 1·9-Ga Great Bear Magmatic Zone, Wopmay Orogen, Northwestern Canada. *Journal of Volcanology and Geothermal Research* **32**, 99–118.

Hirschmann, M. M. & Stolper, E. M. (1996). A possible role for garnet pyroxenite in the origin of the 'garnet signature' in MORB. *Contributions to Mineralogy and Petrology* **124**, 185–208.

Hoffman, P. F. (1989). Precambrian geology and tectonic history of North America. In: Bally, A. W. & Palmer, A. R. (eds) *The Geology of North America: an Overview. Geological Society of America, The Geology of North America* **A**, 447–512.

Huang, J.-X., Gréau, Y., Griffin, W. L., O'Reilly, S. Y. & Pearson, N. J. (2012). Multi-stage origin of Roberts Victor eclogites: Progressive metasomatism and its isotopic effects. *Lithos* **142–143**, 161–181.

Hunt, L., Stachel, T., Grütter, H., Armstrong, J., McCandless, T. E., Simonetti, A. & Tappe, S. (2012). Small mantle fragments from Renard kimberlites, Quebec: powerful recorders of mantle lithosphere formation and modification beneath the eastern Superior Craton. *Journal of Petrology* **53**, 1597–1635.

Ireland, T. R., Rudnick, R. L. & Spetsius, Z. (1994). Trace elements in diamond inclusions from eclogites reveal link to Archean granites. *Earth and Planetary Science Letters* **128**, 199–213.

Irvine, G., Pearson, D. G., Kjarsgaard, B. A., Carlson, R. W., Kopylova, M. G. & Dreibus, G. (2003). A Re–Os isotope and PGE study of kimberlite-derived peridotite xenoliths from Somerset Island and a comparison to the Slave and Kaapvaal cratons. *Lithos* **71**, 461–488.

Jacob, D. E. (2004). Nature and origin of eclogite xenoliths from kimberlites. *Lithos* **77**, 295–316.

Jacob, D. E. & Foley, S. F. (1999). Evidence for Archean ocean crust with low high field strength element signature from diamondiferous eclogite xenoliths. *Lithos* **48**, 317–336.

Jacob, D., Jagoutz, E., Lowry, D., Mattey, D. & Kudrjavtseva, G. (1994). Diamondiferous eclogites from Siberia—Remnants of Archean oceanic crust. *Geochimica et Cosmochimica Acta* **58**, 5191–5207.

Jacob, D. E., Viljoen, K. S. & Grassineau, N. V. (2009). Eclogite xenoliths from Kimberley, South Africa—A case study of mantle metasomatism in eclogites. *Lithos* **112S**, 1002–1013.

Jagoutz, E., Dawson, J. B., Hoernes, S., Spettel, B. & Wänke, H. (1984). Anorthositic oceanic crust in the Archean Earth. *Proceedings of the 15th Lunar Planetary Science Conference. Journal of Geophysical Research* **90**, Supplement: 395–396.

Jerde, E. A., Taylor, L. A., Crozaz, G., Sobolev, N. V. & Sobolev, V. N. (1993). Diamondiferous eclogites from Yakutia, Siberia: evidence for a diversity of protoliths. *Contributions to Mineralogy and Petrology* **114**, 189–202.

Kelemen, P. B., Shimizu, N. & Dunn, T. (1993). Relative depletion of niobium in some arc magmas and the continental crust: partitioning of K, Nb, La and Ce during melt/rock reaction in the upper mantle. *Earth and Planetary Science Letters* **120**, 111–134.

Klein-BenDavid, O., Izraeli, E. S., Hauri, E. & Navon, O. (2007). Fluid inclusions in diamonds from the Diavik mine, Canada and the evolution of diamond-forming fluids. *Geochimica et Cosmochimica Acta* **70**, 723–744.

Klemme, S., van der Laan, S. R., Foley, S. F. & Gunther, D. (1995). Experimentally determined trace and minor element partitioning between clinopyroxene and carbonatite melt under upper mantle conditions. *Earth and Planetary Science Letters* **133**, 439–448.

Klemme, S., Blundy, J. D. & Wood, B. J. (2002). Experimental constraints on major and trace element partitioning during partial melting of eclogite. *Geochimica et Cosmochimica Acta* **66**, 3109–3123.

Kogiso, T., Hirschmann, M. M. & Pertermann, M. (2004). High-pressure partial melting of mafic lithologies in the mantle. *Journal of Petrology* **45**, 2407–2422.

König, S., Münker, C., Schuth, S. & Garbe-Schönberg, D. (2008). Mobility of tungsten in subduction zones. *Earth and Planetary Science Letters* **274**, 82–92.

Kopylova, M. G., Russell, J. K. & Cookenboo, H. (1999*a*). Mapping the lithosphere beneath the North Central Slave Craton. In: Dawson, J. B. & Nixon, P. H. (eds) *Proceeding of the 7th International Kimberlite Conference, Vol. 1.* Red Roof Design, pp. 468–479.

Kopylova, M. G., Russell, J. K. & Cookenboo, H. (1999*b*). Petrology of peridotite and pyroxenite xenoliths from the Jericho kimberlite: Implications for the thermal state of the mantle beneath the Slave craton, Northern Canada. *Journal of Petrology* **40**, 79–104.

Kopylova, M. G., Lo, J. & Christensen, N. I. (2004). Petrological constraints on seismic properties of the Slave upper mantle (Northern Canada). *Lithos* **77**, 493–510.

Kopylova, M. G., Nowell, G. M., Pearson, D. G. & Markovic, G. (2009). Crystallization of megacrysts from protokimberlitic

fluids: Geochemical evidence from high-Cr megacrysts in the Jericho kimberlite. *Lithos* **112S**, 284–295.

Krogh Ravna, E. (2000). The garnet–clinopyroxene Fe^{2+}–Mg geothermometer: an updated calibration. *Journal of Metamorphic Geology* **18**, 211–219.

Kwon, S.-T., Tilton, G. R. & Grunenfelder, M. H. (1989). Lead isotope relationships and alkali complexes: an overview. In: Bell, K. (ed.) *Carbonatites: Genesis and Evolution*. Unwin Hyman, pp. 360–387.

Larsen, T. E. & Sharp, Z. D. (2005). Interpreting the prograde-growth histories of Al_2SiO_5 triple-point rocks using oxygen-isotope thermometry: an example from the Truchas Mountains, USA. *Journal of Metamorphic Geology* **23**, 847–863.

Le Cheminant, A. N. & Heaman, L. M. (1989). Mackenzie igneous events, Canada: Middle Proterozoic hotspot magmatism associated with ocean opening. *Earth and Planetary Science Letters* **96**, 38–48.

Le Cheminant, A. N. & van Breemen, O. (1994). U–Pb ages of Proterozoic dyke swarms, Lac de Gras area, N.W.T.: Evidence for progressive break-up of an Archean supercontinent. *GAC Programs with Abstracts* **19**, 62.

MacGregor, I. D. & Carter, J. L. (1970). The chemistry of clinopyroxenes and garnets of eclogite and peridotite xenoliths from the Roberts Victor mine, South Africa. *Physics of the Earth Planetary Interiors* **3**, 391–397.

MacGregor, I. D. & Manton, W. I. (1986). Roberts Victor eclogites: ancient oceanic crust. *Journal of Geophysical Research* **91(B14)**, 14063–14079.

Mattey, D., Lowry, D. & Macpherson, C. (1994). Oxygen isotope composition of mantle peridotite. *Earth and Planetary Science Letters* **128**, 231–241.

McDonough, W. F. & Sun, S. S. (1995). The composition of the Earth. *Chemical Geology* **120**, 223–253.

Muehlenbachs, K. & Clayton, R. N. (1972). Oxygen isotope geochemistry of submarine greenstones. *Canadian Journal of Earth Sciences* **9**, 471–478.

Norman, M., Garcia, M. O. & Pietruszka, A. J. (2005). Trace-element distribution coefficients for pyroxenes, plagioclase, and olivine in evolved tholeiites from the 1955 eruption of Kilauea Volcano, Hawai'i, and petrogenesis of differentiated rift-zone lava. *American Mineralogist* **90**, 888–899.

O'Hara, M. J. & Yoder, H. S. (1967). Formation and fractionation of basic magmas at high pressures. *Scottish Journal of Geology* **3**, 67–117.

Pearson, D. G. (1999). The age of continental roots. *Lithos* **48**, 171–194.

Pearson, D. G. & Wittig, N. (2008). Formation of Archaean continental lithosphere and its diamonds: the root of the problem. *Journal of the Geological Society, London* **165**, 895–914.

Pearson, D. G., Canil, D. & Shirey, S. B. (2003). Mantle samples included in volcanic rocks: xenoliths and diamonds. In: Carlson, R. W. (ed.) *The Mantle and Core. Treatise on Geochemistry, Vol. 2.* Elsevier–Pergamon, pp. 171–275.

Polat, A., Hofmann, A. W. & Rosing, M. T. (2002). Boninite-like volcanic rocks in the 3·7–3·8 Ga Isua greenstone belt, West Greenland: geochemical evidence for intra-oceanic subduction zone processes in the early Earth. *Chemical Geology* **184**, 231–254.

Polat, A., Appel, P. W. U., Frei, R., Pan, Y., Dilek, Y., Ordonez, J. C., Fryer, B., Hollis, J. A. & Raith, J. G. (2007). Field and geochemical characteristics of Mesoarchean (~3075 Ma) Ivisaartoq greenstone belt, southern West Greenland: Evidence for seafloor hydrothermal alteration in supra-subduction oceanic crust. *Gondwana Research* **11**, 69–91.

Polat, A., Frei, R., Appel, P. W. U., Dilek, Y., Fryer, B., Ordonez, J. C. & Yang, Z. (2008). The origin and compositions of Mesoarchean oceanic crust: Evidence from the 3075 Ma Ivisaartoq greenstone belt, SW Greenland. *Lithos* **100**, 293–321.

Price, S. E., Russell, J. K. & Kopylova, M. G. (2000). Primitive magma from the Jericho pipe, N.W.T., Canada: constraints on primary kimberlite melt chemistry. *Journal of Petrology* **41**, 789–808.

Purves, M. (2007). Origin and isotopic evolution of the Muskox Intrusion, Nunavut, MSc thesis, University of Alberta, Edmonton.

Rapp, R. P. & Watson, B. (1995). Dehydration melting of metabasalt at 8–32 kbar: Implications for continental growth and crust–mantle recycling. *Journal of Petrology* **36**, 891–931.

Richardson, S. H., Harris, J. W. & Gurney, J. J. (1993). Three generations of diamonds from old continental mantle. *Nature* **366**, 256–258.

Ringwood, A. E. & Green, D. H. (1966). An experimental investigation of the gabbro–eclogite transformation and some geophysical implications. *Tectonophysics* **3**, 383–427.

Rollinson, H. (1999). Petrology and geochemistry of metamorphosed komatiites and basalts from the Sula Mountain greenstone belt, Sierra Leone. *Contributions to Mineralogy and Petrology* **134**, 86–101.

Rudnick, R. L., McDonough, W. F. & Chappell, B. W. (1993). Carbonatite metasomatism in the northern Tanzanian mantle: petrographic and geochemical characteristics. *Earth and Planetary Science Letters* **114**, 463–475.

Schmickler, B., Jacob, D. E. & Foley, S. F. (2004). Eclogite xenoliths from the Kuruman kimberlites, South Africa: geochemical fingerprinting of deep subduction and cumulate processes. *Lithos* **75**, 173–207.

Schmidberger, S. S. & Francis, D. (2001). Constraints on the trace element composition of the Archean mantle root beneath Somerset Island, Arctic Canada. *Journal of Petrology* **42**, 1095–1117.

Schmidberger, S. S., Simonetti, A. & Francis, D. (2003). Small-scale Sr isotope investigation of clinopyroxenes from peridotite xenoliths by laser ablation MC-ICP-MS—implications for mantle metasomatism. *Chemical Geology* **199**, 317–329.

Schmidberger, S. S., Heaman, L. M., Simonetti, A., Creaser, R. A. & Cookenboo, H. O. (2005). Formation of Paleoproterozoic eclogitic mantle, Slave Province (Canada): Insights from *in-situ* Hf and U–Pb isotopic analyses of mantle zircons. *Earth and Planetary Science Letters* **240**, 621–633.

Schmidberger, S. S., Simonetti, A., Heaman, L. M., Creaser, R. A. & Whiteford, S. (2007). Lu–Hf, *in-situ* Sr and Pb isotope and trace element systematics for mantle eclogites from the Diavik diamond mine: Evidence for Paleoproterozoic subduction beneath the Slave craton, Canada. *Earth and Planetary Science Letters* **254**, 55–68.

Schulze, D. J., Harte, B., Valley, J. W., Brenan, J. M., Channer, D. M. & De, R. (2003). Extreme crustal oxygen isotope signatures preserved in coesite in diamond. *Nature* **423**, 68–70.

Sharp, Z. D. (1990). A laser-based microanalytical method for the *in situ* determination of oxygen isotope ratios of silicates and oxides. *Geochimica et Cosmochimica Acta* **54**, 1353–1357.

Sharp, Z. D. (1995). Oxygen isotope geochemistry of the Al_2SiO_5 polymorphs. *American Journal of Science* **295**, 1058–1076.

Shirey, S. B. & Richardson, S. H. (2011). Start of the Wilson cycle at 3 Ga shown by diamonds from subcontinental mantle. *Science* **333**, 434–436.

Shirey, S. B., Richardson, S. B. & Harris, J. W. (2004). Integrated models of diamond formation and craton evolution. *Lithos* **77**, 923–944.

Simonetti, A., Heaman, L. M., Hartlaub, R. P., Creaser, R. A., MacHattie, T. G. & Bohm, C. (2005). U–Pb zircon dating by laser ablation-MC-ICP-MS using a new multiple ion counting Faraday collector array. *Journal of Analytical Atomic Spectrometry* **20**, 677–686.

Smart, K. A., Heaman, L. M., Chacko, T., Simonetti, A., Kopylova, M., Mah, D. & Daniels, D. (2009). The origin of high-MgO diamond eclogites from the Jericho kimberlite, Canada. *Earth and Planetary Science Letters* **284**, 527–537.

Smart, K. A., Chacko, T., Stachel, T., Muehlenbachs, K., Stern, R. A. & Heaman, L. M. (2011). Diamond growth from oxidized carbon sources beneath the Northern Slave Craton, Canada: A δ^{13}C-N study of eclogite-hosted diamonds from the Jericho kimberlite. *Geochimica et Cosmochimica Acta* **75**, 6027–6047.

Smart, K. A., Chacko, T., Stachel, T., Tappe, S., Stern, R. A., Ickert, R. B. & EIMF (2012). Eclogite formation beneath the northern Slave craton constrained by diamond inclusions: Oceanic lithosphere origin without a crustal signature. *Earth and Planetary Science Letters* **319–320**, 165–177.

Smit, K. V., Stachel, T., Creaser, R. A., Ickert, R. B., DuFrance, S. A., Stern, R. A. & Seller, M. (2013). Origin of eclogite and pyroxenite xenoliths from the Victor kimberlite, Canada, and implications for Superior craton formation. *Geochimica et Cosmochimica Acta* **125**, 308–337.

Smith, C. B. (1983). Pb, Sr and Nd isotopic evidence for sources of southern African Cretaceous kimberlites. *Nature* **304**, 51–54.

Smithies, R. H., Champion, D. C. & Sun, S-S. (2004). The case for Archean boninites. *Contributions to Mineralogy and Petrology* **147**, 705–721.

Smyth, J. R., Caporuscio, F. A. & McCormick, T. (1989). Mantle eclogites: evidence of igneous fractionation in the mantle. *Earth and Planetary Science Letters* **93**, 133–141.

Spetsius, Z. V., Wiggers de Vries, D. F. & Davies, G. R. (2009). Combined C isotope and geochemical evidence for a recycled origin for diamondiferous eclogite xenoliths from kimberlites of Yakutia. *Lithos* **112S**, 1032–1042.

Stacey, J. S. & Kramers, J. D. (1975). Approximation of terrestrial lead isotope evolution by a two-stage model. *Earth and Planetary Science Letters* **26**, 207–221.

Stachel, T., Viljoen, K. S., Brey, G. & Harris, J. W. (1998). Metasomatic processes in lherzolitic and harzburgitic domains of diamondiferous lithospheric mantle: REE in garnets from xenoliths and inclusions in diamonds. *Earth and Planetary Science Letters* **159**, 1–12.

Sun, S.-S. & McDonough, W. F. (1989). Chemical and isotopic systematics of oceanic basalts: implications for mantle composition and processes. In: Saunders, A. D. & Norry, M. J. (eds) *Magmatism in the Ocean Basins. Geological Society, London, Special Publications* **42**, 313–345.

Tappe, S., Foley, S. F., Stracke, A., Romer, R. L., Kjarsgaard, B. A., Heaman, L. M. & Joyce, N. (2007). Craton reactivation on the Labrador Sea margins: ^{40}Ar/^{39}Ar age and Sr–Nd–Hf–Pb isotope constraints from alkaline and carbonatite intrusives. *Earth and Planetary Science Letters* **256**, 433–454.

Tappe, S., Smart, K. A., Pearson, D. G., Steenfelt, A. & Simonetti, A. (2011). Craton formation in Late Archean subduction zones revealed by first Greenland eclogites. *Geology* **39**, 1103–1106.

Tappe, S., Steenfelt, A. & Nielsen, T. (2012). Asthenospheric source of Neoproterozoic and Mesozoic kimberlites from the North Atlantic craton, West Greenland: New high-precision U–Pb and Sr–Nd isotope data on perovskite. *Chemical Geology* **320**, 113–127.

Tappe, S., Pearson, D. G., Kjarsgaard, B. A., Nowell, G. & Dowall, D. (2013). Mantle transition zone input to kimberlite magmatism near a subduction zone: Origin of anomalous Nd–Hf isotope systematics at Lac de Gras, Canada. *Earth and Planetary Science Letters* **317–372**, 235–251.

Taylor, L. A. & Neal, C. R. (1989). Eclogites with oceanic crustal and mantle signatures from the Bellsbank kimberlite, South Africa, Part 1: Mineralogy, petrology, and whole-rock chemistry. *Journal of Geology* **97**, 551–567.

Valley, J. W., Kitchen, N., Kohn, M. J., Niendorf, C. R. & Spicuzza, M. J. (1995). UWG-2, a garnet standard for oxygen isotope ratios: Strategies for high precision and accuracy with laser heating. *Geochimica et Cosmochimica Acta* **59**, 5223–5231.

van Achterbergh, E., Ryan, C., Jackson, S. & Griffin, W. L. (2001). Appendix 3; Data reduction software for LA-ICP-MS. In: Sylvester, P. (ed.) *Laser-Ablation-ICPMS in the Earth Sciences. Mineralogical Association of Canada, Short Courses* **29**, 239–243.

van Achterbergh, E., Griffin, W. L., Ryan, C. G., O'Reilly, S. Y., Pearson, N. J., Kivi, K. & Doyle, B. J. (2002). Subduction signature for quenched carbonatites from the deep lithosphere. *Geology* **30**, 743–746.

Veizer, J. & Compston, W. (1976). ^{87}Sr/^{86}Sr in Precambrian carbonates as an index of crustal evolution. *Geochimica et Cosmochimica Acta* **40**, 905–914.

Wallace, M. E. & Green, D. H. (1988). An experimental determination of primary carbonatite magma composition. *Nature* **335**, 343–346.

Westerlund, K. J., Shirey, S. B., Richardson, S. H., Carlson, R. W., Gurney, J. J. & Harris, J. W. (2006). A subduction wedge origin for Paleoarchean peridotitic diamonds and harzburgites from the Panda kimberlite, Slave craton, evidence from Re–Os isotope systematics. *Contributions to Mineralogy and Petrology* **152**, 275–294.

Williams, H. M., Nielsen, S. G., Renac, C., Griffin, W. L., O'Reilly, S. Y., McCammon, C. A., Pearson, N., Viljoen, F., Alt, J. C. & Halliday, A. N. (2009). Fractionation of oxygen and iron isotopes by partial melting processes: Implications for the interpretation of stable isotope signatures in mafic rocks. *Earth and Planetary Science Letters* **283**, 156–166.

Wittig, N., Webb, M., Pearson, D. G., Dale, C. W., Ottley, C. J., Hutchinson, M., Jensen, S. M. & Luguet, A. (2010). Formation of the North Atlantic Craton: Timing and mechanisms constrained from Re–Os isotope and PGE data of peridotite xenoliths from S.W. Greenland. *Chemical Geology* **276**, 166–187.

Woodhead, J. D. & Hergt, J. M. (2001). Strontium, neodymium and lead isotope analyses of NIST glass certified reference materials: SRM 610, 612, 614. *Geostandards Newsletter* **25**, 261–266.

Workman, R. K. & Hart, S. R. (2005). Major and trace element composition of the depleted MORB mantle (DMM). *Earth and Planetary Science Letters* **231**, 53–72.

Wyllie, P. J. (1988). Solidus curves, mantle plumes and magma generation beneath Hawaii. *Journal of Geophysical Research* **93B**, 4171–4181.

Wyman, D. A. (1999). A 2·7 Ga depleted tholeiite suite: evidence of plume–arc interaction in the Abitibi Greenstone Belt, Canada. *Precambrian Research* **97**, 27–42.

Yamashita, K., Creaser, R. A., Jensen, J. E. & Heaman, L. M. (2000). Origin and evolution of mid- to late-Archean crust in the Hanikahimajuk Lake area, Slave Province, Canada; evidence from U–Pb geochronological, geochemical and Nd–Pb isotopic data. *Precambrian Research* **99**, 197–224.

Yaxley, G. M. & Sobolev, A. V. (2007). High-pressure partial melting of gabbro and its role in the Hawaiian magma source. *Contributions to Mineralogy and Petrology* **154**, 371–383.